



Contents lists available at ScienceDirect

Journal of the Mechanics and Physics of Solids

journal homepage: www.elsevier.com/locate/jmps

Unified nano-mechanics based probabilistic theory of quasibrittle and brittle structures: I. Strength, static crack growth, lifetime and scaling

Jia-Liang Le^{a,1}, Zdeněk P. Bažant^{b,*}, Martin Z. Bazant^c

^a University of Minnesota, Minneapolis, MN 55455, United States

^b Northwestern University, 2145 Sheridan Road, CEE/A135, Evanston, IL 60208, United States

^c Massachusetts Institute of Technology, Cambridge, MA 02139, United States

ARTICLE INFO

Article history:

Received 20 May 2010

Received in revised form

16 January 2011

Accepted 2 March 2011

Available online 10 March 2011

Keywords:

Strength statistics

Fracture

Probabilistic mechanics

Size effect

Activation energy

ABSTRACT

Engineering structures must be designed for an extremely low failure probability such as 10^{-6} , which is beyond the means of direct verification by histogram testing. This is not a problem for brittle or ductile materials because the type of probability distribution of structural strength is fixed and known, making it possible to predict the tail probabilities from the mean and variance. It is a problem, though, for quasibrittle materials for which the type of strength distribution transitions from Gaussian to Weibullian as the structure size increases. These are heterogeneous materials with brittle constituents, characterized by material inhomogeneities that are not negligible compared to the structure size. Examples include concrete, fiber composites, coarse-grained or toughened ceramics, rocks, sea ice, rigid foams and bone, as well as many materials used in nano- and microscale devices.

This study presents a unified theory of strength and lifetime for such materials, based on activation energy controlled random jumps of the nano-crack front, and on the nano-macro multiscale transition of tail probabilities. Part I of this study deals with the case of monotonic and sustained (or creep) loading, and Part II with fatigue (or cyclic) loading. On the scale of the representative volume element of material, the probability distribution of strength has a Gaussian core onto which a remote Weibull tail is grafted at failure probability of the order of 10^{-3} . With increasing structure size, the Weibull tail penetrates into the Gaussian core. The probability distribution of static (creep) lifetime is related to the strength distribution by the power law for the static crack growth rate, for which a physical justification is given. The present theory yields a simple relation between the exponent of this law and the Weibull moduli for strength and lifetime. The benefit is that the lifetime distribution can be predicted from short-time tests of the mean size effect on strength and tests of the power law for the crack growth rate. The theory is shown to match closely numerous test data on strength and static lifetime of ceramics and concrete, and explains why their histograms deviate systematically from the straight line in Weibull scale.

Although the present unified theory is built on several previous advances, new contributions are here made to address: (i) a crack in a disordered nano-structure (such as that of hydrated Portland cement), (ii) tail probability of a fiber bundle (or parallel coupling) model with softening elements, (iii) convergence of this model to the Gaussian distribution, (iv) the stress-life curve under constant load, and (v) a detailed random walk analysis of crack front jumps in an atomic lattice. The nonlocal behavior is

* Corresponding author. Tel.: +1 847 491 4025; fax: +1 847 491 4011.

E-mail address: z-bazant@northwestern.edu (Z.P. Bažant).

¹ Formerly Graduate Research Assistant, Northwestern University.

captured in the present theory through the finiteness of the number of links in the weakest-link model, which explains why the mean size effect coincides with that of the previously formulated nonlocal Weibull theory. Brittle structures correspond to the large-size limit of the present theory. An important practical conclusion is that the safety factors for strength and tolerable minimum lifetime for large quasibrittle structures (e.g., concrete structures and composite airframes or ship hulls, as well as various micro-devices) should be calculated as a function of structure size and geometry.

© 2011 Elsevier Ltd All rights reserved.

1. Introduction

The design of engineering structures, such as bridges, dams, ships, aircraft and microelectronic components, must ensure an extremely low failure probability, typically $P_f < 10^{-6}$ (Duckett, 2005; NKB, 1978; Melchers, 1987). A direct experimental verification by histogram testing is, for such a low failure probability, virtually impossible (as $> 10^8$ test repetitions would be required). So the determination of probability distributions of structural strength and lifetime must rely on some physically based theory that can be verified and calibrated indirectly, based on tests other than histograms.

The strength distributions of structures have so far been well understood for two limiting behaviors:

- (1) Perfectly plastic structures, in which the failure does not localize and the failure load is a weighted sum of the random material strengths of all the representative volume elements (RVEs) along the failure surface. By virtue of central limit theorem of the theory of probability, the cumulative distribution function (cdf) of structure strength must then be the Gaussian (or normal) distribution (except in the remote tails).
- (2) Perfectly brittle structures, in which the failure localizes into one RVE and thus the failure of the entire structure is triggered by the failure of one RVE (like in a chain). For structures of extremely large size (compared to material inhomogeneities), which can be statistically represented by a chain with an infinite number of RVEs, the strength distribution is then necessarily the (two-parameter) Weibull distribution.

Therefore, for both perfectly plastic and perfectly brittle structures, the failure load corresponding to the tolerable failure probability $P_f = 10^{-6}$ can be easily determined by extrapolating from the mean and variance.

This is not the case for quasibrittle structures, which consist of brittle heterogeneous materials, called quasibrittle materials. They include concrete (as the archetypical example), rocks, coarse-grained and toughened ceramics, fiber composites, rigid foams, sea ice, dental ceramics, dentine, bone, biological shells, many bio- and bio-inspired materials, fiber-reinforced concretes, rocks, masonry, mortar, stiff cohesive soils, grouted soils, consolidated snow, wood, paper, carton, coal, cemented sand, etc. On the micro- and nano-scales, also fine grained ceramics, fatigue-embrittled metals and other brittle materials become quasibrittle. These materials have brittle constituents and are incapable of plastic deformation (except under extreme confining pressure). The salient feature of quasibrittle structures is that the fracture process zone (FPZ) is not negligible compared to the structure size.

For quasibrittle structures with positive geometry, which are those that fail (under controlled load) right at the initiation of a macrocrack from a damaged RVE and are characterized by an initially positive derivative of the stress intensity factor with respect to crack length, the probabilistic aspects of strength and lifetime are more complex than they are for brittle or ductile structures. It has been demonstrated in various ways that the behavior of quasibrittle materials transitions from quasi-plastic to brittle as the structure size increases (Bažant, 1984; Bažant and Kazemi, 1990; Bažant, 1997; Bažant and Planas, 1998; Bažant, 2004, 2005). This transition causes a size effect on the type of strength distribution, in which the cdf of structural strength gradually changes with increasing size from predominantly Gaussian to purely Weibullian (Bažant and Pang, 2006, 2007). This complicates extrapolation from laboratory tests to structures of large sizes or complex geometries, and causes that the safety factors guarding against the uncertainty of structural strength, which are in practice still determined empirically, are the most uncertain aspect of design. For such structures, a rational reliability analysis is of paramount importance.

This article reviews in a unified way and common context several parts of the theory that have already been published separately (Pang et al., 2008; Le and Bažant, 2009; Bažant et al., 2008, 2009; Bažant and Le, 2009; Le et al., 2009) and presents several new advances needed to achieve a unified and complete theory. These advances include: (1) a derivation of failure statistics and the nano-crack growth that is not contingent upon assuming a regular atomic lattice, (2) a derivation of the probability distribution of strength of a bundle model with gradually softening elements, (3) the stress-life curve of quasibrittle structures under constant load and its size effect, (4) a detailed analysis of random walk of an atomistic crack front in a 1-D setting, and (5) further comparisons with experimental histograms for quasibrittle materials. In Part II of this study (Le and Bažant, *in press*), the present theory is further extended to the probability distribution of fatigue strength and lifetime of quasibrittle structures.

2. Review of previous studies

2.1. Strength statistics

The two-parameter Weibull theory has been widely used for the strength distribution of quasibrittle materials (Weibull, 1939; Munz and Fett, 1999; Lohbauer et al., 2002; Tinschert et al., 2000). Freudenthal (1968) proposed to physically justify the two-parameter Weibull distribution of strength by the statistics of material flaws. On closer scrutiny, however, the flaw statistics is not a physical justification since three simplifying hypotheses are implied:

- (1) The Griffith theory is used to calculate the strength from the flaw sizes, even though the cracks are usually cohesive.
- (2) The largest flaws in adjacent material elements are assumed not to interact although they undoubtedly do.
- (3) The maximum flaw size a_m in the volume element is assumed to follow the Fréchet distribution $\exp[-(a_m/u)^{-p}]$ ($u, p = \text{constants} > 0$), which is obtained upon assuming that the probability distribution density of maximum flaw size converges to zero with a power-law decay as $a_m \rightarrow \infty$.

Hypothesis 3 is strictly a mathematical, rather than a physical, argument, which is based on the extreme value statistics (Fisher and Tippett, 1928; Gumbel, 1958; Haldar and Mahadevan, 2000). The Fréchet distribution for the largest flaw size in each RVE is what is needed to obtain the Weibull distribution of macro-strength. But the Fréchet distribution is mathematically required only as an asymptotic case, which might not be approached closely enough until the number of flaws becomes unreasonably large, say 10^{12} . This is a weak point of this argument.

Furthermore, while for ceramics the flaws are often sparse and can be clearly identified, for materials such as concrete the definition of a flaw is ambiguous. The reason is that the material is totally disordered from the nano-scale up and, even before any load is applied, the material is full of pre-existing densely packed “flaws” which must strongly interact. Yet, the fracture statistics of concrete and ceramics share the same characteristics.

Therefore, the statistical distribution of flaws itself does not seem to suffice to explain the statistics of quasibrittle fracture, and it does not predict the size effect on the type of strength distribution. So Freudenthal's theory merely represents a useful macro–micro relationship applicable to some perfectly brittle materials, but not a physical proof.

The testing of concrete, engineering ceramics and fiber composites, revealed systematic deviations of the strength histograms from the two-parameter Weibull distribution, even though the number of test repetitions (< 100) did not suffice to reveal the tails (Weibull, 1939; Lohbauer et al., 2002; Munz and Fett, 1999; Salem et al., 1996; Santos et al., 2003; Schwartz, 1987; Tinschert et al., 2000). As a remedy, a switch to the three-parameter Weibull distribution, which has a finite threshold, has recently been widely adopted to achieve better fits (Duffy et al., 1993; Gross, 1996; Stanley and Inanc, 1985).

This switch, however, amounts to a radical and risky change since the predicted failure load for $P_f = 10^{-6}$ can increase even by a factor 1.5 or more (Pang et al., 2008). For broad enough histograms (> 1000 tests), this switch still does not give an optimum fit since significant deviations still exist in the high probability range (Bažant and Pang, 2007). Furthermore, the value of Weibull modulus m obtained by fitting the three-parameter Weibull distribution is unrealistically low ($m \approx 1.5–5$). More seriously, at the large size limit, the three-parameter Weibull distribution with the weakest-link model predicts a vanishing size effect for very large sizes and an unreasonably strong size effect for medium sizes, which contradicts various experimental observations (Le and Bažant, 2009; Pang et al., 2008) as well as the predictions of the nonlocal Weibull theory (Bažant and Xi, 1991).

Recent studies (Bažant and Pang, 2006, 2007; Bažant et al., 2008, 2009) showed that the crux of the problem lies in the usual tacit assumption that the number of links in the chain underlying the weakest-link model for structural strength statistics is infinite. Instead, for all quasibrittle structures, one must adopt a finite weakest-link model, in which the number of links in the chain is finite, and possibly as small as 5–50. The reason is that the RVE is not negligible compared to the structure size (and also that the fracture mode is often two-dimensional since a row of RVEs along the front edge of fracture in the third dimension must fail nearly simultaneously).

For large size structures, the cdf's strength depends only on the far-left tail of the cdf's strength of one RVE, which must follow a power law. This essential tail property, along with the Weibull distribution itself, was first derived in 1928 by Fisher and Tippett (1928) from the stability postulate of extreme value statistics of a set of independent, identically distributed, random variables. Of course, the RVEs in a material are not perfectly statistically independent, but the stability postulate can also be justified for correlated random systems (such as percolation models, Bazant, 2000, 2002; van der Hofstad and Redig, 2006) using renormalization group methods, which homogenize the system recursively up to a scale (of the RVE) where correlations become negligible. Aside from the assumption of independence, however, the Fisher–Tippett argument has nothing to do with physics per se, and for a long time it has not been clear whether the power-law tail would apply only for probabilities so small (e.g. $< 10^{-9}$) that they would be irrelevant to structural strength.

In recent research (Bažant and Pang, 2006, 2007), a simplified justification of the power-law tail was given on the basis of the thermally activated fracture of a nano-structure and a multiscale statistical model. Further it was established (Bažant and Pang, 2006, 2007) that the type of cdf of strength of quasibrittle structures depends on the structure size and geometry, varying gradually from the Gaussian cdf at small sizes (modified by a remote Weibull tail) to a fully Weibull cdf at large enough sizes.

For ductile (or plastic) materials, by contrast, the strength distribution in the “central region” (within several standard deviations of the mean, not in the remote tail) must be Gaussian, based on the central limit theorem. The lognormal

distribution has sometimes been used to describe material strength, with the argument that negative strength values are impossible. However, this argument is mathematically incorrect because, for a sum of positive independent random variables, the negative tail is always beyond the range of the central limit theorem (note that even the sum of independent positive random variables converges to Gaussian distribution). This argument is also physically incorrect because a lognormal distribution would imply the load to be a product, rather than a sum, of statistically independent strength contributions from all the elements along the failure surface, which makes little physical sense.

2.2. Lifetime statistics

Ensuring a tolerable lifetime probability of a structure is another important aspect of engineering design. For decades, extensive efforts have been devoted to both deterministic and statistical predictions of lifetime of engineering materials.

The deterministic models of structural lifetime under constant loads were anchored in the kinetics of breakage of atomic bonds (Tobolsky and Eyring, 1943; Zhurkov, 1965; Zhurkov and Korsukov, 1974; Hsiao et al., 1968; Henderson et al., 1970). But the structural lifetime was in these models derived directly from the frequency of forward jumps over the activation energy barrier of one interatomic bond, while the statistics of nano-fracture growth, the statistical multiscale nano–macro transition, and the slow crack growth at macro-scale were not taken into consideration. Therefore, the size and geometry dependence of structural lifetime cannot be captured by these classical deterministic models.

Meanwhile, many phenomenological models of the lifetime probability distribution have been developed for various engineering materials. The lifetime statistics was first studied for fibrous materials (Coleman, 1957, 1958) and later for fiber composites (Phoenix, 1978a; Tierney, 1983; Ibnabdeljalil and Phoenix, 1995; Mahesh and Phoenix, 2004). These models were derived by assuming the infinite weakest-link model for a single fiber, which is questionable because experimentally observed strength histograms of single fibers consistently showed deviations from the classical Weibull distribution (Schwartz, 1987; Wanger et al., 1984; Schwartz et al., 1986), and the size effect was not checked.

A more general approach for lifetime statistics has more recently been based on the kinetics of crack growth (Munz and Fett, 1999; Fett and Munz, 1991; Lohbauer et al., 2002). For stress-driven creep crack growth, a power law was proposed to describe the dependence of crack growth velocity on the applied stress (Evans, 1972; Thouless et al., 1983; Evans and Fu, 1984). A partial theoretical justification of the power-law form for crack growth rate has also been suggested (Fett, 1991; Munz and Fett, 1999), based on the break frequency of a bond between a pair of two atoms. Such a justification, however, is insufficient, for three reasons: (1) The derivation was limited to the case of a pair potential, such as the Morse potential, which neglects the major contribution of surrounding atoms. (2) The propagation of a nano-crack consists of many jumps between subsequent potential wells with many very small decrements in the overall potential. (3) The statistical scale bridging between the atomic scale and the macro-scale was lacking. Thus the power law for creep crack growth rate still remained to be empirical.

In the recent studies of lifetime statistics of ceramics, the structural strength was calculated from the linear elastic fracture mechanics (LEFM) based on the initial flaw size, and was related to the structural lifetime by the crack growth law (Munz and Fett, 1999; Fett and Munz, 1991; Lohbauer et al., 2002). In these models, however, the two-parameter Weibull cdf structure strength, from which the Weibull cdf of lifetime followed, was assumed rather than derived. Yet it has not been explained why the lifetime histograms of quasibrittle specimens, particularly those of ceramics and fiber composites, consistently deviate from the two-parameter Weibull distribution (Chiao et al., 1977; Munz and Fett, 1999; Fett and Munz, 1991), and the corresponding size effect has not been checked.

3. Probabilistic fracture mechanics at the nano-scale

The macro-scale fracture originates from the breakage of interatomic bonds at the nano-scale. Thus it is logical to relate the statistics of structural failure to the statistics of interatomic bond breakage. This seems also inevitable since the only scale on which the probabilistic properties can be deduced mathematically appears to be the atomistic scale.

Although some researchers suggest multiscale modeling based on disordered mesostructure, at the mesoscale level there exists no fundamental physical law for the probability of microstructural breaks. Only intuitive hypotheses can be made. On the atomic level, though, a well established physical theory for the frequency of bond breaks exists. It is the rate process theory (Eyring, 1936; Glasstone et al., 1941; Tobolsky and Eyring, 1943; Krausz and Krausz, 1988; Kaxiras, 2003), which theoretically justifies the Arrhenius thermal factor and has long been used to transit from the atomic scale to the material scale, yielding the temperature and stress dependence of the rates of creep, diffusion, phase changes, adsorption, chemical reactions, etc. In this theory, the rates of breakage of interatomic bonds are characterized by the distribution of thermal energies among atoms and the frequency of passage over the activation energy barriers of the interatomic potential. The probability of failure of interatomic bonds is proportional to their failure frequency because, on the atomic level, the process is quasi-stationary.

To justify the quasi-stationarity hypothesis, consider a missile of speed 200 m/s breaking a single row of atoms along the missile path. The atomic spacing is about 2×10^{-10} m, and so the rate of bond breakage is $(200 \text{ m/s}) / (2 \times 10^{-10} \text{ m}) = 10^{12} / \text{s}$. Since the frequency of atomic vibrations is about $10^{14} / \text{s}$, one jump over the activation energy barrier occurs after every 100 vibrations; for accelerated missiles, after about every 20 vibrations; for a crack propagating at Raleigh wave speed in concrete, after about 10 vibrations (but the hypothesis is invalid for collisions in space, or for nuclear explosions, for which the frequency of bond breakage exceeds $10^{14} / \text{s}$).

The same hypothesis is also easily justified by energetic arguments. The natural energy scale for chemical bonds, and thus also for activation barriers in molecular rearrangements between long-lived well-defined molecular states, is the electron-volt. This scale is larger by at least one order of magnitude than the thermal energy scale since $kT=0.025$ eV at room temperature ($k=1.381 \times 10^{-23}$ J/K = Boltzmann constant and T = absolute temperature). As such, transitions between local minima of free energy can typically be described by the asymptotic Kramer's formula for the first passage time, which predicts an exponential dependence on the barrier energy relative to kT (which is also an Arrhenius dependence on temperature).

Consider a nano-scale element, such as an atomic lattice block representing a crystal grain of brittle ceramic (Fig. 1a), or a completely disordered system of nano-particles of the calcium silicate hydrate in concrete (Fig. 1b). In a continuum approximation, the fracturing behavior of this nano-scale element is characterized by a curve of equilibrium load P versus deflection u , in which hardening is followed by softening (Fig. 2a). The integral of this curve yields the curve of potential Π versus u , shown as the dash line in Fig. 2d.

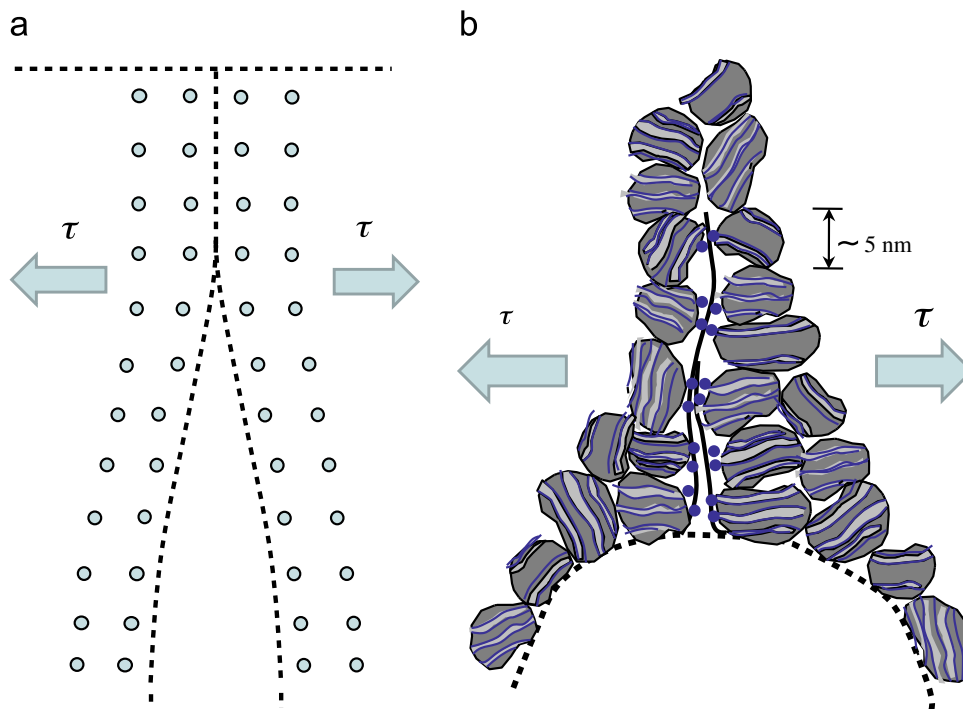


Fig. 1. Fracture of nano-scale element.

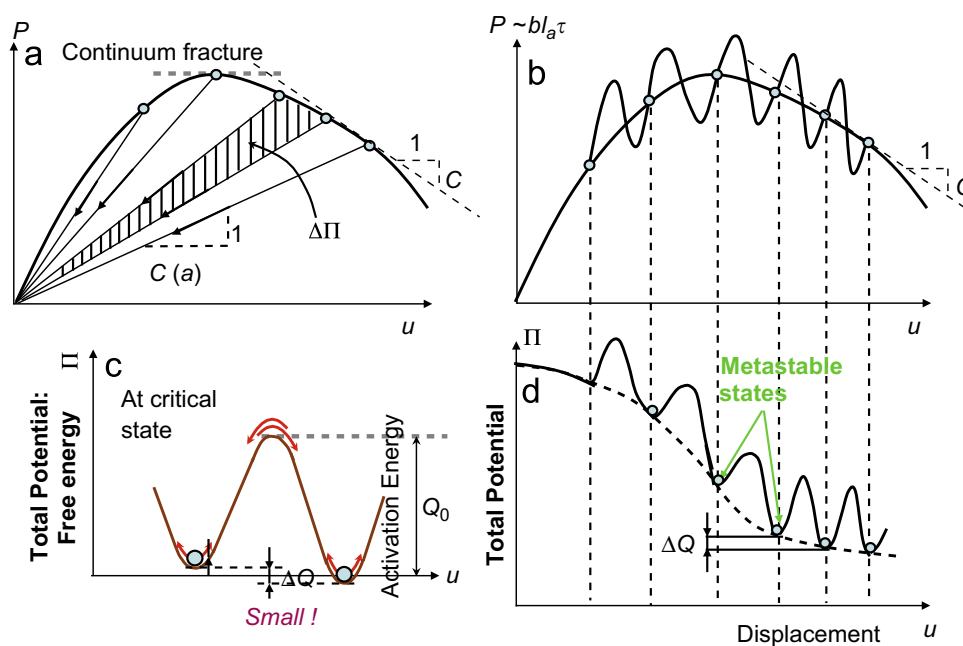


Fig. 2. (a) and (b) Load–displacement curve of lattice block, (c) change of activation energy barrier due to fracture.

A crack in the nano-scale element does not advance smoothly. Rather, it advances in numerous discrete jumps which correspond to the jumps over the activation energy barriers of interatomic bonds (Fig. 1a) or nano-particle connections (Fig. 1b). The length of these jumps is the spacing δ_a of the atoms or the nano-particles. The jumps cause that an undulation must be superposed on the load–deflection curve, and a corresponding undulation on the potential curve; see Fig. 2b in which $P = \tau b l_a = \text{load}$, $u = \text{displacement in the sense of } P$, $l_a = \text{characteristic size of the nano-element}$, $b = \text{width in the third dimension}$, and $\tau = \text{remote stress applied on the nano-element}$.

Now the crucial point is that many interatomic bonds (Fig. 1a) or many nano-particle connections (Fig. 1b) must be broken before reaching the critical crack length at which the nano-fracture becomes unstable and begins to advance dynamically, with sound emission. Consequently, there must be many undulation waves on the $\Pi(u)$ curve and on the corresponding potential curve (Fig. 2b and d). It follows that the difference ΔQ between two adjacent potential wells must be small (Fig. 2c) compared to the activation energy barrier Q_0 . In previous work (Bažant and Pang, 2006, 2007), the smallness of ΔQ was assumed on the basis of shear displacement of atoms over a lattice, which is not too realistic. With reference to Fig. 2d, the necessity of ΔQ being small is thus clear.

Consider, for the sake of simplicity, planar three-dimensional cracks that grow in a self-similar manner, expanding, e.g., in concentric circles or squares. According to LEFM, the stress intensity factor may generally be expressed as

$$K_a = \tau \sqrt{l_a} k_a(\alpha) \tag{1}$$

where $\alpha = a/l_a = \text{relative crack length}$ and $k_a(\alpha) = \text{dimensionless stress intensity factor}$. In the context of linear elasticity, the remote stress applied on the nano-scale element τ can be related to the macro-scale stress σ by setting $\tau = c\sigma$, where $c = \text{nano-macro stress concentration factor}$. Therefore, the energy release rate per unit crack front advance is

$$\mathcal{G}(\alpha) = \frac{K_a^2}{E_1} = \frac{k_a^2(\alpha) l_a c^2 \sigma^2}{E_1} \tag{2}$$

where $E_1 = \text{elastic modulus of the nano-element}$. Let $\gamma_1 = \text{geometry constant such that } \gamma_1 a = \text{perimeter of the radially growing crack front}$. The energy release along the entire perimeter, caused by crack advance δ_a , is

$$\Delta Q = \delta_a \left[\frac{\partial \Pi^*(P, a)}{\partial a} \right]_P = \delta_a (\gamma_1 \alpha l_a) \mathcal{G} = V_a(\alpha) \frac{c^2 \sigma^2}{E_1} \tag{3}$$

Here $\Pi^* = \text{complementary energy potential of the nano-element}$, and $V_a(\alpha) = \delta_a (\gamma_1 \alpha l_a^2) k_a^2(\alpha) = \text{activation volume}$ (note that if the stress tensor is written as $\tau \mathbf{s}$ where $\tau = \text{stress parameter}$, one could more generally write $V_a = \mathbf{s} : \mathbf{v}_a$ where $\mathbf{v}_a = \text{activation volume tensor}$, as in the atomistic theories of phase transformations in crystals (Aziz et al., 1991)).

A sharp LEFM crack is, of course, an idealization. In reality, there is always a finite FPZ. However, for the global response, which is what matters here, a crack with a finite FPZ may be treated by an equivalent sharp LEFM crack giving the same energy release rate. Its tip is located roughly in the middle of the FPZ.

Due to thermal activation, the energy states of the nano-element fluctuate and lead to jumps over the activation energy barriers. The jumps occur both forward and backward, albeit with different frequencies (Fig. 2c). The energies required for the forward and backward jumps are $Q_0 - \Delta Q/2$ and $Q_0 + \Delta Q/2$, respectively, where $Q_0 = \text{activation energy at no stress}$.

One might object that, generally, there are multiple activation energy barriers Q_1, Q_2, \dots instead of Q_0 . However, the lowest one always dominates. The reason is that the factor $e^{-Q_i/kT}$ is very small, typically 10^{-12} . Thus, if for example $Q_2/Q_1 = 1.2$ or 2 , then $e^{-Q_2/kT} = 0.0043 e^{-Q_1/kT}$ or $10^{-12} e^{-Q_1/kT}$, and so the higher barrier makes a negligible contribution. And if for example $Q_2/Q_1 = 1.02$, then Q_1 and Q_2 can be replaced by a single activation energy $Q_0 = 1.01 Q_1$.

Since the nano-crack attains its critical length a_c only after overcoming many activation energy barriers (Fig. 2b and d), the barrier for each forward jump, $Q_0 - \Delta Q/2$, must differ only little from the barrier for the backward jump, $Q_0 + \Delta Q/2$. Consequently, the forward and backward jumps must be happening with only slightly different frequencies. According to the transition rate theory (Kaxiras, 2003; Philips, 2001), the first-passage time for each state transition (for the limited case of a large free-energy barrier, $Q_0 \gg kT \gg \Delta Q$), which gives the net frequency of the forward crack front jumps, is given by Kramer's formula (Risken, 1989):

$$f_1 = \nu_T (e^{-(Q_0 + \Delta Q/2)/kT} - e^{-(Q_0 - \Delta Q/2)/kT}) = 2\nu_T e^{-Q_0/kT} \sinh[V_a(\alpha)/V_T] \tag{4}$$

where $V_T = 2E_1 kT/c^2 \sigma^2$; ν_T is the characteristic attempt frequency for the reversible transition, $\nu_T = kT/h$ where $h = 6.626 \times 10^{-34} \text{ Js} = \text{Planck constant} = (\text{energy of a photon})/(\text{frequency of its electromagnetic wave})$.

A comment on the classical empirical theory of structural lifetime (Zhurkov, 1965; Zhurkov and Korsukov, 1974; Kausch, 1978) is in order. This theory implied that only forward jumps take place. In that case, as a generalization of the Arrhenius factor, the jump frequency is assumed to be an exponential function of the applied stress. This situation is approached by the present formulation when the stress is sufficiently large, in which case the frequency of forward jumps is far higher than the frequency of backward jumps. Then the second term in Eq. (4) can be neglected, which gives approximately an exponential instead of the hyperbolic sine.

When, however, the stress is small, such a one-way jump model, which corresponds to the classical empirical theory, underestimates the lifetime by orders of magnitude. In Zhurkov (1965) it was observed that, for a low stress such as 20% of the short-time strength, the predicted lifetime was three orders of magnitude shorter than that observed experimentally on polymers, glass and alumina.

The atomic spacing is typically on the order of 0.1 nm, and so $V_a \sim 10^{-26} \text{ m}^3$. Volume V_T is a function of $\tau = c\sigma$, where the stress concentration factor c is probably larger than 10. The elastic modulus E_1 of the atomic lattice is doubtless larger, though not much larger, than the macroscopic elastic modulus E . For example, for the nano-structure of hardened Portland cement gel, the remote stress at nano-scale is perhaps on the order of 20–30 MPa, which gives $V_T \sim 10^{-25} \text{ m}^3$, and $V_a/V_T < 0.1$. Since $\sinh x \approx x$ for small x , Eq. (4) thus becomes (Bažant et al., 2009):

$$f_1 \approx e^{-Q_0/kT} [V_T V_a(\alpha)/kT] c^2 \sigma^2 / E_1 \tag{5}$$

The essential point here is that the frequency of each jump follows a power-law function of stress τ with a zero threshold.

So far we have determined the rate of jumps over one activation energy barrier. For a nano-scale crack to propagate up to the critical crack length a_c at which stability is lost, a certain number, n , of activation energy barriers must be overcome (up to point A in Fig. 2b). We do not know (and need not know) what number n is, but we know it must exist and be finite. Assuming that each jump is an independent process, the frequency of reaching the critical crack length is the sum of the net frequencies of forward jumps over all these barriers (for a subtle refinement see Appendix A). Then, since the failure probability P_f of the nano-element is proportional to this frequency, we may write

$$P_f(\sigma) \propto \sum_{i=1}^n f_{1i}(\sigma) = \int_{\alpha_0}^{\alpha_c} f_1 d\alpha \tag{6}$$

where f_{1i} = jump frequency of a crack of length a_i , whose tip is located at the i th interatomic bond on the crack path either through the atomic lattice block or through the block of nano-particles. Substituting Eq. (5) into Eq. (6), we obtain:

$$P_f(\sigma) \propto C_T c^2 \sigma^2 \tag{7}$$

with the notations $C_T = H_T \gamma_1 \int_{\alpha_0}^{\alpha_c} \alpha k_a^2(\alpha) d\alpha$, and $H_T = e^{-Q_0/kT} (\delta a^2_a / E_1 h)$.

4. Statistical multiscale transition of strength distribution

To relate the strength distributions of a nano-scale element and an RVE at the macro-scale, a certain statistical multiscale transition framework is needed. The numerical stochastic multiscale approaches proposed so far (e.g. Xu, 2007; Graham-Brady et al., 2006; Williams and Baxer, 2006) do not suffice for handling multiscale transitions of probability distributions and their tails. Here we try to determine the type of strength distribution of an RVE analytically, using for the scale transitions two basic statistical models: the fiber bundle model (or parallel coupling model) and the chain model (or weakest-link model, or series coupling model). These two models represent statistically two basic phenomena:

- (1) The weakest-link model (Fig. 3a), failing in one link only, statistically models the localization of failure into one FPZ at one location, within one scale.
- (2) The fiber bundle model (Fig. 3b) statistically models the condition of compatibility between one scale and its sub-scale—namely the condition that the deformations of several cracked material sub-elements located along the crack

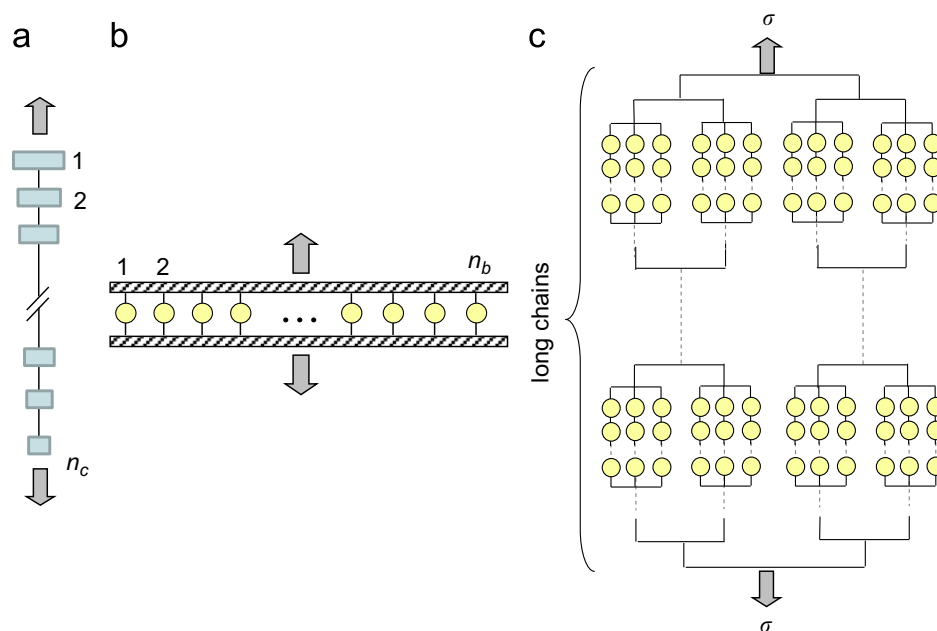


Fig. 3. (a) Chain model, (b) bundle model, (c) hierarchical model.

path within the FPZ must be compatible with the overall deformation of this FPZ on a higher scale. In contrast to the weakest-link model, the bundle model represents a material element that fails by distributed cracking.

4.1. Weakest-link model (a chain or series coupling)

The strength of the chain is determined by the strength of its weakest-link. To determine the failure probability P_f of a chain, note that the whole chain survives if and only if all the elements survive. So, the survival probability, $1 - P_f$, of a chain is the joint probability of survival of all its links. Therefore, if the failure probability (or strength distribution) of the i -th link (or element) under stress σ_i is denoted as $P_i(\sigma)$ where σ =stress in the chain, and if all the P_i are statistically independent, then the failure probability of a chain of n_c elements is given by the following well-known formula:

$$P_{f,chain}(\sigma) = 1 - \prod_{i=1}^{n_c} [1 - P_i(\sigma)] \tag{8}$$

For a detailed discussion, see, e.g., Bažant and Pang (2007). Suffice to say that the chain has the following two simple asymptotic properties: If the cdf's of strength of all the elements (or links) have a power-law tail of exponent p , then the cdf of strength of the whole chain has also a power-law tail and its exponent is also p ; and for large enough n_c , $P_f = 1 - e^{-n_c(\sigma/s_0)^p}$ = Weibull distribution (where s_0 is a constant).

4.2. Bundle model (parallel coupling)

In the bundle model (Fig. 3b), after one element (called a 'fiber') fails, the load gets redistributed among the other elements. The load is reduced to zero when all the elements break, but the maximum load is reached when a only certain fraction of the elements breaks. The bundle model statistically represents the load redistribution when the microstructure is partially damaged. The load redistribution after a fiber breaks depends on the load sharing rule. Various rules have been assumed (Daniels, 1945; Phoenix, 1978a, 1978b; Phoenix and Tierney, 1983; Mahesh and Phoenix, 2004), but many of them were merely phenomenological hypotheses, such as the load sharing by the nearest neighbors of the failing element in the bundle. A more realistic rule should be based on a mechanical model.

Since any fiber can be replaced by several fibers having different cross section areas or different lengths but the same combined elastic stiffness, it is not unduly restrictive to assume that all the fibers have equal elastic stiffness and are subjected to the same displacement. So, we consider initially elastic fibers spanning two parallel rigid plates. The load sharing rule is then fully determined by the failure behavior of the fibers.

Two limiting cases are by now well understood: (1) brittle failure, in which the stress in the fiber drops to zero immediately after its strength limit (peak stress) is reached, (2) plastic (or ductile) failure, in which the fiber extends at constant stress after its strength limit is reached. Two asymptotic properties are of particular interest here—the tail of the cdf of bundle strength and the type of cdf's of the strength of large bundles.

A surprisingly simple property applies to power-law tails. The power-laws are always preserved and their exponents are additive. Specifically, if the strength cdf of each of n_b fibers in a bundle has a power-law tail of exponent p_i ($i=1, \dots, n_b$), then the cdf of bundle strength has also a power-law tail and its exponent is $p = \sum_{i=1}^{n_b} p_i$.

For a brittle bundle, this remarkable property was proven by induction based on the set theory (Harlow et al., 1983; Phoenix et al., 1997). Later it was also proven by a simpler approach Bažant and Pang (2007) using the asymptotic expansion of Daniel's (1945) exact recursive equation for the strength of cdf of bundles of increasing n_b . For a plastic bundle, this property was proven by the asymptotic expansion of cdf (Bažant and Pang, 2007). Alternatively, it can be proven through the Laplace transform of cdf. A recent study (Lam et al., submitted for publication) provided a general proof of the additivity of power-law tail exponents based on the generalization of the central limit theorem. For the general case of fibers that exhibit gradual post-peak softening, the tail exponent additivity has been verified numerically but an analytical proof has been lacking. It is presented next.

Consider a bundle with two fibers having the same cross section area, although a generalization to any number of fibers is easy. Assume that each element has a bilinear stress–strain curve (Fig. 4a), which has an elastic modulus E and softening modulus E_t ($E_t \leq 0$). Let the only random variable be the peak strength σ_i ($i=1,2$). Then the peak of average stress in the bundle can be written as:

$$\sigma_b = \max_{\epsilon} [s_1(\epsilon) + s_2(\epsilon)]/2 \tag{9}$$

where ϵ = strain in the fiber, and s_1, s_2 = stresses in fibers 1 and 2. We seek the critical strain ϵ^* at which the load on the bundle reaches its maximum. The critical strain depends on the ratio $\alpha = -E_t/E$ ($\alpha \geq 0$). Two cases must be distinguished, depending on whether the weaker element fails completely (i) before or (ii) after the stronger element reaches its peak.

Let the two fibers be numbered such that $\sigma_1 \leq \sigma_2$. Then the peak stress of the bundle, σ_b , can be written as follows:

Case 1: $0 \leq \alpha \leq 1$

if $(1 + \alpha)\sigma_1/\alpha > \sigma_2$: $\sigma_b = [(1 + \alpha)\sigma_1 + (1 - \alpha)\sigma_2]/2$, (10)

if $(1 + \alpha)\sigma_1/\alpha \leq \sigma_2$: $\sigma_b = \sigma_2/2$, (11)

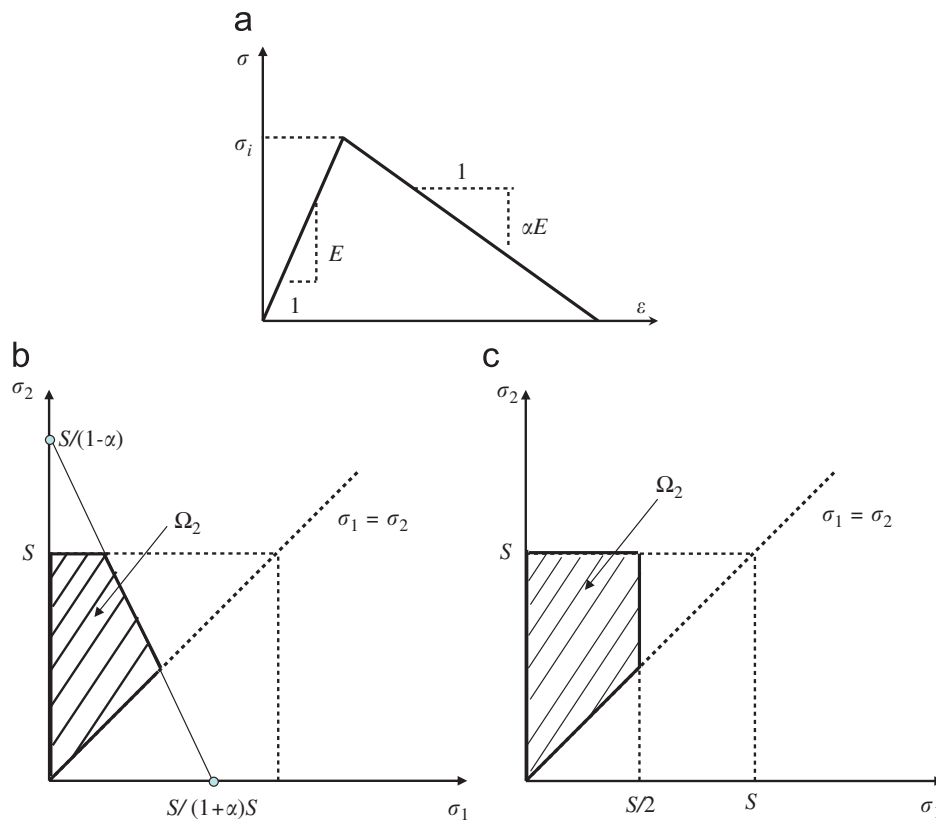


Fig. 4. (a) Mechanical behavior of fiber. (b) and (c) Feasible region of strength of fibers.

Case2: $\alpha > 1$

$$\text{if } (1 + \alpha)\sigma_1/\alpha > \sigma_2 : \sigma_b = \sigma_1, \tag{12}$$

$$\text{if } (1 + \alpha)\sigma_1/\alpha \leq \sigma_2 : \sigma_b = \max(\sigma_1, \sigma_2/2), \tag{13}$$

Note that these results cover not only the softening bundles but also the limit cases of both the plastic and brittle bundles. When $\alpha = 0$, the element is plastic and the peak average stress in the bundle is $(\sigma_1 + \sigma_2)/2$ (which was statistically analyzed in Bažant and Pang (2007)). When $\alpha \rightarrow \infty$, the element is brittle and the peak stress of the bundle is $\max(\sigma_1, \sigma_2/2)$ (Daniels, 1945).

If the average bundle strength is less than some prescribed value S , i.e. $\sigma_b \leq S$, then, based on Eqs. (10)–(13), the strength of each fiber must lie in the domain $\Omega_2(S)$, shown in Fig. 4b and c. Since the strengths of these two fibers are independent random variables, we may use the joint probability theorem to express the cdf of the average bundle strength;

$$G_2(S) = 2 \int_{\Omega_2(S)} f_1(\sigma_1) f_2(\sigma_2) d\sigma_1 d\sigma_2 \tag{14}$$

where f_i = probability density function (pdf) of the strength of the i th element ($i=1,2$). For the limiting cases of brittle and plastic bundles, Eq. (14) becomes equivalent to Daniels' (1945) formulation for the brittle bundle and the convolution integral for the plastic bundle becomes equivalent to the formulation in Bažant and Pang (2007).

Now we assume that the strength of each fiber has a cdf with a power-law tail, i.e. $P_i(\sigma) = (\sigma/s_0)^{p_i}$. Considering the transformation: $y_i = \sigma_i/S$, we can write the cdf of bundle strength as:

$$G_2(S) = 2S^{(p_1 + p_2)} \int_{\Omega_2(1)} \frac{p_1 p_2}{s_0^{p_1 + p_2}} y_1^{p_1 - 1} y_2^{p_2 - 1} dy_1 dy_2 \tag{15}$$

where $\Omega_2(1)$ denotes the feasible region $\Omega_2(S)$ normalized by S . Since the integral in Eq. (15) results in a constant, the cdf of bundle strength has a power-law tail whose exponent is $p_1 + p_2$.

By induction, the foregoing analysis is then easily extended to a bundle with n_b fibers, for which the cdf of average bundle strength can be written as:

$$G_{n_b}(S) = n_b! \int_{\Omega_{n_b}(S)} \prod_{i=1}^{n_b} f_i(\sigma_i) d\sigma_1 d\sigma_2, \dots, d\sigma_{n_b} \tag{16}$$

$$G_{n_b}(S) = n_b! S^{p_1 + p_2 + \dots + p_{n_b}} \int_{\Omega_{n_b}(1)} \left(\prod_{i=1}^{n_b} \frac{p_i y_i^{p_i-1}}{S_0^{p_i}} \right) dy_1 dy_2, \dots, dy_{n_b} \quad (17)$$

Here $\Omega_{n_b}(S)$ is the feasible region of stresses in all the fibers, which defines an n_b -dimensional space, and $\Omega_{n_b}(1)$ is the corresponding feasible region of normalized stresses, $y_i = \sigma_i/S$. Q.E.D.

Thus, regardless of the post-peak slope E_t of each fiber, it is proven that, if each fiber strength has a cdf with a power-law tail, then the cdf of bundle strength will also have a power-law tail, and the power-law exponent will be the sum of the exponents of the power-law tails of the cdf of all the fibers in the bundle.

In Bažant and Pang (2006, 2007), the reach of power-law tail of the strength cdf of softening bundle was shown to be another important consideration. It can be calculated from Eq. (16). However, for large bundles, it is difficult to handle the integral in Eq. (16) numerically. Previous studies (Bažant and Pang, 2006, 2007) showed that the reach of power-law tail decreases with the number n_b of elements rapidly as $P_{tn_b} \sim (P_{t1}/n_b)^{n_b} - (P_{t1}/3n_b)^{n_b}$ for brittle bundles, or $(P_{t1}/n_b)^{n_b}$ for plastic bundles, where P_{t1} =failure probability at the terminal point of the power-law tail of one fiber. Since the behavior of softening bundles is bounded between these two extreme cases, the rate of shortening of power-law tail of strength cdf of the softening bundles must lie between them; i.e.

$$P_{tn_b} \sim (P_{t1}/n_b)^{n_b} - (P_{t1}/3n_b)^{n_b} \quad (18)$$

The series coupling, by contrast, was shown to extend the power-law tail (Bažant and Pang, 2007)—roughly by one order of magnitude for each ten-fold increase in the number links.

The foregoing framework can be applied to a bundle with fibers whose strength has any kind of cdf. Recently, many papers (Duffy et al., 1993; Gross, 1996; Stanley and Inanc, 1985) assumed that the cdf of strength has a non-zero threshold σ_i . So, consider that, for each fiber, $P_i(\sigma) \sim \langle \sigma - \sigma_i \rangle^{p_i}$. Then the cdf of average strength of a bundle of n_b fibers with bilinear stress–strain relations will have the tail:

$$P_{tn_b} \sim \langle \sigma - \sigma_0 \rangle^{p_1 + p_2 + \dots + p_k} \prod_{i=k+1}^{n_b} \langle \sigma - \sigma'_i \rangle^{p_i} \quad (19)$$

where $\sigma_0 = \sum_{i=1}^k A_i \sigma_i$ and $\sigma'_i = B_i \sigma_i$; A_i , B_i and k are constants which depend on the softening stiffness of the fibers. Obviously, when $\sigma_i = 0, (i = 1, \dots, n_b)$, Eq. (19) indicates additivity of the power-law tail exponents. For perfectly plastic bundles, the strength cdf of the bundle has one threshold, i.e. $P_{tn_b} \sim \langle \sigma - \sigma_0 \rangle^{p_1 + p_2 + \dots + p_{n_b}}$. For perfectly brittle bundles, the strength cdf of bundle has n_b thresholds, i.e. $P_{tn_b} \sim \prod_{i=1}^{n_b} \langle \sigma - \sigma'_i \rangle^{p_i}$. Hence, for general bundles with softening behavior, the strength cdf will have multiple thresholds.

Another important asymptotic property is the type of cdf of strength of large bundles. For brittle bundles, Daniels derived a recursive equation for the strength cdf of a bundle with n_b fibers and showed that the strength cdf of large bundles approaches the Gaussian (or normal) distribution (Daniels, 1945). This property is obviously also true for plastic bundles; it is a natural consequence of the central limit theorem since the strength of a plastic bundle is the sum of strengths of all the fibers.

To prove that this asymptotic property applies to all the bundles regardless of their post-peak softening stiffness E_t , consider a bundle of $3n_b$ fibers (or elements). The load carried by the bundle is given by $F(\epsilon) = \max[\sum_{j=2}^{3n_b+1} \sigma_j(\epsilon)A_f]$, where A_f =cross section area of each fiber, σ_j =stress in j th element, and ϵ =strain in each element. The mechanical behavior of each fiber can be random and independent. This causes randomness of the critical value ϵ^* of strain ϵ , at which F reaches its maximum. We label the $3n_b$ elements by $j=2, 3, 4, \dots, 3n_b+1$, arrange them according to their breaking order, and divide them into two groups with different load resultants:

$$F_A(\epsilon) = \sum_{i=3k} \sigma_i(\epsilon)A_f, F_B(\epsilon) = \sum_{i=3k \pm 1} \sigma_i(\epsilon)A_f \quad (k = 1, 2, 3, \dots, n_b) \quad (20)$$

The maximum load carried by the bundle is

$$F_{max} = F_A(\epsilon^*) + F_B(\epsilon^*) \quad (21)$$

If n is large, then the stress distribution over the elements in these two groups will be similar to that in the bundle (Fig. 5). It follows that the cdf of F_{max} (i.e. the strength of bundle) and the cdf of $F_A(\epsilon^*)$ and $F_B(\epsilon^*)$ are of the same type. Then, to satisfy Eq. (21), the only possible distribution of F_{max} is the Gaussian distribution (note that this argument would not apply if the we divided the bundle into two groups with the same number of elements and the same resultant for large n_b).

However, the rate of convergence depends on the post-peak softening stiffness E_t of the elements. The slowest convergence, of the order of $O(n_b^{-1/3}(\log n_b)^2)$ (Smith, 1982), occurs for brittle bundles. The fastest convergence, of the order of $O(n_b^{-1/2})$, occurs for plastic bundles (Bažant and Pang, 2007).

4.3. Hierarchical model for strength distribution of one RVE

At low probabilities, the strength cdf of typical quasibrittle materials asymptotically terminates with a power-law of exponent m (i.e. Weibull modulus), which is generally observed to be between 15 and 60. But for the nano-scale, the cdf tail was found to have the exponent of 2. How to explain such a drastic increase of exponent? Let us now briefly review the

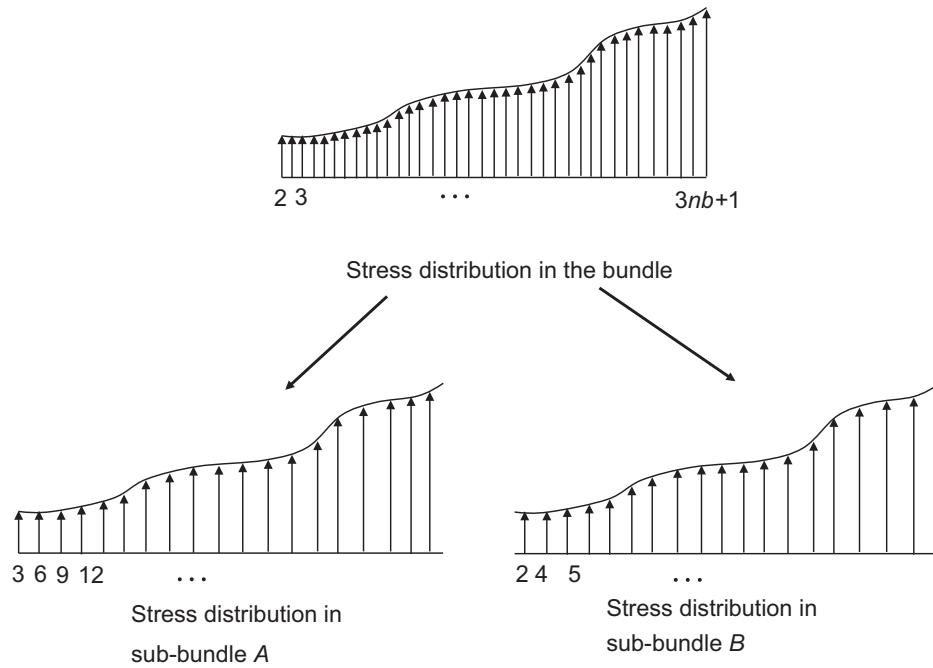


Fig. 5. Stress distribution of fibers in a large bundle.

previous work (Bažant and Pang, 2006, 2007) which showed that the explanation can be given in terms of multiscale transitions.

Aside from the exponent, we must also consider the reach of the power-law tail. Based on studies of experimental strength histograms and the mean size effect for typical quasibrittle materials, it was shown (Bažant and Pang, 2007) that the cdf of RVE strength must have a Weibullian (or power-law) tail extending up to $P_f = 10^{-4} - 10^{-3}$.

Why cannot the extent of the power-law tail be $\leq 10^{-5}$? If it were, then the histograms of strength tests of structures with $> 10^4$ RVEs would not be predominantly Weibullian and the mean size effect would not approach a power-law, contrary to observations (Bažant and Pang, 2007). And why cannot the extent of the power-law tail be $> 10^{-3}$? If it were, then the histograms of strength tests of structures with $< 10^3$ RVEs would not yield the observed kinked deviations from the Weibull cdf and the mean size effect would not deviate from the power-law at the observed locations.

From these tail properties, it has been concluded (Bažant and Pang, 2006, 2007) that the RVE must be statistically represented by a hierarchy of series and parallel connections shown in Fig. 3c, which consists of a bundle of only two long sub-chains, each of which consists of sub-bundles of two sub-sub-chains, each of which consists of sub-sub-bundles, etc., until the nano-scale element is reached (Bažant and Pang, 2006, 2007). In this model, the parallel connections involve no more than two elements (except at nano-scale where three can be coupled in parallel), provided that each chain consists of about 10–20 elements (which seems to reflect damage localization patterns). If there were more elements coupled in parallel, the reach of the power-law tail would be shorter than the aforementioned limit of 10^{-4} (unless the chains had hundreds of elements).

In the hierarchical model, the strength of each element is assumed to be statistically independent, although statistical correlations must in fact exist. However, a certain statistical correlation is indirectly introduced by the parallel coupling (or bundle model), through its load distribution rules. The lack of an explicit statistical correlation cannot be a serious problem because the choice of the rule of load distribution in the bundle model is found to have a negligible effect on the functional form of the cdf of strength of the hierarchical model.

4.4. Calculation of the cdf of strength of one RVE

To figure out the type of cdf of strength of one RVE, one must specify the mechanical behavior of the bundles in the hierarchical model. Although different assumptions yield about the same results, here the following assumption is made: For the bundles at the lowest scale, three types of stress–strain behaviors, i.e. brittle, softening, and plastic, are considered for each element. Bundles at higher scales have brittle behavior.

The strength cdf needs to be calculated in a hierarchical manner. At the lowest scale, each element represents a nano-structure whose strength cdf has a power-law tail. One can then calculate the strength cdf of the sub-chain that connects these elements. At the next scale, the strength cdf of the sub-bundle, which consists these sub-chains, can be calculated based on the strength cdf of these sub-chains. In this manner, one could move up through the scales, and finally obtain the strength cdf of one RVE.

As an example, we calculate the strength cdf of the hierarchical model shown in Fig. 3c. Every element in the hierarchical model represents one nano-scale element, whose strength cdf is a power-law (Eq. (7)). Three cases are considered:

- (1) Each element has an elastic–brittle behavior.
- (2) Each element exhibits a linear post-peak softening, where the softening modulus magnitude is 40% of the elastic modulus of the element.
- (3) Each element has an elastic–plastic behavior.

Fig. 6a shows the calculated strength cdf of the hierarchical model for these three cases on the Weibull scale. For all these cases, the lower portion of the calculated strength cdf is a straight line on the Weibull plot, which indicates that it follows the Weibull distribution (i.e., the tail is a power-law). This property is, of course, expected since, in the chain and bundle models, the power-law tail of the cdf of strength is indestructible.

For the upper portion, the strength cdf deviates from the straight line in Fig. 6a. Among the three cases considered, case 1 (i.e., elements with brittle behavior) gives the shortest Weibull tail, which terminates at the probability of about 0.7×10^{-4} , while case 3 (elements with plastic behavior) gives the longest Weibull tail, which terminates at the probability of about 0.7×10^{-3} .

To identify the type of distribution for the upper portion of the cdf, the cdf's of strengths are plotted on the normal probability paper; see Fig. 6 b–d where the upper portion of the cdf is seen to be fitted quite closely by a straight line. The straight line is not too close for case 1 and for $P_f \geq 0.8$. For the cases 2 and 3, the straight line fits quite closely, with a slight deviation occurring only for $P_f \geq 0.99$. This means that, the upper portion of the strength cdf can be approximated as the Gaussian distribution. Since, for real quasibrittle structures, the nano-element is expected to have a softening behavior (Fig. 2b), the strength cdf of one RVE should be close to case 2.

In general, the strength distribution of one RVE can be approximately described by a Gaussian distribution with a Weibull tail grafted on the left at a point of the probability of about 10^{-4} – 10^{-3} . The grafted cdf of strength of one RVE may

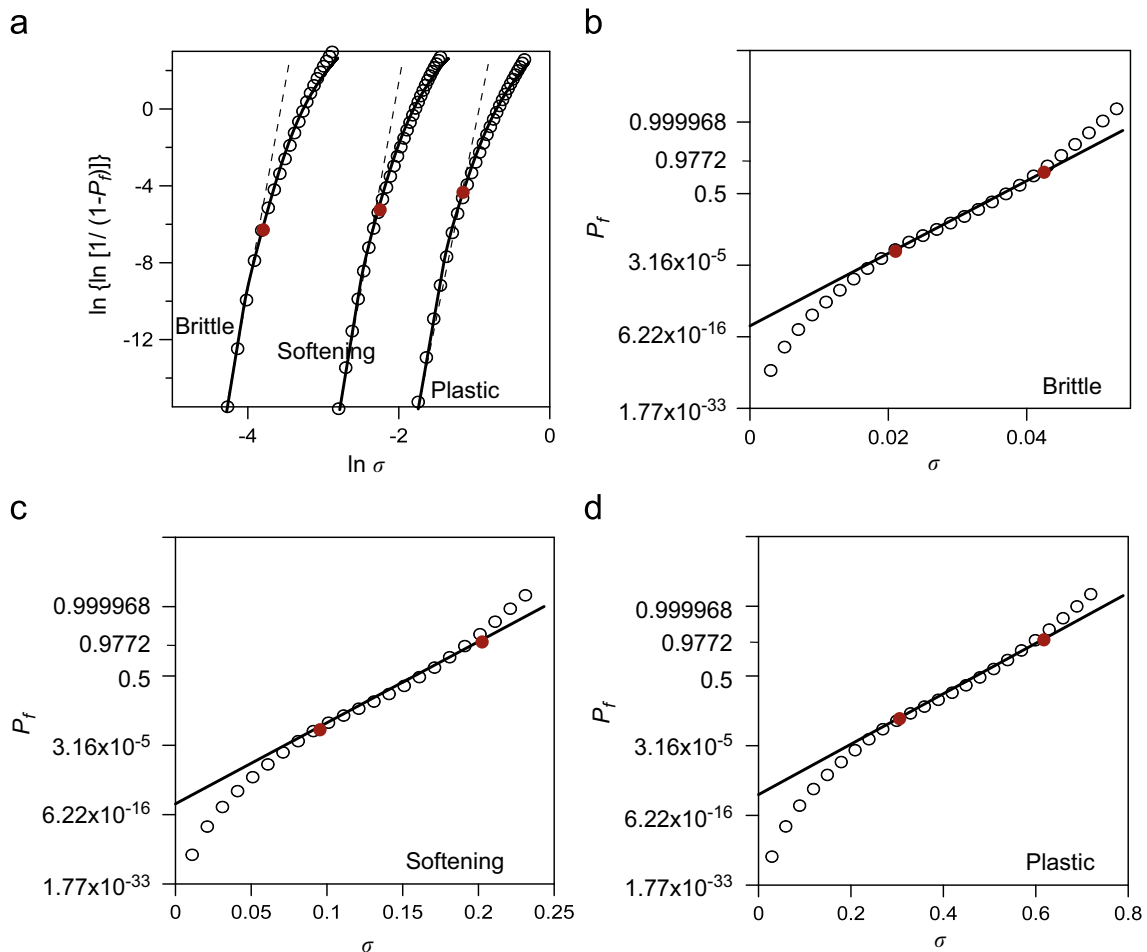


Fig. 6. (a) Calculated strength cdf of one RVE on the Weibull scale. (b)–(d) Calculated strength cdf of one RVE on the normal distribution paper.

be mathematically described as (Bažant and Pang, 2006, 2007):

$$P_1(\sigma_N) = 1 - e^{-(\sigma_N/s_0)^m} \quad (\sigma_N \leq \sigma_{gr}) \quad (22)$$

$$P_1(\sigma_N) = P_{gr} + \frac{r_f}{\delta_G \sqrt{2\pi}} \int_{\sigma_{gr}}^{\sigma_N} e^{-(\sigma' - \mu_G)^2 / 2\delta_G^2} d\sigma' \quad (\sigma_N > \sigma_{gr}) \quad (23)$$

Here σ_N = nominal strength, which is a maximum load parameter of the dimension of stress, in general defined as $\sigma_N = c_n P_{max} / bD$ or $c_n P_{max} / D^2$ for two- or three-dimensional scaling P_{max} = maximum load of the structure or parameter of load system; c_n = parameter chosen such that σ_N represent the maximum principal stress in the structure, b = structure thickness in the third dimension, D = characteristic structure dimension or size. Furthermore, m (Weibull modulus) and s_0 are the shape and scale parameters of the Weibull tail, and μ_G and δ_G are the mean and standard deviation of the Gaussian core if considered extended to $-\infty$; r_f is a scaling parameter required to normalize the grafted cdf such that $P_1(\infty) = 1$, and P_{gr} = grafting probability = $1 - \exp[-(\sigma_{gr}/s_0)^m]$. Finally, continuity of the probability density function at the grafting point requires that $(dP_1/d\sigma_N)|_{\sigma_{gr}^+} = (dP_1/d\sigma_N)|_{\sigma_{gr}^-}$.

Note that, in the framework of present theory, P_{gr} depends on the failure behavior of sub-scale structures, from micro to nano, which is statistically represented by the hierarchical model. One cannot determine P_{gr} directly from the hierarchical model since it is essentially a qualitative statistical model which only yields the functional form of the cdf of strength of one RVE. Therefore, P_{gr} must be calibrated from macro-scale tests. The simplest is the size effect test of the mean structural strength, where P_{gr} can be identified from the location where the size effect curve deviates from the classical Weibull size effect (Bažant and Pang, 2007).

4.5. Probability distribution of structure strength

Consideration is here limited to the broad class of structures having the so-called positive geometry (which is a geometry characterized by $\partial K_I / \partial a > 0$, K_I = stress intensity factor, a = crack length). Such structures fail under controlled load as soon as a macro-crack initiates from one RVE. Therefore, their macroscopic failure behavior follows the weakest-link model in which each link corresponds to one RVE if the structure is subdivided into many RVEs (Fig. 3a). The definition of RVE is necessarily different from the homogenization theory: The RVE is the smallest material volume whose failure causes the whole structure to fail (Bažant and Pang, 2006, 2007).

The survival probability of the structure is the joint probability of survival of all the RVEs, numbered as $i = 1, \dots, N$. Therefore, under the assumption of statistical independence of the random strengths of the RVEs, $1 - P_f = \prod_{i=1}^N [1 - P_1]_i$ or

$$P_f(\sigma_N) = 1 - \prod_{i=1}^N [1 - P_1(\langle s(\mathbf{x}_i) \rangle \sigma_N)] \quad \langle \mathbf{x} \rangle = \max(\mathbf{x}, 0) \quad (24)$$

where $P_1(\sigma)$ = cdf of strength of one RVE, P_f = failure probability of the structure, σ_N = nominal strength of the structure, $\sigma_i(\mathbf{x}_i) = \sigma_N s(\mathbf{x}_i)$ = maximum principal stress at the center of i th RVE with the coordinate \mathbf{x}_i , and $s(\mathbf{x}_i)$ = field of dimensionless maximum principal stress in the structure. Here it is assumed that the principal stresses in each RVE are fully statistically correlated to the maximum one, which seems realistic. If they were uncorrelated, each principal stress would require one element in the chain.

Eq. (24) is further contingent upon the hypothesis that the strengths of different RVEs are statistically uncorrelated. This is certainly a simplification, though probably quite realistic. Strictly speaking, the strength field within the structure is an autocorrelated random process. But previous studies of random particle-lattice model (Grassl and Bažant, 2009) showed that the autocorrelation length is approximately equal to size l_0 of the RVE. So, the strength correlations, though existing, should be negligible for distances larger than the RVE size (anyway, even if the maximum autocorrelation length were larger than the RVE, then the RVE size could be enlarged to this length and the uncorrelated weakest-link model could still be used on the larger scale).

Eq. (24) directly implies the size effect on structure strength in terms of number N . For small-size structures (small N), the cdf of strength is predominantly Gaussian, which corresponds to the case of quasi-plastic behavior. This implies that the failure of one RVE is caused by distributed cracking instead of localization of damage. When the structure size increases but is not too large, the core of the cdf of structure strength is still predominantly governed by the lower part of the Gaussian core of the strength cdf of one RVE lying close to the grafting point but above it. According to the stability postulate used by Fisher and Tippett (1928) (or a renormalization group analysis Bazant, 2000; van der Hofstad and Redig, 2006), the core of cdf of structural strength should thus approach the Gumbel (or Fisher–Tippett–Gumbel) distribution, in the sense of intermediate asymptotics (Barenblatt, 1978).

However, for sufficiently large structures (large N), what matters for P_f is the tail of the strength cdf of one RVE, i.e. $P_1(\sigma) = (\sigma/s_0)^m$. Therefore, Eq. (24) can be re-written as:

$$P_f(\sigma_N) = 1 - \exp \left[- \left(\int_V \langle s(\mathbf{x}_i) \rangle^m \frac{dV(\mathbf{x})}{V_0} \right) \left(\frac{\sigma_N}{s_0} \right)^m \right] \quad (25)$$

where $V_0 = l_0^3$ = volume of one RVE, and l_0 = size of one RVE, which is a material property (material length).

As shown in Eq. (25), the cdf of strength of large-size structures tends to the Weibull distribution, which corresponds to the case of perfectly brittle behavior. Here, it is convenient to define $N_{eq,\sigma} = \int_V \langle s(\mathbf{x}_i) \rangle^m dV(\mathbf{x})/V_0$. $N_{eq,\sigma}$ represents the equivalent number of RVEs, which is the number of RVEs under uniform stress for which σ_N gives the same cdf of structure strength as does Eq. (24) under the assumption that the strength cdf follows the Weibull distribution (Bažant and Pang, 2006, 2007).

Therefore, $N_{eq,\sigma}$ depends on the structure size relative to the RVE size, V/V_0 , as well as the stress field $s(\mathbf{x}_i)$. For the grafted distribution, $N_{eq,\sigma}$ is expected to be a function of both σ_N and stress field.

The strength distribution of one RVE has sometimes been assumed as Weibullian. However, it is simple to prove that this is impossible. Consider that the strength of a presumed “RVE” has the Weibull distribution. But this distribution can arise only from the weakest-link model for a chain, described by Eq. (24). But in a chain, the fracture must always localize into one failing link. So the presumed “RVE” cannot be the true RVE. Rather the failing link must represent the true RVE, which is the smallest material volume whose failure triggers the failure of the entire structure.

Using the weakest-link model (Eq. (24)) to calculate the strength cdf of structure, one needs to subdivide the structure into equal-size elements, having approximately the same size as the RVE. However, such a subdivision is possible only for rectangular boundaries. For structures with general geometry, a nonlocal boundary layer (NBL) approach has been recently proposed to deal with arbitrary boundaries and at the same time avoid the subjectivity of subdivision (Bažant et al., 2010).

In this approach, a boundary layer of thickness $h_0 \approx l_0$ along all the surfaces is separated from the structure. For the boundary layer, one only needs to evaluate the stress for the points of the middle surface Ω_M of the layer. For the interior domain V_I , the conventional nonlocal continuum approach (Bažant and Jirásek, 2002) can be adopted. The original weakest-link model may be rewritten as:

$$\ln[1 - P_f(\sigma_N)] = h_0 \int_{\Omega_M} \ln\{1 - P_1[\sigma(\mathbf{x}_M)]\} \frac{d\Omega(\mathbf{x}_M)}{V_0} + \int_{V_I} \ln\{1 - P_1[\bar{\sigma}(\mathbf{x})]\} \frac{dV(\mathbf{x})}{V_0} \quad (26)$$

For very large structures, the boundary layer becomes very thin compared to the structure size (i.e. the first integral becomes negligible), the nonlocal stress in the domain becomes the local stress, and Eq. (26) eventually leads to Eq. (25). Note that, in the original weakest-link model, the element size is roughly equal to the auto-correlation length and the element strength is essentially independent of the other elements. In the nonlocal model, the element can be smaller than the auto-correlation length and the spatial correlation is represented through the nonlocal averaging (Breyse and Fokwa, 1992).

5. Formulation of lifetime distribution

To ensure a sufficiently small probability that a structure would not achieve its specified lifetime, the cdf of creep lifetime must be determined. When a long lifetime is required, it is often impossible or unacceptable to obtain the histogram of lifetime by waiting until the structure fails. Recently it was proposed (Bažant and Le, 2009; Le et al., 2009) that how the cdf of lifetime of quasibrittle structures could be predicted theoretically from experiments of much shorter durations. Here we review this approach in a unified context and present in detail its physical justification, which consists of fracture kinetics and its multiscale transition.

Attention is here limited to the simplest loading history—the creep rupture case, although a generalization to other monotonic loading histories is straightforward. An extension to fatigue lifetime is presented in Part II which follows.

5.1. Crack growth law and its physical justification

Consider again the nano-element in which the frequency of each crack jump is given by Eq. (5). Since the propagation of the nano-crack is governed by stress-induced drift, the velocity of nano-crack propagation is simply given by:

$$\dot{a}_{nano} = \delta_a f_1 = v_1 e^{-Q_0/kT} K_a^2 \quad (27)$$

where $\dot{a}_{nano} = da_{nano}/dt$, $v_1 = \delta_a^2 (\gamma_1 \alpha l_a) / E_1 h = \text{constant}$, and $K_a = \text{stress intensity factor of the nano-element}$, which is given by Eq. (1) and is proportional to the remote stress $\tau = c\sigma$, and thus also to σ .

At macro-scale, when the crack starts to propagate, there will be a FPZ at the tip of the crack. In this FPZ, there are N_a active nano-cracks. To link the fracture kinetics of macro- and nano-cracks, we follow Bažant et al. (2009, Eq. (9)) in imposing the condition of equality of energy dissipation rates, which states that the rate of energy dissipation of the macro-crack must be equal to the sum of energy dissipation rates of all the active nano-cracks a_i ($i = 1, \dots, N_a$) in the FPZ of the macro-crack (this condition, of course, ignores dissipations by frictional slips within the FPZs, but since this additional dissipation should be roughly proportional to the fracturing dissipations, the argument is not affected qualitatively). This condition reads:

$$G\dot{a} = \sum_{i=1}^{N_a} G_i \dot{a}_i \quad (28)$$

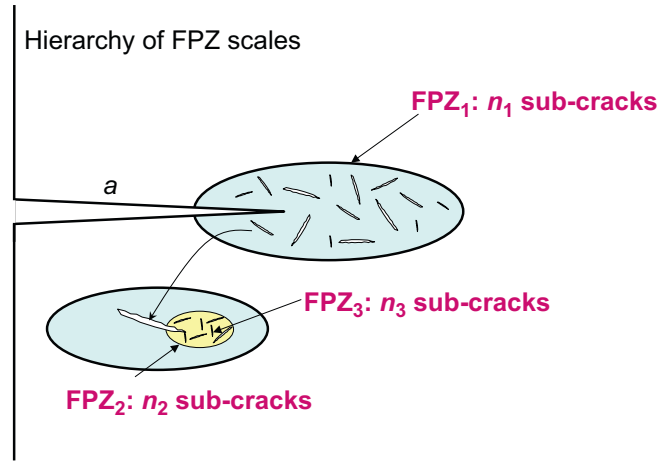


Fig. 7. Hierarchy of fracture process zone scales.

where \mathcal{G} and \mathcal{G}_i denote the energy release rate functions for the macro-crack a and nano-crack a_i , respectively. By substituting Eq. (27) for \dot{a}_i and expressing the energy release rate function in terms of the stress intensity factor, one has:

$$\dot{a} = e^{-Q_0/kT} \phi(K) \quad \text{where} \quad \phi(K) = \sum_{i=1}^{N_a} \frac{v_i K_i^4 E}{K^2 E_i} \quad (29)$$

where K_i =stress intensity factors of nano-cracks a_i within the nano-elements in the FPZ, E_i =elastic modulus of each nano-element, and $v_i = \delta_a^2(\gamma_1 \alpha_i l_i)/E_i h$. K_i may be assumed to be linearly proportional to the macro-scale stress σ as well as the nano-scale remote stress τ . So, one may set $K_i = \omega_i K$ where ω_i =constants. Hence, $\phi(K)$ can be re-written as:

$$\phi(K) = K^2 \sum_{i=1}^{N_a} \frac{v_i \omega_i^4 E}{E_i} \quad (30)$$

The number of active nano-cracks in the FPZ of the macro-crack may be added up through the hierarchy of FPZ scales (Fig. 7): The FPZ of the macro-crack contains q_1 meso-cracks, each of which has a meso-FPZ at its tip. Each of the meso-FPZ contains q_2 micro-cracks, each of which has at its tip a micro-FPZ with q_3 sub-micro-cracks, ..., and so forth, all the way down to the nano-scale. If there are s different scales between the macro-scale and nano-scale, then the total number of nano-cracks in the macro-FPZ is simply given by:

$$N_a = q_1 q_2 \cdots q_s \quad (31)$$

On scale μ , the number q_μ of activated cracks within the FPZ must be a function of the relative stress intensity factor K/K_μ , i.e. $q_\mu = q_\mu(K/K_\mu)$, where K_μ = typical critical value of K for cracks of scale μ .

It appears plausible that function $q_\mu(K/K_\mu)$ increases rapidly with increasing K/K_μ while the ratios in $\phi(K)$ change far less. Therefore, one may replace E_i , ω_i , and v_i by some effective mean values E_a , ω_a , and v_a :

$$\phi(K) = v_a \omega_a^4 (E/E_a) K^2 \prod_{\mu=1}^s q_\mu(K/K_\mu) \quad (32)$$

It may be expected that there is no characteristic value of K at which the behavior of function $q_\mu(K/K_\mu)$ would qualitatively change, and so function $q_\mu(K/K_\mu)$ should be self-similar. The only self-similar functions are power laws, i.e. $q_\mu(K/K_\mu) = (K/K_\mu)^r$ (Barenblatt, 2003). It follows that function $\phi(K)$ should also be a power law:

$$\phi(K) = \frac{v_a \omega_a^4 E}{E_a \left(\prod_{\mu} K_\mu^r \right)} K^{rs+2} \quad (33)$$

Substituting Eq. (33) into Eq. (29) and setting $rs+2 = n$, one has:

$$\dot{a} = A e^{-Q_0/kT} K^n \quad (34)$$

where $A = (v_a \omega_a^4 E)/E_a (\prod_{\mu} K_\mu^r)$. Eq. (34) is the well-known power law for the rate of creep crack growth, which was proposed in Evans (1972), Evans and Fu (1984), Thouless et al. (1983) and used widely as an empirical law (Bažant and Prat, 1988; Bažant and Planas, 1998; Munz and Fett, 1999; Lohbauer et al., 2002; Fett and Munz, 1991). The foregoing analysis providing the theoretical justification of the power law for crack growth rate was recently sketched in Bažant and Le (2009), Le et al. (2009). Note that Eq. (34) has the same form as Eq. (27) except for two aspects:

1. While v_1 in Eq. (27) depends on the relative nano-crack length α , parameter A in Eq. (34) is a constant. The reason is that the FPZ does not change significantly as the macro-crack propagates, which is an essential concept leading to the

constancy of the fracture energy G_f . Therefore, all the different relative nano-crack lengths α_i in the nano-elements of a FPZ must average out to give a constant A , as mathematically described by Eq. (32).

- The power-law exponent for the nano-crack growth rate is 2 while the power-law exponent for the macro-crack growth rate is about 10–30, as observed in experiments (Munz and Fett, 1999; Kawakubo, 1995). This is because, for a certain applied stress and structural geometry, the number of activated nano-cracks rapidly increases on passing to higher scales with larger FPZs, as implied by the increasing value of s in Eq. (31).

The present analysis proves that the growth rate of nano-cracks follows a power-law with an exponent equal to 2, and it shows that, under a certain plausible assumption (self-similarity of function $q_\mu(K)$), the power-law form of crack growth rate at macro-scale can be physically justified. Nevertheless, the foregoing analysis does not present a mathematical proof of the power-law for macro-crack growth rate. The experimental validation is essential.

5.2. Distribution of structural lifetime

The crack growth rate is a crucial aspect of time-dependent failure, which relates the strength and lifetime of one RVE. Consider the load history in the creep-rupture test (or lifetime test), in which the load F is rapidly raised to some value F_0 , then is held constant for various lengths of time, t_1 , and finally is rapidly increased to some random value F_1 at which the failure occurs (Fig. 8a). When $t_1 \rightarrow \lambda = \text{lifetime}$, we have $F_1 \rightarrow F_0$. For $t_1 \rightarrow 0$, $F_1 \rightarrow F_{\max}$, which is the strength test. In between there must be a continuous transition, and so the statistics of failure load F_{\max} must be related to the statistics of lifetime λ .

Now consider one RVE which contains a dominant subcritical crack a_R with initial length a_0 . Based on the equivalent linear elastic fracture mechanics, this subcritical crack is considered to have its tip at the center of the FPZ, thus representing the effect of distributed damage in the RVE. Under a certain loading history, this crack grows to its critical length a_c , at which the RVE fails. The growth rate of the subcritical crack can be described by Eq. (34), in which one may further express the stress intensity factor as:

$$K_R = \sigma \sqrt{l_0} k_R(\alpha) \tag{35}$$

where σ is a load parameter of the stress dimension, called the nominal stress, and is defined as $\sigma = F/l_0^2$; $l_0 = \text{RVE size}$, $\alpha = a_R/l_0$ relative crack length.

For the case of strength test, the load is linearly increased till the failure of RVE with loading rate r (i.e. $F=rt$); Fig. 8b. Denoting $\sigma_N = F_{\max}/l_0^2$ and integrating Eq. (34), one obtains the nominal strength σ_N :

$$\sigma_N^{n+1} = r(n+1)e^{Q_0/kT} \int_{\alpha_0}^{\alpha_c} \frac{d\alpha}{Al_0^{(n-2)/2} k_R^n(\alpha)} \tag{36}$$

For the case of lifetime test (Fig. 8b), the load is rapidly increased to F_0 , which is smaller than the load capacity of the RVE, and the lifetime of interest is typically far longer than the duration of laboratory strength tests. Therefore, the initial rapidly increasing portion of the load history makes a negligible contribution compared to the overall structural lifetime. By letting the applied nominal stress to be $\sigma_0 = F_0/l_0^2$ and integrating Eq. (34) for the constant σ_0 , one obtains the lifetime, λ :

$$\sigma_0^n \lambda = e^{Q_0/kT} \int_{\alpha_0}^{\alpha_c} \frac{d\alpha}{Al_0^{(n-2)/2} k_R^n(\alpha)} \tag{37}$$

Comparison of Eqs. (36) and (37) leads to a surprisingly simple relationship between σ_N and λ :

$$\sigma_N = \beta \sigma_0^{n/(n+1)} \lambda^{1/(n+1)} \tag{38}$$

where $\beta = [r(n+1)]^{1/(n+1)} = \text{constant}$.

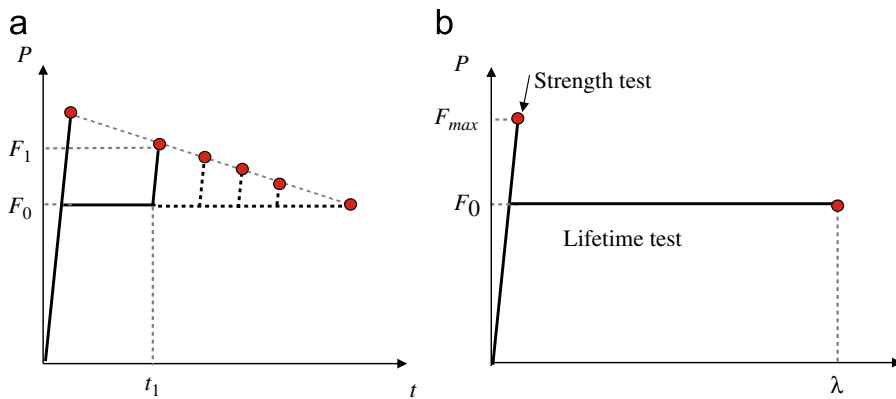


Fig. 8. Loading histories of strength and lifetime tests.

Note that although the power-law for creep crack growth has been derived as the mean behavior, it is now used to relate the randomness of strength and of lifetime in one RVE. This is certainly a simplification. Eqs. (36) and (37) indicate that the randomness of strength and lifetime of RVE is caused by the geometrical randomness of the dominant subcritical crack. In the framework of equivalent linear elastic fracture mechanics, this reflects the randomness of micro-structures and local fracture energy. This randomness can be captured by the random particle model (Grassl and Bažant, 2009).

Since the distribution of RVE strength is given by Eqs. (22) and (23), the lifetime distribution of one RVE can easily be obtained by substituting Eq. (38) for σ_N in Eqs. (22) and (23):

$$\text{for } \lambda < \lambda_{gr} : P_1(\lambda) = 1 - \exp[-(\lambda/s_\lambda)^{\bar{m}}]; \tag{39}$$

$$\text{for } \lambda \geq \lambda_{gr} : P_1(\lambda) = P_{gr} + \frac{r_f}{\delta_G \sqrt{2\pi}} \int_{\gamma \lambda_{gr}^{1/(n+1)}}^{\gamma \lambda^{1/(n+1)}} e^{-(\lambda' - \mu_G)^2 / 2\delta_G^2} d\lambda' \tag{40}$$

where $\gamma = \beta \sigma_0^{n/(n+1)} \lambda_{gr} = \beta^{-1} \sigma_0^{-n} \sigma_{N,gr}^{n+1}$, $s_\lambda = s_0^{n+1} \beta^{-(n+1)} \sigma_0^{-n}$, and $\bar{m} = m/(n+1)$.

Similar to the strength distribution of one RVE, the lifetime cdf of one RVE, too, has a Weibull tail (power-law tail). The grafting probability P_{gr} for the lifetime distribution of one RVE is the same as that for the strength cdf of one RVE. However, as Eq. (40) suggests, the rest of the lifetime cdf of one RVE does not exactly follow the Gaussian distribution.

Since the lifetime of a chain is the shortest lifetime of its links, the weakest-link model may again be used to compute the lifetime cdf of a structure consisting of any number of RVEs. Similar to the definition of nominal strength, here we can define the nominal stress, $\sigma_0 = c_n P/bD$ or $c_n P/D^2$ for two- or three-dimensional scaling, and P is the applied load. By the joint probability theorem, the lifetime distribution of structure can be expressed as:

$$P_f(\sigma_0, \lambda) = 1 - \prod_{i=1}^N \{1 - P_1[\langle \sigma_0 s(\mathbf{x}_i) \rangle, \lambda]\} \tag{41}$$

where $s(\mathbf{x}) =$ dimensionless stress field. Similar to the chain model for the cdf of the structural strength, the lifetime of the i -th RVE is here assumed to be governed by the maximum average principal stress $\sigma_0 s(\mathbf{x}_i)$ within the RVE, which is valid provided that the other principal stresses are fully statistically correlated. Similar to the calculation of strength cdf, the lifetime cdf of a structure of any geometry can be calculated by using the nonlocal boundary layer model (Bažant and Le, 2009).

As shown in Eq. (40), the core of lifetime cdf of one RVE, denoted as $\Phi_u(\lambda)$, is a Gaussian cdf transformed by the power-law for crack growth, i.e., is such that the lifetime power $\xi = (r/\kappa)^\kappa \sigma_0^{1-\kappa} \lambda^\kappa$ ($\kappa = 1/(n+1)$) would have the Gaussian distribution;

$$\Phi_u = \int_{-\infty}^{\xi} (2\pi s_u^2)^{-1/2} e^{-(t' - \mu_u)^2 / 2s_u^2} dt' \tag{42}$$

When κ is very small, the foregoing transformation can be approximated by the logarithmic transformation for the region of λ that is near some prescribed lifetime λ_0 (Ibnabdeljalil and Phoenix, 1995):

$$\xi = (r/\kappa)^\kappa \sigma_0^{1-\kappa} \lambda_0^\kappa [\kappa \ln(\lambda/\lambda_0) + 1] \tag{43}$$

This approximation rests on the fact that, when κ is small enough, $(\lambda/\lambda_0)^\kappa$ is close to 1. Therefore, $\ln[(\lambda/\lambda_0)^\kappa] \approx (\lambda/\lambda_0)^\kappa - 1$ and $\lambda_0^\kappa [\kappa \ln(\lambda/\lambda_0) + 1] \approx \lambda^\kappa$.

To ensure the continuity of both cdf and pdf at the grafting point, we choose $\lambda_0 = \lambda_{gr}$. From Eqs. (42) and (43), one finds that the core of lifetime distribution can be approximated as the lognormal distribution for a range of λ that is near λ_{gr} . This range is typically very narrow because the lifetime is widely scattered and $(\lambda/\lambda_{gr})^\kappa$ for the main part of the core is not close to 1.

As κ decreases (or n increases), one might expect that the range of applicability of the logarithmic transformation would increase. Interestingly, this is not really the case. The reason is as follows: A larger value of n would doubtless make $(\lambda/\lambda_{gr})^\kappa$ converge to 1. At the same time, however, a larger value of n means a much broader scatter of the lifetime. This would greatly increase the ratio λ/λ_{gr} for the main part of the core, and thus it would make $(\lambda/\lambda_{gr})^\kappa$ deviate further from 1. Calculations show that these two effects cancel each other. As a result, the logarithmic transformation gives only an approximation of the core near λ_{gr} , albeit a good one, and does so even for a large value of n .

Fig. 9 shows the lifetime distributions of structures consisting of different numbers of RVEs with $n=20$ (or $\kappa = 1/21$), calculated by both the exact transformation from the power-law of crack growth and its logarithmic approximation. For the lifetime distribution of one RVE, the logarithmic approximation works well only for a very narrow range of λ . When the number of RVEs increases, the logarithmic approximation gets closer to the exact solution. This is because, if the structure is sufficiently large, the portion of the core of lifetime cdf of one RVE that matters for the lifetime cdf of the entire structure is small and is very close to the grafting lifetime. Since that part of the core can be modelled by the log-normal distribution, the deviation of lifetime cdf from the Weibull distribution can be approximated as a chain of elements with lognormal distribution provided that the structure is large enough.

For very large structures, the weakest-link model shows the lifetime cdf to be determined by the far-left tail of the lifetime cdf of one RVE: $P_1(\lambda) = (\lambda/s_\lambda)^{\bar{m}}$. An analysis similar to that for the strength cdf for large-size structures leads to the

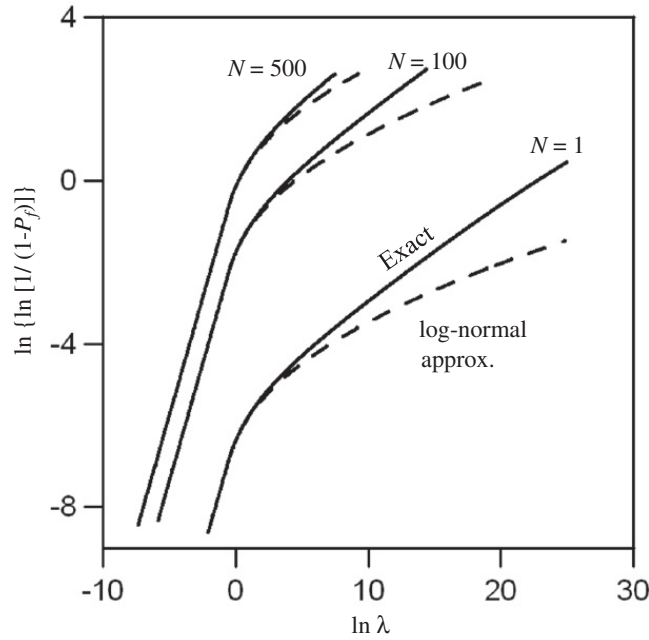


Fig. 9. Lifetime distributions calculated by Eq. (40) and its logarithmic approximation.

cdf of lifetime for large size structure:

$$P_f(\lambda) = 1 - \exp \left[- \left(\int_V \langle s(\mathbf{x}_i) \rangle^{n\bar{m}} \frac{dV(\mathbf{x})}{V_0} \right) \left(\frac{\lambda}{s_\lambda} \right)^{\bar{m}} \right] \quad (44)$$

Similar to the cdf of structural strength, the lifetime cdf of large-size structures asymptotically approaches the Weibull cdf. Here one may also define the equivalent number of RVEs for the lifetime distribution of large-size structures: $N_{eq,\lambda} = \int_V \langle s(\mathbf{x}_i) \rangle^{n\bar{m}} dV(\mathbf{x}) / V_0$. This integral physically represents the number of RVEs for which a chain of $N_{eq,\lambda}$ elements subjected to a uniform stress σ_0 would give the same lifetime cdf as Eq. (41) does.

Note that the equivalent numbers of RVEs for the strength and lifetime distributions are different. The reason is that the corresponding loading histories for strength and lifetime tests are different. However, the difference is small because $mn/(n+1) \approx m$ for large n .

The present theory yields for the Weibull moduli of strength and lifetime distributions a strikingly simple relation involving the exponent of the power-law for crack growth:

$$\bar{m} = \frac{m}{n+1} \quad (45)$$

where \bar{m} = Weibull modulus of lifetime distribution. This relation indicates an efficient way to obtain the Weibull modulus of lifetime distribution without any testing of the lifetime histograms, which is time consuming and costly, and for realistically long lifetimes virtually impossible. Aside from exponent n , one merely needs the Weibull modulus m of strength distribution, which can be most easily determined by tests of the mean size effect (Pang et al., 2008). Exponent n of power-law for crack growth can be obtained by the standard test of not too long duration, which measures the mean crack growth velocity.

Note from Eq. (45) that the Weibull modulus for lifetime is typically 10–30 times smaller than that for strength. This means that, for lifetime, the size effect must be far stronger than it is for structural strength. Regrettably, there seem to be no experiments in the literature to document it.

6. Validation by optimum fits of strength and lifetime histograms

For decades, tremendous efforts have been devoted to experimentally study the strength and lifetime distributions of structures made of quasibrittle materials such as concrete (Weibull, 1939), fiber composites (Chiao et al., 1977; Wanger et al., 1984; Wagner et al., 1986; Wagner, 1989) and industrial or dental ceramics (Weibull, 1939; Stanley and Inanc, 1985; Okabe and Hirata, 1995; Salem et al., 1996; Munz and Fett, 1999; Tinschert et al., 2000; Lohbauer et al., 2002; Santos et al., 2003). The two-parameter Weibull distribution (having zero threshold) has been widely used to fit these histograms. However, systematic deviations have been observed—first for concrete strength (Weibull, 1939), for which the sizes with N_{eq} large enough to render brittle response are unattainable, and recently for the strength of coarse-grained or toughened ceramics on the normal testing scale and fine-grained ceramics on the microscale. The present theory can fit these deviations, which serves as a partial validation of the theory. The detail fitting algorithm is outlined in Le and Bažant (2009).

6.1. Strength

Fig. 10a–f shows the plots of the strength histograms of various industrial and dental ceramics on the Weibull scale (zero threshold). The details of the experiments may be summarized as follows: (a) Sintered nitride ceramics (Si_3N_4), intended for dense, high strength and high toughness materials for reciprocating engine components and turbo-chargers, and for metal cutting tools. Gross (1996) tested 27 beams with dimensions $3.1 \times 4 \times 40.4$ mm under four-point bending. (b) Silicon nitride with sintering additive ($\text{Si}_3\text{N}_4\text{-Al}_2\text{O}_3, \text{O}_3\text{-Y}_2\text{O}_3$), which enhances the bending strength and fracture toughness. Four-point bending tests were carried out on 27 specimens with dimensions $3 \times 4 \times 40$ mm (Santos et al., 2003). (c) Dicor dental ceramic (tetrasilicic fluoromica glass ceramic), tested by four-point-bend beams (Tinschert et al., 2000). Tested were 30 specimens with dimensions $1.5 \times 3 \times 30$ mm. (d) Alumina glass composites. Tested were 30 specimens (Lohbauer et al., 2002) with dimensions $3 \times 4 \times 45$ mm under four-point-bend loading. (e) Vitadur Alpha Core dental ceramics (Alumina-reinforced feldspathic porcelain). Tested were 30 four-point-bend beams Tinschert et al., 2000 with dimensions $1.5 \times 3 \times 30$ mm. (f) Zirconia-ZTP dental ceramics (partially stabilized zirconia ceramic). Tested were 30 four-point-bend beams (Tinschert et al., 2000) with dimensions $1.5 \times 3 \times 30$ mm.

Despite rather low numbers of the specimens tested, one can discern from Fig. 10a–f that the strength histograms plotted in Weibull scale are not straight lines, as required by the two-parameter Weibull distribution. As shown by the solid curves in Fig. 10a–f, these histograms can be fitted as closely as the scatter permits by the present theory, in which the Weibull scale histogram consists of two parts separated by a relatively abrupt kink. The left tail is a Weibull straight line, and the core deviates from it to the right as strength σ_N increases. The core results from a chain of elements with the Gaussian part of the RVE strength. The kink is smooth but so abrupt that it may be approximated by a point transition at which both parts are grafted with a continuous cdf slope. The height of the grafting point characterizes the degree of brittleness of structure, which depends on the ratio of the structure size to the material inhomogeneity size.

To fit this kind of histograms, many investigators recently switched to the three-parameter Weibull distribution, which has a non-zero threshold. This way, they obtained better fits (Gross, 1996; Duffy et al., 1993; Stanley and Inanc, 1985) which, however, had a somewhat higher coefficient of variation of errors and an unreasonably low modulus m of the Weibull part.

Aside from the conflict of the three-parameter Weibull cdf with the present nano-mechanical derivation, there is experimental evidence that this cdf is not correct. Weibull (1939) tested 2868 specimens of Portland cement mortar, and

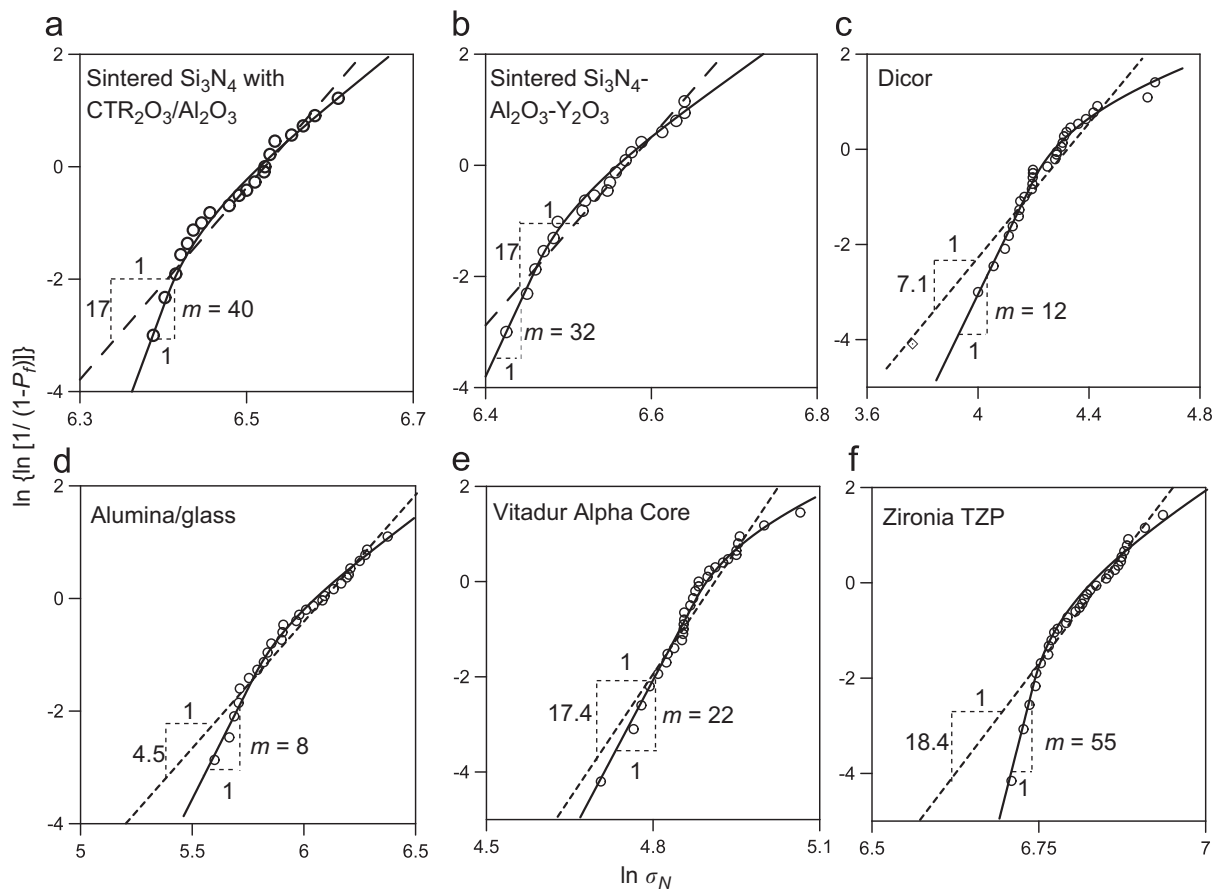


Fig. 10. Optimum fits of strength histograms of engineering and dental ceramics: (a) Sintered Si_3N_4 (Gross, 1996), (b) Sintered $\text{Si}_3\text{N}_4\text{-Al}_2\text{O}_3\text{-Y}_2\text{O}_3$ (Santos et al., 2003), (c) Dicor dental ceramics (Tinschert et al., 2000), (d) Alumina glass composites (Lohbauer et al., 2002), (e) Vitadur Alpha Core dental ceramics (Tinschert et al., 2000), (f) Zirconia-ZTP dental ceramics (Tinschert et al., 2000).

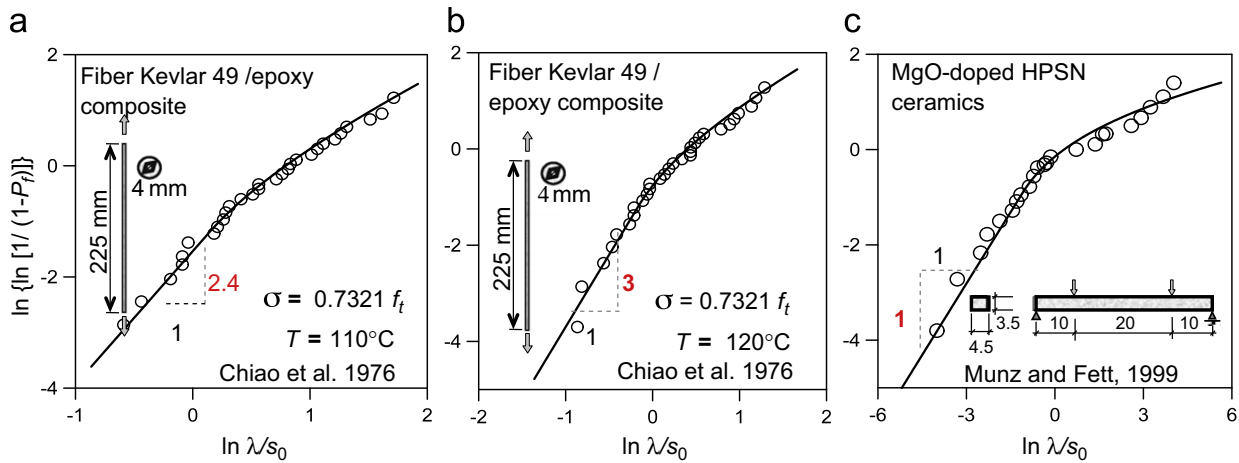


Fig. 11. Optimum fits of lifetime histograms of fiber composites and ceramics: (a) Kevlar-49 fiber composites at 110 °C (Chiao et al., 1977), (b) Kevlar-49 fiber composites at 120 °C (Chiao et al., 1977), (c) MgO-doped HPSN (Munz and Fett, 1999).

even if these data are plotted in a scale that gives, for the three-parameter Weibull cdf, a straight line, there is a systematic kink and deviation to the right in the high-probability range (see Fig. 10 in Bažant and Pang (2007)).

A more extensive experimental evidence against the three-parameter Weibull distribution is available for the mean size effect curve. The three parameter Weibull distribution implies, for the large size limit, a vanishing size effect, with the strength approaching a horizontal asymptote (Le and Bažant, 2009; Pang et al., 2008). This does not agree with the experimental observations of the size effect curve for the large size limit (Bažant et al., 2007).

Furthermore, the present theory shows that the zero threshold is a necessary consequence of the activation energy controlled crack jumps on the nano-scale, and of the hierarchical series-parallel coupling model for the multiscale transition of strength statistics. In fact, based on the present analysis of chain and bundle models, the three-parameter Weibull distribution cannot be analytically derived even if one assumes a non-zero threshold of strength cdf at nano-scale since the parallel couplings will produce multiple thresholds (Eq. (19)).

6.2. Lifetime

Fig. 11a–c presents the lifetime histograms of various fiber composites and engineering ceramics fitted by the present theory and the two-parameter Weibull distributions. Chiao et al. (1977) studied the lifetime histograms of Kevlar-49 fiber composites. A total of 30 prismatic bar specimens were loaded in tension at elevated temperature (100–120 °C) under a constant uniaxial tensile stress, which is about 70% of the mean short-time strength. Munz and Fett (1999) investigated the lifetime histograms of MgO-doped HPSN (hot-pressed silicon nitride) loaded at the temperature of 1100 °C. Standard four-point bend tests were used and the applied stress was about 50% of the mean short-time strength.

Similar to the strength histogram, the lifetime histogram is also seen to exhibit two parts in Weibull scale. The lower part, which has for one RVE the same reach as the tail of the cdf of strength (i.e., cca $P_f < 0.001$), is a straight line. The upper part is a curve deviating to the right. It is obvious that the two-parameter Weibull distribution cannot fit both parts simultaneously, and neither can the three-parameter Weibull distribution. The present theory is found to give optimum fits for these histograms.

Fett and Munz (1991) studied the strength and lifetime histograms of four-point bend beams made of 99.9% Al_2O_3 . Thirty specimens were used for each histogram testing. Fig. 12 shows experimentally observed strength and lifetime histograms with the optimum fits by the present theory. With one and the same set of parameters, the present theory is seen to give excellent fits of both the strength and lifetime histograms. By the optimum fitting, the Weibull moduli for strength and lifetime distributions are estimated to be about 30 and 1.1, respectively. Based on Eq. (45), the exponent n of the power-law for creep crack growth in this materials (99.9% Al_2O_3) can be obtained, and is found to be about 26.

The fitting of these histograms reveals that the grafting probabilities of the strength and lifetime cdf's are about the same. This agrees well with the present theory, in which the grafting probability can be calculated as: $P_{gr} = 1 - [1 - P_{gr,1}]^{N_{eq}}$. Since the grafting probabilities $P_{gr,1}$ of strength and lifetime cdf for one RVE are the same and the equivalent numbers N_{eq} of the RVEs for strength and lifetime distributions are about the same, then P_{gr} for strength and lifetime cdf's must be about the same.

The most severe check on the theory would be to test the size effect on the mean lifetime. But again, no such test data seem to exist.

7. Determination of RVE size for highly orthotropic materials, and way to achieve different N_{eq}

It is clear that, to calibrate the strength and lifetime cdf, one must roughly know the RVE size. From experience with statistically isotropic materials such as concrete and ceramics, l_0 is roughly equal to, and only slightly larger than, the FPZ

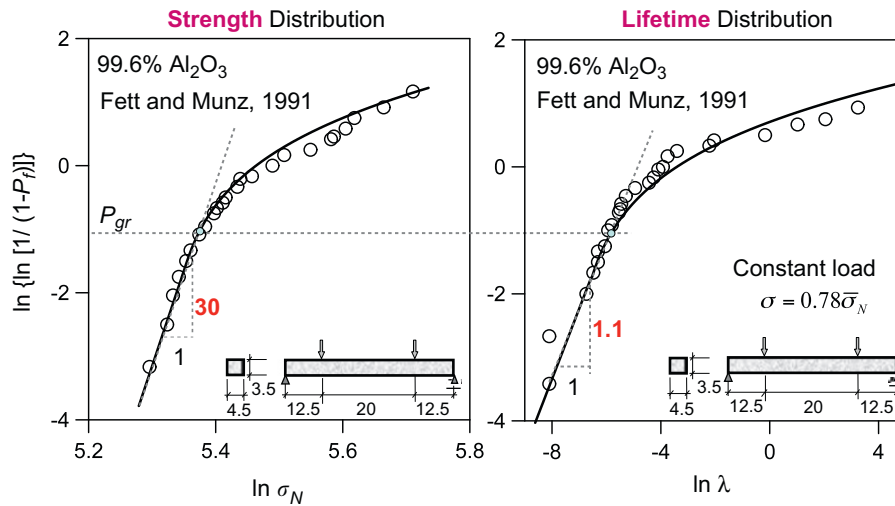


Fig. 12. Optimum fits of strength and lifetime histograms of 99.9% Al₂O₃ (Fett and Munz, 1991).

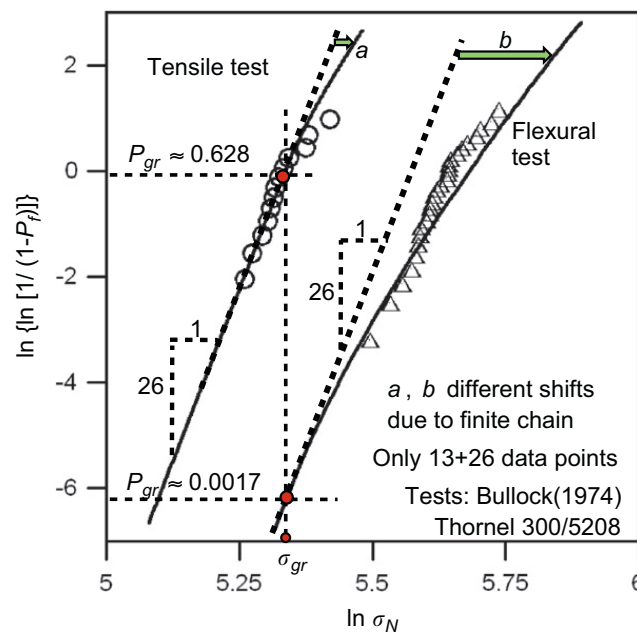


Fig. 13. Optimum fits of strength histograms of Thornel 300/5208 composite under direct tension and three-point bending (Bullock, 1974).

width in large notched specimens. The latter is easily identified from the tests of size effect on the mean strength (Bažant and Kazemi, 1990; Bažant, 2005, 2004; Bažant and Planas, 1998).

In highly orthotropic materials such as uniaxial fiber composites and biological nanocomposites (Gao et al., 2003; Chen et al., 2007), the problem is more complicated, since the length and width of the RVE are not the same. However, for fracture initiation under axial tension, the RVE length is probably again roughly equal to the length of the fracture process zone obtained from the size effect tests (Bažant et al., 1996). This is, of course, a point to be verified.

Within the framework of the present theory, the RVE size can also be determined from the optimum fits of strength histograms of structures with different sizes or geometries. Unfortunately, it has not been a common practice to test strength histograms at significantly different sizes. One main difficulty associated with histogram testing at different structure sizes is that the size range is always limited by the capacity and set-up of loading machines.

Since N_{eq} depends on both the structure size and the stress field, an easier way to obtain different equivalent numbers N_{eq} of RVEs is to test strength histograms of unnotched specimens with the same overall dimensions but different modes of loading. For example, if we assume the Weibull statistics, a concrete beam (of length-depth ratio 4:1) in direct tension is equivalent to a three-point bend beam whose depth is 50-times larger (Bažant and Planas, 1998).

Bullock (1974) tested strength histograms of unidirectional fiber composites (Thornel 300/5208) under both direct tension and three-point bending. The specimens were made of NARMCO's 5208 epoxy resin with Union Carbide's Thornel 300 fibers. The specimens for tensile tests were six-ply coupons, and the volume of specimen was estimated to be about 2117 mm³. The three-point bend specimens had 15 plies and the dimensions of 76.2 × 12.7 × 2.25 mm.

Fig. 13 shows that the optimum fits of the strength histograms of these two specimens are reasonably good. The reason why the histograms are not smooth is that too few specimens were tested (13 specimens in direct tension and 26 in flexure). The deviations of these histograms from the two-parameter Weibull distribution are different because of the finiteness of the chain. The grafting probabilities for the strength of the cdf's of these two specimens are seen to differ by two orders magnitude. The reason is that, in the bending specimen, the decay of stress from the maximum stress point in both the transverse and longitudinal directions causes N_{eq} to be much smaller. According to the fits, the volume of one RVE, V_0 , for Thornel 300/5208 under tension is found to be around 0.11 mm^3 .

Due to the excessively small number of test specimens, these histograms can be fitted equally well by the two-parameter Weibull distribution. The difference could be detected only if the number of data points were large enough for the Weibull tail of one RVE to get sampled.

Previously, the strength statistics of highly orthotropic materials such as unidirectional composites has been modeled by a chain of wide bundles (Harlow and Phoenix, 1978, 1979). However, such a model is insufficient because the Weibull tail for one RVE would be so remote (e.g. $P_f < 10^{-8}$) that, contrary to experience, the Weibull distribution of strength would be reached only for abnormally large structures (e.g. $N_{eq} > 10^9$). Yet, the Weibull distribution is seen to occupy in Fig. 13 a major portion of the cdf of strength. It is for this reason that the RVE strength statistics requires hierarchical model with no more than two elements coupled in parallel.

8. Size effects on mean structural strength and lifetime

Based on the weakest-link model, the mean structural strength and lifetime can be calculated as:

$$\text{Mean strength : } \bar{\sigma}_N = \int_0^\infty \prod_{i=1}^N [1 - P_1(\sigma_N S_i(\mathbf{x}_i))] d\sigma_N \tag{46}$$

$$\text{Mean lifetime : } \bar{\lambda} = \int_0^\infty \prod_{i=1}^N [1 - P_1(\sigma_0 S_i(\mathbf{x}_i), \lambda)] d\lambda \tag{47}$$

where P_1 = cdf of the strength or lifetime of one RVE. The cdf of both the structure strength and lifetime can then be calculated by the nonlocal boundary layer method. Fig. 14 shows the calculated size effect on both the mean structural strength and lifetime of 99.9% Al_2O_3 , based on the strength and lifetime cdf's calibrated by Fett and Munz's histograms (Fig. 12). It can be seen that, for the large size limit, the curves of size effect on both the mean strength and the lifetime tend to straight lines in the logarithmic plot. This agrees well with the power-law size effects of Weibull statistics because the strength and lifetime cdf's approach the Weibull distribution (Eqs. (25) and (44)) as the structure size increases. For small sizes, both size effect curves deviate from the straight line, because the fracture process zone size (or the size of material inhomogeneities) is not negligible compared to the structure size.

It is impossible to obtain analytical expressions for $\bar{\sigma}_N$ and $\bar{\lambda}$, but an approximate analytical formula for the mean strength has been obtained by asymptotic matching (Bažant, 2004, 2005):

$$\bar{\sigma}_N = \left[\frac{N_a}{D} + \left(\frac{N_b}{D} \right)^{\psi/m} \right]^{1/\psi} \tag{48}$$

Here parameters N_a , N_b , ψ and m are to be determined by asymptotic properties of the size effect curve. It has been shown that this size effect formula agrees well with the experiments on concrete (Bažant et al., 2007) and on fiber composite

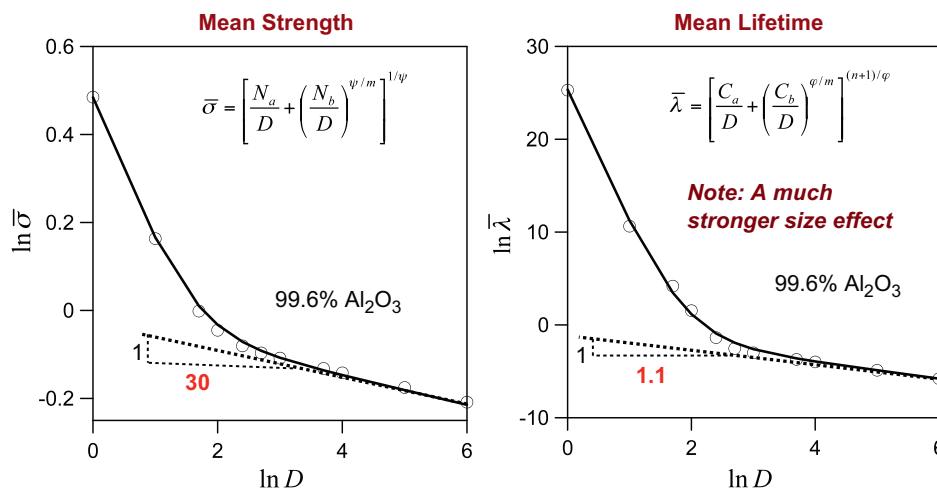


Fig. 14. Calculated size effect curves on the mean structural strength and lifetime of 99.9% Al_2O_3 .

(Bažant et al., 2006), as well as with the predictions of the nonlocal Weibull theory (Bažant and Novák, 2000a, 2000b), which is an older theory (Bažant and Xi, 1991) capable of describing the mean statistical size effect and the failure statistics of quasibrittle structures in the central range of cdf but not in the tail.

The size effect equation (Eq. (48)) converges to the large-size asymptote $(N_b/D)^{1/m}$, which is a power-law represented by a straight line of slope $-1/m$ in the size effect plot of $\log \sigma_N$ versus $\log D$. Calculation of the mean strength from the Weibull distribution shows that the size effect exponent, m , must be equal to the Weibull modulus of strength distribution, which represents the slope of the left tail of strength histogram plotted in Weibull scale. The other three parameters, N_a , N_b , and ψ , can be determined by solving three simultaneous equations expressing three asymptotic conditions, $[\bar{\sigma}_N]_{D \rightarrow l_0}$, $[d\bar{\sigma}_N/dD]_{D \rightarrow l_0}$, and $[\bar{\sigma}_N D^{1/m}]_{D \rightarrow \infty}$.

Within the framework of the present theory, the structural strength statistics must evolve with increasing size D through three asymptotic regimes:

- (1) for small sizes [roughly $N_{eq} \in (1,20)$], the cdf of strength is virtually Gaussian.
- (2) In the intermediate range of not too large sizes [roughly $N_{eq} \in (50,500)$], the chance that the strength of the weakest RVE would fall into the power-law tail $P_f < 10^{-3}$ is still very small, and so the weakest RVE is likely to be in the Gaussian core. This means that the strength distribution should tend to the extreme value distribution of Gaussian variables, which is the Gumbel distribution (Fisher and Tippett, 1928; Ang and Tang, 1984; Gumbel, 1958; Haldar and Mahadevan, 2000; Bazant, 2000; van der Hofstad and Redig, 2006), representing the so-called intermediate asymptotic regime in the sense of Barenblatt (1978, 2003).
- (3) For large sizes (roughly $N_{eq} > 5000$), there is a very high chance that the strength of the weakest element would be in the power-law tail $P_f < 10^{-3}$. This means that the strength cdf must converge to the extreme value distribution for power-law tails, which is the Weibull distribution (Fisher and Tippett, 1928; Ang and Tang, 1984; Haldar and Mahadevan, 2000).

Computations show, however, that the Gumbel statistics is not approached closely, and that the cdf for any size may be well approximated as a Gauss–Weibull grafted distribution, with the grafting point moving from left to right as the structure size increases.

Some researchers proposed that the deviations from the classical Weibull statistics can be explained by size and shape dependence of the Weibull modulus, m . Batdorf (1982) derived a failure envelope of unidirectional fiber composites, which relates the failure stress to the critical number of fiber breaks. Based on this envelope, he found the curve of the size effect on failure stress to consist, on the log–log scale, of a sequence of linear segments of decreasing slopes, m , supposed to imply a size-dependent Weibull modulus (Batdorf, 1982). However, this interpretation is questionable for two reasons:

- (1) The failure envelope represents the mean behavior, which cannot predict the size effect on the cdf of strength, and so it is impossible to infer a size effect on the Weibull modulus from this kind of analysis.
- (2) The Weibull modulus is obtained from the mean size effect curve, which implies the hypothesis that Weibull statistics applies. However, the present theory shows that the Weibull statistics applies only if the size of structure is sufficiently large.

The present theory implies that Weibull modulus, m is an intrinsic material property, determined by the multiscale transition from the nano-scale to the RVE scale; m is equal to the minimum of the sum of the Weibull tail powers among all the possible cuts separating the hierarchical model into two halves (Bažant et al., 2009). At macro-level, if the structure follows the weakest-link model, then the exponent of the power-law tail, which is equal to the Weibull modulus, remains unchanged.

It has been argued that the mean lifetime and the mean strength can be related by an equation of the same form as Eq. (38) (Bažant et al., 2009; Bažant and Le, 2009; Le et al., 2009). This is true for sufficiently large structures ($N_{eq} > 500$) for which the strength and lifetime cdf are approaching the Weibull distribution.

For small size structures, whose strength cdf is predominantly Gaussian, the mean strength and mean lifetime are not related by a simple power-law. However, calculation (Fig. 14) shows that the size effect on mean lifetime can be reasonably approximated by an equation of a similar form as Eq. (48):

$$\bar{\lambda} = \left[\frac{C_a}{D} + \left(\frac{C_b}{D} \right)^{\varphi/m} \right]^{(n+1)/\varphi} \quad (49)$$

where m =Weibull modulus of strength cdf, and n =exponent of power-law for creep crack growth. Similar to the size effect on the mean strength, the values of C_a , C_b and s can be derived by matching three asymptotic conditions: $[\bar{\lambda}]_{D \rightarrow l_0}$, $[d\bar{\lambda}/dD]_{D \rightarrow l_0}$, and $[\bar{\lambda} D^{(n+1)/m}]_{D \rightarrow \infty}$. Note that parameter φ in Eq. (49) is generally not equal to parameter ψ in Eq. (48) based on the fitting of the size effects on the mean strength and lifetime for the entire size range. Nevertheless, in the previous studies (Bažant et al., 2009; Bažant and Le, 2009; Le et al., 2009) it was assumed that $\psi = \varphi$, which is good enough only for the fitting of size effect curves on the strength and lifetime of large structures, particularly for $N_{eq} > 500$.

It is obvious that the size effect on the mean structural lifetime is much stronger than that on the mean strength. This is physically plausible. Consider two geometrically similar beams, with size ratio 1:8. Let the nominal strength of the small beam be ζ . Due to the size effect on the mean strength, the nominal strength of the large beam is about $\zeta/2$. If one applied a nominal load $\zeta/2$ to both beams, the large beam will fail within standard laboratory testing period (i.e. about 5 min) while the small beam is expected to survive at that load for decades if not forever.

An important practical merit of the present theory is that it provides a way to determine the strength and lifetime distributions without any histogram testing. If the test data on the mean curve of the size effect on the mean strength and on the rate of crack growth are available, they can be used to calibrate the present model. This will then yield not only the strength distribution but also the lifetime distribution.

Although the need to fabricate similar specimens of significantly different sizes may be regarded as inconvenient, the curve of mean size effect can be calibrated with much fewer tests. This curve also exhibits much less error because the mean generally has a much smaller coefficient of variation than the individual data (precisely $1/\sqrt{N_d}$ times smaller, where N_d =number of individual data points). A similar property applies to the regression line (such as the size effect curve). Testing for the mean size effect requires three to four different sizes with only 3–6 specimens for each size. For the histogram testing, at least a few hundred specimens are needed in order to obtain any information on the left tail of probability distribution.

9. The stress-life curve of quasibrittle structures under constant load and its size effect

In Section 5.2, the power-law for creep crack growth was applied to the lifetime test for one RVE to derive its lifetime distribution (Eq. (37)). Now we use the same equation to study the stress-life curve. Let us consider constant stresses of two levels, σ_{01} and σ_{02} , to be applied separately to the same RVE. By Eq. (37), the random lifetimes associated with these two stress levels can be related as:

$$\lambda_2 = \frac{\sigma_{01}^n}{\sigma_{02}^n} \lambda_1 \tag{50}$$

Similarly, we can consider nominal stresses of two levels (σ_1 and σ_2) to be applied to a structure with many RVEs. The stress in each RVE may be considered to be proportional to the nominal stress, and so the ratio of stresses on each RVE for these two load cases is σ_1/σ_2 . Therefore, we can use Eq. (50) to describe the relation between the random lifetime and the applied stress for each RVE.

At the reference stress σ_1 , the failure probability of entire structure is $P_f = 1 - \prod_{i=1}^N [1 - P_1(\lambda)]$. Then, by Eq. (50), the failure probability of structure subjected to nominal stress σ_2 is $P_f = 1 - \prod_{i=1}^N \{1 - P_1[(\sigma_1^n/\sigma_2^n)\lambda]\}$. Therefore, the mean structural lifetimes for these two stresses can be related by $\sigma_1^n \bar{\lambda}_1 = \sigma_2^n \bar{\lambda}_2$, which means that the stress-life under constant load follows the law:

$$\bar{\lambda} = C/\sigma_0^n \tag{51}$$

where C =constant. This inverse power-law has the same form as the stress-life curve of structures under fatigue load (Basquin's law, 1910), although the exponents for these two load cases are very different.

As shown in Fig. 15a and b, Eq. (51) agrees well with the recent experimental results on the stress-life curve of 99.9% Al_2O_3 and tetragonal zirconia polycrystal (TZP) (Kawakubo, 1995). Eq. (51) predicts the structural lifetime at low stress based on the structural lifetime at high stress. From the temperature effect on the fracture energy of concrete (Bažant and Prat, 1988), one finds that $n \approx 24$. Let f_t denote the tensile strength of concrete obtained in a test lasting about 5 min. For applied stress $0.2f_t$, Eq. (51) predicts the lifetime of the specimen to be about 5.7×10^{11} years, which is longer than the age of universe (1.375×10^{10} years); for $0.5f_t$, Eq. (51) predicts about 160 years.

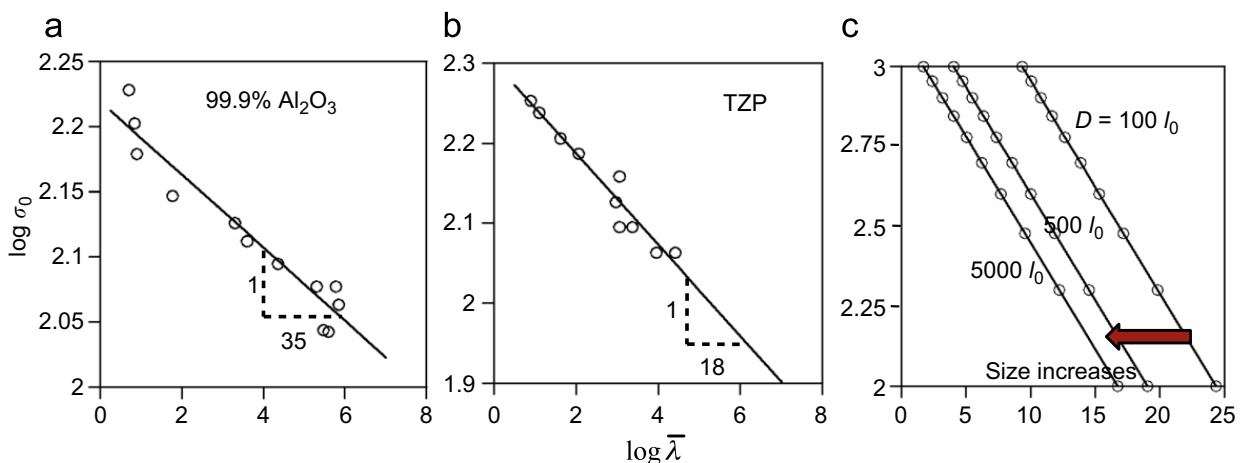


Fig. 15. (a) Stress-life curve for TZP and (b) size effect on stress-life curve.

Analyzing the size effect on the mean structural lifetime (Eq. (49)), one obtains the constant C in Eq. (51), which yields:

$$\sigma_0^n \bar{\lambda} = C = \sigma_0^n \left[\frac{C_a}{D} + \left(\frac{C_b}{D} \right)^{\varphi/m} \right]^{(n+1)/\varphi} \quad (52)$$

As shown in the log–log plot of Fig. 15c, the stress-life curve shifts to the left horizontally as the structure size increases. Eq. (52) makes it possible to predict the mean lifetime of large engineering structures under moderate stress from the lifetime tests of a small structure under high stress.

10. Effect of temperature on strength and lifetime distributions

The present theory justifies the Arrhenius factor for the temperature dependence of strength and lifetime distributions. This dependence naturally arises from the temperature dependence of the crack growth rate on the nano-scale, which is transferred over the scales without any change to the crack growth rate on the macro-scale. The Arrhenius type of temperature effect on the growth rate of macro-cracks in concrete has been shown to lead to the correct temperature dependence of the fracture energy of concrete (Bažant and Prat, 1988).

Generally, many activation energy barriers exist on the surface of the free energy potential of a nano-element (Krausz and Krausz, 1988). Various extraneous factors, such as temperature range and corrosive agents, influence the dominant activation energy barrier, Q_0 . Its value may be assumed to dominate and to be approximately independent of temperature, T , within a certain range. This simplification allows avoiding the details of the transition rate theory, with its changing activation energy barriers.

Consider that one RVE is subjected to two different temperatures T_1 and T_2 , and assume that this temperature difference causes no change in Q_0 . Based on Eq. (36), the RVE strengths at these two temperatures are related as:

$$\sigma_2 = \sigma_1 \exp \left[\frac{Q_0}{(n+1)k} \left(\frac{1}{T_2} - \frac{1}{T_1} \right) \right] \quad (53)$$

provided that the change of T causes no chemical reactions altering the material properties. Eq. (53) makes it possible to predict the cdf of structure strength at temperature T_2 if the cdf of strength at temperature T_1 is known:

$$P_f(\sigma)_{|T_2} = P_f(C_1 \sigma)_{|T_1} \quad (54)$$

where

$$C_1 = \exp \left[\frac{Q_0}{(n+1)k} \left(\frac{1}{T_2} - \frac{1}{T_1} \right) \right]. \quad (55)$$

Similar analysis also applies to the lifetime distribution. Based on Eq. (37), the cdf of structural lifetime at temperature T_2 can be deduced from the lifetime cdf at temperature T_1 :

$$P_f(\lambda)_{|T_2} = P_f(C_2 \lambda)_{|T_1} \quad (56)$$

where

$$C_2 = \exp \left[\frac{Q_0}{k} \left(\frac{1}{T_2} - \frac{1}{T_1} \right) \right] \quad (57)$$

On the Weibull scale, the strength cdf or lifetime cdf at temperature T_2 can simply be obtained through a horizontal shift of the strength or lifetime cdf at temperature T_1 by the distance of $\ln C_1$ or $\ln C_2$, respectively.

Chiao et al. (1977) investigated the lifetime histograms of organic fiber (Kevlar 49) composites at elevated temperature (100 and 110 °C). Bar specimens were subjected to a constant uniform tensile stress equal to 67% of the mean tensile strength. Here the lifetime histogram at 100 °C is first fitted by the nonlocal boundary layer approach, and the lifetime histogram at 110 °C is then obtained by extrapolating the calibrated lifetime cdf for 100 °C, based on Eq. (56).

Fig. 16 shows that the horizontal shift predicted by the present theory yields excellent fits of both histograms. These fits show that the dominant activation energy barrier of this organic fiber composite in the temperature range 100–110 °C is $Q_0 = 0.79$ eV (and $Q_0/k = 9225$ K).

The temperature dependence of the strength and lifetime cdf's thus provides an effective way to determine the dominant Q_0 . Eq. (53) indicates not only the effect of temperature on the random strength of one RVE, but also the temperature dependence of the mean strength of structure. If the mean structural strengths, $\bar{\sigma}_1$ and $\bar{\sigma}_2$, are measured at two different temperatures T_1 and T_2 , and if the temperature difference is not so large as to cause a change of Q_0 , then

$$Q_0 = (n+1)k \log \left(\frac{\bar{\sigma}_2}{\bar{\sigma}_1} \right) \left(\frac{1}{T_2} - \frac{1}{T_1} \right)^{-1} \quad (58)$$

where exponent n of the power law for crack growth rate can be obtained by the standard test measuring the crack growth velocity. Alternatively, if the mean structural lifetimes $\bar{\lambda}_1$ and $\bar{\lambda}_2$ are measured at two different temperatures, then the

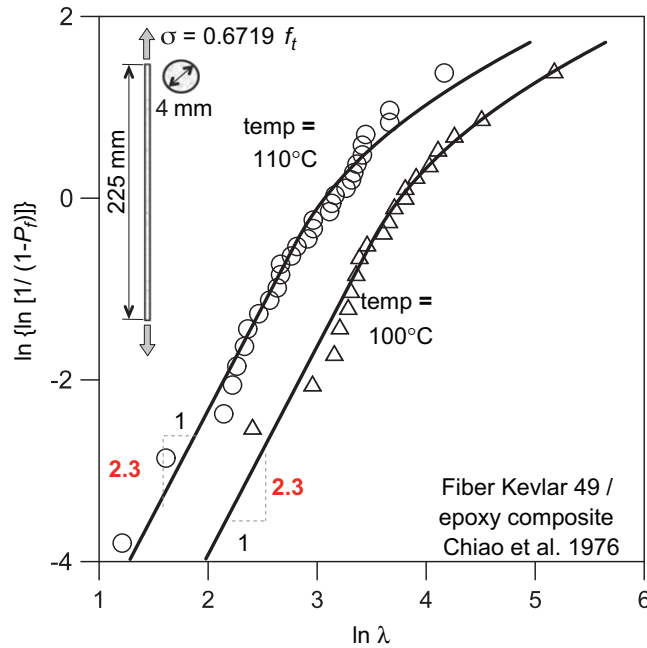


Fig. 16. Optimum fits of Kevlar-49 fiber composites at temperature 100 and 110 °C (Chiao et al., 1977).

dominant activation energy barrier can be determined without knowing n , i.e.,

$$Q_0 = k \log \left(\frac{\bar{\lambda}_2}{\bar{\lambda}_1} \right) \left(\frac{1}{T_2} - \frac{1}{T_1} \right)^{-1} \quad (59)$$

If test data are available for both the mean structural strengths and the lifetimes at two different temperatures, then, based on Eqs. (58) and (59), one can determine both the dominant activation energy barrier Q_0 and the exponent n of the power-law for crack growth rate.

11. Summary of new results

Various recently published results are given better and more coherent justifications, and are amalgamated into a common context to set up a unified theory of statistical strength, crack growth rate and lifetime of structures. Furthermore, several new results are obtained here to complete the theory. They are as follows:

1. The nano-crack propagating through an atomic lattice is an unnecessarily restrictive basis for the theory. The same results are obtained if the nano-scale crack propagates through a disordered nano-structure in a sequence involving many jumps over activation energy barriers.
2. The previous analytical proof of the additivity of power-law tail exponents of the cdf of bundle strength (or parallel coupling) model (Bažant and Pang, 2006, 2007) was restricted to perfectly brittle and perfectly ductile elements. Here it is shown that the analytical proof can be extended to gradually softening elements.
3. Daniels' proof that the strength of a bundle of brittle elements converges to the Gaussian distribution is extended to a bundle of gradually softening elements, and the additivity of tail exponents is also proven.
4. The stress-life curve of quasibrittle structures under constant load and its size effect are derived theoretically.
5. A random walk model for the propagation of crack front through atomic lattice is here refined by proper boundary conditions and solved for a simplified situation by Laplace transform.
6. Further comparisons with experimental data strengthen the support for the present theory.

12. Concluding remark

The present research demonstrates that the size effect on structure strength or lifetime is a crucial distinguishing characteristic of the failure properties of quasibrittle materials. Without testing for the size effect, the identification of material properties is ambiguous, and also more tedious. So far mostly ignored in the testing of ceramics and composites, the size effect has long been studied in concrete research.

Acknowledgements

The theoretical development was partially supported under Grant CMS-0556323 to Northwestern University (NU) from the U.S. National Science Foundation. The applications to concrete and composites were partially supported from the U.S. Department of Transportation through the NU Infrastructure Technology Institute under Grant 20118, and also under Grant N007613 to NU from Boeing, Inc.

Appendix A. The random walk of a crack in an atomic lattice

Atomic lattice crack: As a crack propagates through an atomic lattice, the separation δ between the opposite atoms across the nano-crack gradually increases by jumps, as shown in Fig. 17a. The force F_b transmitted between the opposite atoms and the corresponding interatomic potential function $\Pi_b(\delta)$ are related as $F_b = \partial\Pi_b(\delta)/\partial\delta$ and plotted in Fig. 17b and c. The pair with the peak value of the bond force, which corresponds to the point of maximum slope of the curve $\Pi_b(\delta)$ (state 3 in Fig. 17b and c), is normally defined as the front of a nano-scale cohesive crack. The real nano-crack ends at the atomic pair where the bond force drops to 0 (state 5 in Fig. 17b and c), at which point the adjacent lattice cells may undergo a gross distortion.

The atomic pairs between states 3 and 5 represent the cohesive zone (or the FPZ), defined as the zone in which the bond force decreases with increasing separation (Barenblatt, 1959). State 4 represents the limit of stability, at which the curve $\Pi_b(\delta)$ reaches a certain critical downward slope (equal in magnitude to the stiffness of the confinement within the surrounding solid). State 5, at which the atomic pair separation greatly increases, must lie immediately next to state 4 because the transition from state 4 to state 5 is unstable, and thus dynamic and fast. A continuum model of this process leads to the diagram already shown in Fig. 2b, where the undulations correspond to the successive jumps δ_a over the activation energy barriers.

Random walk model: The possibility of both forward and backward crack front jumps suggests that the nano-crack propagation should be treated as a random walk problem. The movement of the front of the cohesive crack (state 3 in Fig. 17a) represents a random walk biased by the energy release rate favoring the forward jumps and restricted by the tip (state 5) of the real crack (this contrasts with a macro-scale cohesive crack whose front cannot jump backward because of irreversible damage at the macro-level).

The lattice boundary at $x=l_a$, in front of the crack, is an absorbing boundary of the random walk of crack front. Before the real crack opens, the opposite boundary at $x=0$ is a reflecting boundary of the random walk. However, the situation gets more complicated after the bonds of the atomic pair at crack mouth separate by several atomic spacings. This break, which produces the real crack (state 5), is irreversible. It is a sudden instability emitting a sound wave carrying energy which cannot be recovered. The tip of the real crack (state 5) represents a reflecting boundary that moves forward as a function of the random walk. One thus faces a generalized random walk problem, which is beyond the present study.

The simplest model for nano-crack propagation is a one-dimensional biased random walk on a lattice with a constant stress-driven drift. The probability density for the position of the random walk satisfies the Fokker–Planck equation, whose solution is related to the first passage problem (Redner, 2001). As shown below, the diffusion of a crack becomes

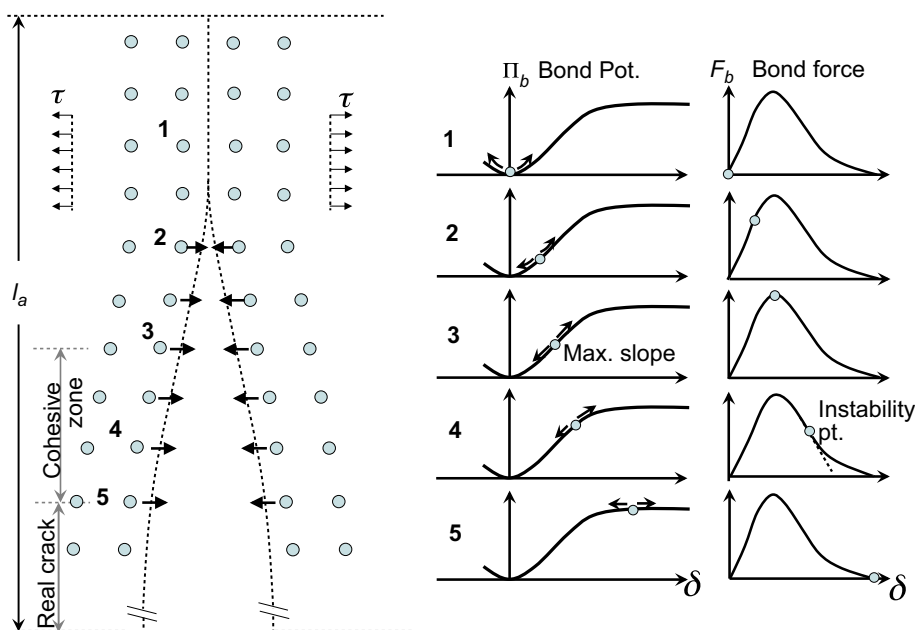


Fig. 17. Fracture of atomic lattice block.

significant compared to its stress-driven drift only if the Péclet number roughly satisfies the criterion $Pe < 4$, where $Pe = 2(l_a/\delta_a)(V_a/V_T)$. Although diffusion always dominates in the limit of zero stress, this condition is not met in normal situations. Indeed, for $l_a \approx 300\delta_a$ and the aforementioned values of V_a and V_T , one gets $Pe \approx 80$, and the failure probability corresponding to $Pe=2$ is of the order of 10^{-12} per lifetime, which is far too low to be of practical interest. Hence, the random walk aspect can safely be neglected compared to nano-crack drift driven purely by stress, which justifies the preceding analysis.

The random walk can nevertheless be important for certain situations, such as corrosion assisted fracture at very low applied stress. So, to show the nature of the problem, let us consider here at least a simplified one-dimensional random walk with fixed boundaries, in which the crack tip, initially located at x_0 , moves at the drift velocity $v = \delta_a f_1$ (Fig. 18a). For simplicity, the forcing (or bias) is assumed to be constant (uniform), even though in fracture mechanics it actually varies with the crack length.

When the crack-tip moves to the right, the crack propagates; when to the left, it shortens (i.e., is closing). At $x = 0$, there is a reflecting boundary, and at $x_1 = l_a$ an absorbing boundary. When the crack tip forms at $x=0$, it will begin to move in the positive x direction. The random walk of the crack tip can at most reach $x=l_a$, which represents a complete fracture of the lattice block (in reality, the lattice block will fail earlier due to instability, which is not captured by the random walk model). The probability $p(x,t)$ at time t of the crack tip being at position x , called the occupation probability, satisfies the Fokker–Plank equation (Redner, 2001; Risken, 1989):

$$\frac{\partial p(x,t)}{\partial t} + v \frac{\partial p(x,t)}{\partial x} - D \frac{\partial^2 p(x,t)}{\partial x^2} = 0 \tag{60}$$

where $D = \frac{1}{2} v_T \delta_a^2 e^{-Q_0/kT}$ = diffusivity. The absorbing and reflecting boundary conditions are $p(x=l_a, t)=0$ and $v p(0,t) - D[\partial p(x,t)/\partial x]_{x=0} = 0$, respectively. The initial condition is: $p(x,0) = \delta(x-x_0)$, where $\delta(x)$ = Dirac delta function.

To solve Eq. (60), one may apply the Laplace transform in the time domain (s =transform parameter):

$$s p(x,s) - p(x,0) + v \frac{\partial p(x,s)}{\partial x} = D \frac{\partial^2 p(x,s)}{\partial x^2} \tag{61}$$

The general solution of Eq. (61) is simply given by:

$$p(x,s) = A_1 \exp(\alpha_1 x) + A_2 \exp(\alpha_2 x) \quad (x \leq x_0) \tag{62}$$

$$p(x,s) = A_3 \exp(\alpha_1 x) + A_4 \exp(\alpha_2 x) \quad (x > x_0) \tag{63}$$

where $\alpha_{1,2} = (v \pm \sqrt{v^2 + 4Ds})/2D = l_a(Pe + P_s)$, $Pe = v l_a/2D = 2(l_a/\delta_a)(V_a/V_T)$ and $P_s = l_a \sqrt{v^2 + 4Ds}/2D$. The Péclet number, Pe , measures the relative dominance of stress-driven drift over stress-independent diffusion. Constants A_1, A_2, A_3 and A_4 are to be determined by the boundary and initial conditions: (1) $p(l_a,s) = 0$, (2) $-v p(0,t) + D[\partial p(x,s)/\partial x]_{x=0} = 0$, (3) Continuity of $p(x,s)$ at $x=x_0$: $p(x=x_0^+,s) = p(x=x_0^-,s)$, (4) Discontinuity of spatial derivative of $p(x,s)$ at $x=x_0$:

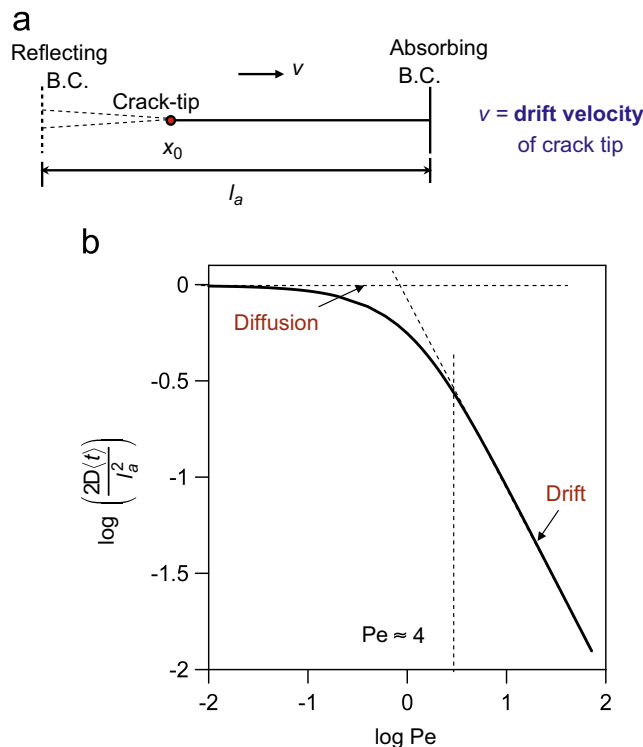


Fig. 18. (a) 1-D idealization of random walk of crack tip and (b) mean failure time as a function of Péclet number.

$[\partial p(x,s)/\partial x]|_{x=x_0^+} - [\partial p(x,s)/\partial x]|_{x=x_0^-} = -1/D$. By solving for these constants, one obtains the flux of occupation probability at the absorbing boundary as:

$$j(l_a, s) = -D \frac{\partial p(x, s)}{\partial x} \Big|_{x=l_a} \quad (64)$$

$$j(l_a, s) = \frac{e^{Pe(1-x_0/l_a)} [Pe \sinh(x_0 P_s / l_a) + P_s \cosh(x_0 P_s / l_a)]}{Pe \sinh P_s + P_s \cosh P_s} \quad (65)$$

The Laplace transform of the flux of occupation probability $j(l_a, s)$ can be written as:

$$j(l_a, s) = \int_0^\infty j(l_a, t) e^{-st} dt \quad (66)$$

$$j(l_a, s) = \int_0^\infty j(l_a, t) \left(1 - st + \frac{s^2 t^2}{2!} \dots \right) dt \quad (67)$$

$$j(l_a, s) = \mathcal{E} \left[1 - s \langle t \rangle + \frac{s^2}{2!} \langle t^2 \rangle \dots \right] \quad (68)$$

where \mathcal{E} is the exit probability at $x=l_a$, which equals 1 because the system is bounded; $\langle t \rangle =$ the mean exit time, which is equivalent to the mean failure time of the lattice block. The Maclaurin expansion of the Laplace transform of the occupation probability thus contains complete information about all the moments of the first passage time. In particular, we can easily compute the mean $\langle t \rangle$:

$$\langle t \rangle = - \frac{\partial j(l_a, s)}{\partial s} \Big|_{s=0} \quad (69)$$

It should be noted that there are other analytical methods to arrive directly at the mean first passage time (Redner, 2001; Risken, 1989), but our approach also provides the variance and all higher moments, if desired.

Substituting Eq. (64) into Eq. (69), one obtains a simple formula for the mean exit time, or the mean failure time, of the lattice block:

$$\langle t \rangle = \frac{l_a^2}{2D} \left[\frac{1-x_0/l_a}{Pe} + \frac{\cosh Pe}{Pe^2 e^{Pe}} - \frac{\cosh(Pe x_0 / l_a)}{Pe^2 e^{Pe x_0 / l_a}} \right] \quad (70)$$

Fig. 18b shows the mean failure time $\langle t \rangle$ as a function of Péclet number Pe . For small Péclet numbers ($Pe \rightarrow 0$), the mean failure time is the characteristic time for nano-crack diffusion across the lattice block, $l_a^2/2D$. For large Pe , the mean failure time approaches $(l_a - x_0)/v$, which is the time for stress-driven drift across the lattice block without significant back diffusion. As shown in Fig. 18b, the transition between diffusion dominance and drift dominance occurs within a relatively narrow range of Pe values. The analytical solution shows that, for $Pe > 4$, the fracture process is well approximated by purely stress-dependent drift.

Nevertheless, at extremely low stress corresponding to a very low Péclet number, diffusion dominates, and the random walk analysis then shows that the far left-tail ($P_f < 10^{-12}$) of strength cdf follows an exponential function instead of a power law. So, an exponential tail of the strength distribution must in fact lie far beyond the power-law tail considered here. However, this tail corresponds to such low failure probability that it is unlikely to be of interest in most practical engineering problems.

References

- Ang, A.H.-S., Tang, W.H., 1984. Probability Concepts in Engineering Planning and Design, vol. II Decision, Risk and Reliability. Wiley, New York.
- Aziz, M.J., Sabin, P.C., Lu, G.Q., 1991. The activation strain tensor: nonhydrostatic stress effects on crystal growth kinetics. Phys. Rev. B 41, 9812–9816.
- Barenblatt, G.I., 1959. The formation of equilibrium cracks during brittle fracture, general ideas and hypothesis, axially symmetric cracks. Prikl. Mat. Mech. 23 (3), 434–444.
- Barenblatt, G.I., 1978. Similarity, self-similarity and intermediate asymptotics (in Russian). Girometeoizdat, Moscow; and English translation, Consultants Bureau, New York, 1979.
- Barenblatt, G.I., 2003. Scaling. Cambridge University Press.
- Basquin, O.H., 1910. The exponential law of endurance tests. Proc. Am. Soc. Testing Mater. ASTEA, 10; 1910, pp. 625–630.
- Batdorf, S.B., 1982. Tensile strength of unidirectionally reinforced composites. J. Reinf. Plast. Compos. 1, 153–164.
- Bazant, M.Z., 2000. The largest cluster in subcritical percolation. Phys. Rev. E 62, 1660–1669.
- Bazant, M.Z., 2002. Stochastic renormalization group in percolation. Physica A 316, 451–477.
- Bažant, Z.P., 1984. Size effect in blunt fracture: concrete, rock, metal. J. Eng. Mech. ASCE 110 (4), 518–535.
- Bažant, Z.P., 1997. Scaling of quasibrittle fracture: asymptotic analysis. Int. J. Fract. 83 (1), 19–40.
- Bažant, Z.P., 2004. Scaling theory of quasibrittle structural failure. Proc. Natl. Acad. Sci. USA 101 (37), 13397–13399.
- Bažant, Z.P., 2005. Scaling of Structural Strength, second ed. Elsevier, London.
- Bažant, Z.P., Daniel, I.M., Li, Z., 1996. Size effect and fracture characteristics of composite laminates. J. Eng. Mater. Technol. ASME 118 (3), 317–324.
- Bažant, Z.P., Jirásek, M., 2002. Nonlocal integral formulations of plasticity and damage: survey of progress. J. Eng. Mech. ASCE 128 (11), 1119–1149.
- Bažant, Z.P., Kazemi, M.T., 1990. Determination of fracture energy, process zone length and brittleness number from size effect, with application to rock and concrete. Int. J. Fract. 44, 111–131.

- Bažant, Z.P., Kazemi, M.T., 1990. Size effect in fracture of ceramics and its use to determine fracture energy and effective process zone length. *J. Am. Ceram. Soc.* 73 (7), 1841–1853.
- Bažant, Z.P., Le, J.-L., 2009. Nano-mechanics based modeling of lifetime distribution of quasibrittle structures. *J. Eng. Failure Anal.* 16, 2521–2529.
- Bažant, Z.P., Le, J.-L., Bazant, M.Z., 2008. Size effect on strength and lifetime distribution of quasibrittle structures implied by interatomic bond break activation. In: *Proceedings of 17th European Conference on Fracture*, Brno, Czech Republic, pp. 78–92.
- Bažant, Z.P., Le, J.-L., Bazant, M.Z., 2009. Scaling of strength and lifetime distributions of quasibrittle structures based on atomistic fracture mechanics. *Proc. Natl. Acad. Sci. USA* 20, 11484–11489.
- Bažant, Z.P., Le, J.-L., Hoover, C.G., 2010. Nonlocal boundary layer (NBL) model: overcoming boundary condition problems in strength statistics and fracture analysis of quasibrittle materials. In: Oh, B.-H. (Ed.), *Fracture Mechanics of Concrete and Concrete Structures—Recent Advances in Fracture Mechanics of Concrete Proceedings FraMCoS-7*, 7th International Conference held in Jeju, Korea, plenary lecture. Korea Concrete Institute, Seoul, pp. 135–143.
- Bažant, Z.P., Novák, D., 2000a. Probabilistic nonlocal theory for quasibrittle fracture initiation and size effect. I. Theory. *J. Eng. Mech. ASCE* 126 (2), 166–174.
- Bažant, Z.P., Novák, D., 2000b. Probabilistic nonlocal theory for quasibrittle fracture initiation and size effect. II. Application. *J. Eng. Mech. ASCE* 126 (2), 175–185.
- Bažant, Z.P., Pang, S.-D., 2006. Mechanics based statistics of failure risk of quasibrittle structures and size effect on safety factors. *Proc. Natl. Acad. Sci. USA* 103 (25), 9434–9439.
- Bažant, Z.P., Pang, S.-D., 2007. Activation energy based extreme value statistics and size effect in brittle and quasibrittle fracture. *J. Mech. Phys. Solids* 55, 91–134.
- Bažant, Z.P., Planas, J., 1998. *Fracture and Size Effect in Concrete and Other Quasibrittle Materials*. CRC Press.
- Bažant, Z.P., Prat, P.C., 1988. Effect of temperature and humidity on fracture energy of concrete. *ACI Mater. J.* 85-M32, 262–271.
- Bažant, Z.P., Vořechovský, M., Novák, D., 2007. Asymptotic prediction of energetic-statistical size effect from deterministic finite element solutions. *J. Eng. Mech. ASCE* 128, 153–162.
- Bažant, Z.P., Xi, Y., 1991. Statistical size effect in quasi-brittle structures: II. Nonlocal theory. *J. Eng. Mech. ASCE* 117 (7), 2623–2640.
- Bažant, Z.P., Zhou, Y., Daniel, I.M., Caner, F.C., Yu, Q., 2006. Size effect on strength of laminate-foam sandwich plates. *J. Eng. Mater. Technol. ASME* 128 (3), 366–374.
- Breyse, D., Fokwa, D., 1992. Influence of disorder of the fracture process of mortar. In: Bažant, Z.P. (Ed.), *Proceedings of 1st International Conference on Fracture Mechanisms of Concrete Structures*. Elsevier, London, pp. 536–541.
- Bullock, R.E., 1974. Strength ratio of composite materials in flexure and in tension. *J. Comp. Mater.* 8, 200–206.
- Chen, L., Ballarini, R., Kahn, H., Heuer, A.H., 2007. A bioinspired micro-composite structure. *J. Mater. Res.* 22 (1), 124–131.
- Chiao, C.C., Sherry, R.J., Hetherington, N.W., 1977. Experimental verification of an accelerated test for predicting the lifetime of organic fiber composites. *J. Comp. Mater.* 11, 79–91.
- Coleman, B.D., 1957. Time dependence of mechanical breakdown in bundles of fibers I Constant total load. *J. Appl. Phys.* 28 (9), 1058–1064.
- Coleman, B.D., 1958. Statistics and time dependent of mechanical breakdown in fibers. *J. Appl. Phys.* 29 (6), 968–983.
- Daniels, H.E., 1945. The statistical theory of the strength of bundles and threads. *Proc. R. Soc. London A* 183, 405–435.
- Duckett, K., 2005. Risk analysis and the acceptable probability of failure. *Struct. Eng.* 83 (15), 25–26.
- Duffy, S.F., Powers, L.M., Starlinger, A., 1993. Reliability analysis of structural ceramic components using a three-parameter Weibull distribution. *Trans. ASME J. Eng. Gas Turbines Power* 115, 109–116.
- Eyring, H., 1936. Viscosity, plasticity, and diffusion as examples of absolute reaction rates. *J. Chem. Phys.* 4, 283–291.
- Evans, A.G., 1972. A method for evaluating the time-dependent failure characteristics of brittle materials—and its application to polycrystalline alumina. *J. Mater. Sci.* 7, 1146–1173.
- Evans, A.G., Fu, Y., 1984. The mechanical behavior of alumina. In: *Fracture in Ceramic Materials*. Noyes Publications, Park Ridge, NJ, pp. 56–88.
- Fett, T., 1991. A fracture-mechanical theory of subcritical crack growth in ceramics. *Int. J. Fract.* 54, 117–130.
- Fett, T., Munz, D., 1991. Static and cyclic fatigue of ceramic materials. In: Vincenzini, P. (Ed.), *Ceramics Today—Tomorrow's Ceramics*. Elsevier Science Publisher B.V., pp. 1827–1835.
- Freudenthal, A.M., 1968. Statistical approach to brittle fracture. In: Liebowitz, H. (Ed.), *Fracture: An Advanced Treatise*, vol. 2. Academic Press, New York, pp. 591–619.
- Fisher, R.A., Tippett, L.H.C., 1928. Limiting forms of the frequency distribution of the largest and smallest member of a sample. *Proc. Cambridge Philos. Soc.* 24, 180–190.
- Gao, H., Ji, B., Jäger, I.L., Arzt, E., Fratz, P., 2003. Materials become insensitive to flaws at nano-scale: lessons from nature. *Proc. Natl. Acad. Sci. USA* 100 (10), 5597–5600.
- Graham-Brady, L.L., Arwade, S.R., Corr, D.J., Gutiérrez, M.A., Breyse, D., Grigoriu, M., Zabarás, N., 2006. Probability and materials: from nano- to macro-scale: a summary. *Probab. Eng. Mech.* 21 (3), 193–199.
- Grassl, P., Bažant, Z.P., 2009. Random lattice-particle simulation of statistical size effect in quasi-brittle structures failing at crack initiation. *J. Eng. Mech. ASCE* 135 (2), 85–92.
- Glasstone, S., Laidler, K.J., Eyring, H., 1941. *The Theory of Rate Processes*. McGraw-Hill, New York.
- Gross, B., 1996. Least squares best fit method for the three parameter Weibull distribution: analysis of tensile and bend specimens with volume or surface flaw failure. *NASA, TM-4721*, 1–21.
- Gumbel, E.J., 1958. *Statistics of Extremes*. Columbia University Press, New York.
- Haldar, A., Mahadevan, S., 2000. *Probability, Reliability, and Statistical Methods in Engineering Design*. Wiley, New York.
- Harlow, D.G., Phoenix, S.L., 1978. The chain-of-bundles probability model for the strength of fibrous materials I: analysis and conjectures. *J. Comput. Mater.* 12, 195–214.
- Harlow, D.G., Phoenix, S.L., 1979. Bounds on the probability of failure of composite materials. *Int. J. Fract.* 15 (4), 312–336.
- Harlow, D.G., Smith, R.L., Taylor, H.M., 1983. Lower tail analysis of the distribution of the strength of load-sharing systems. *J. Appl. Probab.* 20, 358–367.
- Henderson, C.B., Graham, P.H., Robinson, C.N., 1970. A comparison of reaction rate models for the fracture of solids. *Int. J. Fract.* 6 (1), 33–40.
- van der Hofstad, R., Redig, F., 2006. Maximal clusters in non-critical percolation and related models. *J. Statist. Phys.* 122 (4), 671–703.
- Hsiao, C.C., Moghe, S.R., Kausch, H.H., 1968. Time-dependent mechanical strength of oriented media. *J. Appl. Phys.* 39, 3857–3861.
- Ibnabdeljalil, M., Phoenix, S.L., 1995. Creep rupture of brittle matrix composite reinforced with time dependent fibers: scalings and Monte Carlo simulations. *J. Mech. Phys. Solids* 43(6), 897–931.
- Kausch, H.H., 1978. *Polymer Fracture*. Springer-Verlag, Berlin, Heidelberg, New York.
- Kawakubo, T., 1995. Fatigue crack growth mechanics in ceramics. In: Kishimoto, H., Hoshida, T., Okabe, N. (Eds.), *Cyclic Fatigue in Ceramics*. Elsevier Science B. V. and The Society of Materials Science, Japan, pp. 123–137.
- Kaxiras, E., 2003. *Atomic and Electronic Structure of Solids*. Cambridge University Press.
- Krausz, A.S., Krausz, K., 1988. *Fracture Kinetics of Crack Growth*. Kluwer Academic Publisher, Netherlands.
- Lam, H., Blanchet, J., Burch, D., Bazant, M.Z. Corrections to the central limit theorem for heavy-tailed probability densities, submitted for publication, <http://arxiv.org/abs/1103.4306>.
- Le, J.-L., Bažant, Z.P., 2009. Finite weakest link model with zero threshold for strength distribution of dental restorative ceramics. *Dent. Mater.* 25 (5), 641–648.

- Le, J.-L., Bažant, Z.P., Bazant, M.Z., 2009. Crack growth law and its consequences on lifetime distributions of quasibrittle structures. *J. Phys. D: Appl. Phys.* 42, 214008(8 pp.).
- Le, J.-L., Bažant, Z.P. Unified nano-mechanics based probabilistic theory of quasibrittle and brittle structures: II. Fatigue crack growth, lifetime and scaling. *J. Mech. Phys. Solids*, in press.
- Lohbauer, U., Petchelt, A., Greil, P., 2002. Lifetime prediction of CAD/CAM dental ceramics. *J. Biomed. Mater. Res.* 63 (6), 780–785.
- Mahesh, S., Phoenix, S.L., 2004. Lifetime distributions for unidirectional fibrous composites under creep-rupture loading. *Int. J. Fract.* 127, 303–360.
- Melchers, R.E., 1987. *Structural Reliability, Analysis and Prediction*. Wiley, New York.
- Munz, D., Fett, T., 1999. *Ceramics: Mechanical Properties, Failure Behavior, Materials Selection*. Springer-Verlag, Berlin.
- NKB, 1978. Nordic Committee for Building Structures. Recommendation for loading and safety regulations for structural design. NKB Report, No. 36.
- Okabe, N., Hirata, H., 1995. High temperature fatigue properties for some types of SiC and Si₃N₄ and the unified strength estimation method. In: Kishimoto, H., Hoshida, T., Okabe, N. (Eds.), *Cyclic Fatigue in Ceramics*. Elsevier Science B. V. and The Society of Materials Science, Japan, pp. 245–276.
- Pang, S.-D., Bažant, Z.P., Le, J.-L., 2008. Statistics of strength of ceramics: finite weakest link model and necessity of zero threshold. *Int. J. Fract.* 154, 131–145.
- Philips, R., 2001. *Crystals, Defects and Microstructures: Modeling Across Scales*. Cambridge University Press.
- Phoenix, S.L., 1978a. Stochastic strength and fatigue of fiber bundles. *Int. J. Fract.* 14 (3), 327–344.
- Phoenix, S.L., 1978b. The asymptotic time to failure of a mechanical system of parallel members. *SIAM J. Appl. Math.* 34 (2), 227–246.
- Phoenix, S.L., Tierney, L.-J., 1983. A statistical model for the time dependent failure of unidirectional composite materials under local elastic load-sharing among fibers. *Eng. Fract. Mech.* 18 (1), 193–215.
- Phoenix, S.L., Ibnabdeljalil, M., Hui, C.-Y., 1997. Size effects in the distribution for strength of brittle matrix fibrous composites. *Int. J. Solids Struct.* 34 (5), 545–568.
- Redner, S., 2001. *A Guide to First-Passage Processes*. Cambridge University Press.
- Risken, H., 1989. *The Fokker–Planck Equation*, second ed. Springer Verlag.
- Salem, J.A., Nemeth, N.N., Powers, L.P., Choi, S.R., 1996. Reliability analysis of uniaxially ground brittle materials. *J. Eng. Gas Turbines Power* 118, 863–871.
- Santos, C.D., Strecker, K., Piorino Neto, F., Oliveério Moreira de, M.S., Sandro Aparecido, B., Cosme Roberto Moreira da, S., 2003. Evaluation of the reliability of Si₃N₄–Al₂O₃–Cr₂O₃ ceramics through Weibull analysis. *Mater. Res.* 6 (4), 463–467.
- Schwartz, P., 1987. A review of recent experimental results concerning the strength and time dependent behaviour of fibrous poly (paraphenylene terephthalamide). *Polym. Eng. Sci.* 27 (11), 842–847.
- Schwartz, P., Netravali, A., Sembach, S., 1986. Effects of strain rate and gauge length on the failure of ultra-high strength polyethylene fibers. *Textile Res. J.* 56, pp. 502–508.
- Smith, R.L., 1982. The asymptotic distribution of the strength of a series-parallel system with equal load sharing. *Ann. Probab.* 10 (1), 137–171.
- Stanley, P., Inanc, E.Y., 1985. Assessment of surface strength and bulk strength of a typical brittle material. In: Eggwertz, S., Lind, N.C. (Eds.), *Probabilistic Methods. I. The Mechanics of Solids and Structures*. Springer-Verlag, Berlin, pp. 231–251.
- Thouless, M.D., Hsueh, C.H., Evans, A.G., 1983. A damage model of creep crack growth in polycrystals. *Acta Metal.* 31 (10), 1675–1687.
- Tierney, L.-J., 1983. Asymptotic bounds on the time to fatigue failure of bundles of fibers under local load sharing. *Adv. Appl. Probab.* 14 (1), 95–121.
- Tinschert, J., Zvez, D., Marx, R., Ausavice, K.J., 2000. Structural reliability of alumina-, feldspar-, leucite-, mica- and zirconia-based ceramics. *J. Dent.* 28, 529–535.
- Tobolsky, A., Eyring, H., 1943. Mechanical properties of polymeric materials. *J. Chem. Phys.* 11, 125–134.
- Xu, X.F., 2007. A multiscale stochastic finite element method on elliptic problems involving uncertainties. *Comput. Meth. Appl. Mech. Eng.* 196, 2723–2736.
- Wagner, H.D., 1989. Stochastic concepts in the study of size effects in the mechanical strength of highly oriented polymeric materials. *J. Polym. Sci.* 27, 115–149.
- Wagner, H.D., Schwartz, P., Phoenix, S.L., 1986. Lifetime statistics for single Kevlar 49 filaments in creep-rupture. *J. Polym. Sci.* 21, 1868–1878.
- Wanger, H.D., Phoenix, S.L., Schwartz, P., 1984. A study of statistical variability in the strength of single aramid filaments. *J. Comp. Mater.* 18, 312–338.
- Weibull, W., 1939. The phenomenon of rupture in solids. In: *Proceedings of Royal Swedish Institute of Engineering Research*, vol. 153, Stockholm, 1939, pp. 1–55.
- Williams, T., Baxer, S.C., 2006. A framework for stochastic mechanics. *Probab. Eng. Mech.* 21 (3), 247–255.
- Zhurkov, S.N., 1965. Kinetic concept of the strength of solids. *Int. J. Fract. Mech.* 1 (4), 311–323.
- Zhurkov, S.N., Korsukov, V.E., 1974. Atomic mechanism of fracture of solid polymer. *J. Polym. Sci.* 12 (2), 385–398.



Contents lists available at ScienceDirect

Journal of the Mechanics and Physics of Solids

journal homepage: www.elsevier.com/locate/jmps

Unified nano-mechanics based probabilistic theory of quasibrittle and brittle structures: II. Fatigue crack growth, lifetime and scaling

Jia-Liang Le^{a,1}, Zdeněk P. Bažant^{b,*}^a Department of Civil Engineering, University of Minnesota, Minneapolis, Minnesota 55455, United States^b Departments of Civil Engineering and Materials Science, Northwestern University, 2145 Sheridan Road, CEE/A135, Evanston, Illinois 60208, United States

ARTICLE INFO

Article history:

Received 10 July 2010
Received in revised form
16 January 2011
Accepted 2 March 2011
Available online 21 March 2011

Keywords:

Fracture
Statistical modeling
Probabilistic mechanics
Side effect
Structural safety

ABSTRACT

This paper extends the theoretical framework presented in the preceding Part I to the lifetime distribution of quasibrittle structures failing at the fracture of one representative volume element under constant amplitude fatigue. The probability distribution of the critical stress amplitude is derived for a given number of cycles and a given minimum-to-maximum stress ratio. The physical mechanism underlying the Paris law for fatigue crack growth is explained under certain plausible assumptions about the damage accumulation in the cyclic fracture process zone at the tip of subcritical crack. This law is then used to relate the probability distribution of critical stress amplitude to the probability distribution of fatigue lifetime. The theory naturally yields a power-law relation for the stress-life curve (S-N curve), which agrees with Basquin's law. Furthermore, the theory indicates that, for quasibrittle structures, the S-N curve must be size dependent. Finally, physical explanation is provided to the experimentally observed systematic deviations of lifetime histograms of various ceramics and bones from the Weibull distribution, and their close fits by the present theory are demonstrated.

© 2011 Elsevier Ltd. All rights reserved.

1. Introduction

For many structures, such as aircraft, ships, bridges and biomedical implants, the fatigue lifetime is an essential aspect of design. However, when a long lifetime is required, it is next to impossible to obtain the lifetime histogram purely experimentally, by waiting until the test structure or material specimen fails. Therefore, one must rely on a realistic theory of failure probability that can be calibrated and verified indirectly through its predictions other than the histograms of fatigue strength and lifetime.

The concept of fatigue lifetime, which is usually characterized in terms of the stress-life (S-N) curve representing the plot of the applied nominal stress amplitude versus the critical number of load cycles, was pioneered by Wöhler (1860), who conducted rotating bend tests of fatigue lifetime of alloys for railroad car axles. Basquin (1910) subsequently proposed a simple power-law relation between the lifetime and the stress amplitude for fully reversed, constant-amplitude fatigue loading. The minimum-to-maximum stress ratio and the average stress have further been shown to affect the S-N curve significantly (Gerber, 1874; Goodman, 1899; Soderberg, 1939; Morrow, 1968), though not its power-law form.

* Corresponding author. Tel.: +1 847 491 4025; fax: +1 847 491 4011.

E-mail address: z-bazant@northwestern.edu (Z.P. Bažant).

¹ Formerly Graduate Research Assistant, Northwestern University.

After the advent of fracture mechanics, it has generally been agreed that the fatigue lifetime should be determined from the growth rate of a fatigue crack. Paris and Erdogan (1963) proposed a power-law for the fatigue crack growth rate, called the Paris law, which expresses this rate as a power-law function of the stress amplitude. Its integration up to the critical crack length yields the fatigue lifetime. The resulting stress amplitude–lifetime relation follows the same power law as the Basquin law.

Various aspects of the Paris law have been researched for decades. Weertman (1966) and Rice (1967) independently proposed damage accumulation models derived on the basis of tensile yielding or slip in the reversed plastic zone of metals ahead of the crack. Considering the plastic superposition for unloading, Rice (1967) showed that the size of the reversed plastic zone, which is mostly embedded within the FPZ for monotonic loading and determines the propagation of a fatigue crack, is proportional to $\Delta K^2/f_y^2$ (where ΔK = stress intensity factor amplitude and f_y = yield strength of metal). Another type of damage model considers the cyclic plastic strain in the reverse yield zone at the crack tip (Coffin, 1962). These plasticity-based models for metals have predicted the exponent of Paris law to be 4, in agreement with the experimental observations for most metals.

For quasibrittle materials, experiments showed that the Paris law is still applicable but the exponent of Paris law, n , is significantly higher, specifically $n \approx 10$ for concrete (Bažant and Xu, 1991), and $n \approx 30$ for both alumina ceramics (Ogawa, 1995) and zirconia dental ceramics (Studarta et al., 2007a). However, a theoretical justification of Paris law for quasibrittle materials has been lacking and will be attempted here.

For decades, extensive efforts have been devoted to probabilistic modeling of fatigue lifetime based on histogram testing as well as theoretical analysis. A simple way to model the fatigue lifetime is to directly implement the cyclic loading history into the creep lifetime model (Phoenix, 1978a,b; Tierney, 1983). However, such an approach is not consistent with the experimental observations in two respects: (1) The model always predicts that the structure would fail slower under a cyclic load varying between P_{min} and P_{max} than it would fail under a constant load equal to P_{max} , whereas the experiments show that under the cyclic loading the failure may come faster, which is explained by a build-up of residual stresses (Suresh, 1998). (2) The model predicts the exponents of the power laws for the S–N curves for constant and cyclic loading to be the same. However, recent experiments on ceramics show these exponents to be very different (Kawakubo, 1995).

A more sophisticated approach was to model the fatigue crack propagation probabilistically as a Markov process (Sobczyk and Spencer, 1992; Mihashi, 1983). However, various assumptions with no physical justification had to be introduced for the transition rates of this process. A simplified approach was to randomize the parameters of the Paris law by a certain stationary stochastic process (Yang et al., 1983; Yang and Donath, 1983; Yang and Manning, 1991), but the distribution functions for its parameters again lacked physical justifications.

Besides various theoretical attempts for fatigue lifetime distribution, the statistics of fatigue lifetime of quasibrittle materials, such as engineering and dental ceramics and cortical bones, is often modelled, for the sake of simplicity, by some empirical probability density function (pdf). The most widely used pdf's are the two- and three- parameter Weibull distributions (Studarta et al, 2007a,b; Sakai and Hoshide, 1995). However, it is found that the two-parameter Weibull distribution does not fit the histograms well. The three-parameter Weibull distribution improves the fits, but its finite threshold was recently shown to be impossible for strength and lifetime statistics (Bažant et al., 2009; Pang et al., 2008). Furthermore, different types of pdf's with the same mean and same variance have very different tails within the range of design lifetimes corresponding to a tolerable failure probability such as $< 10^{-6}$ (Melchers, 1987; Duckett, 2005; NKB, 1978). For instance, when the Weibull modulus is 24, the distance between the failure load of probability $P_f = 10^{-6}$ and the mean failure load, measured in terms of the standard deviations of strength, nearly doubles when the cdf of structure strength changes from Gaussian to Weibullian. For a much smaller Weibull modulus, which is typical for lifetime distribution of quasibrittle structures, this distance becomes still much larger (Bažant et al., 2009; Le and Bažant, 2009; Pang et al., 2008). Hence, a mechanics-based theory is necessary and is attempted here.

Based on the theoretical framework presented in the preceding Part I (Le et al., this issue), we will first derive the probability distribution of fatigue strength, defined as the critical stress amplitude for a given number of cycles and a given minimum-to-maximum stress ratio. The probability distribution of fatigue lifetime will then be deduced from the cdf of fatigue strength and the law of fatigue crack growth.

2. Statistics of fatigue strength on the nanoscale

A simple and clear physical basis for the probability of fracture growth exists only on the atomic scale. The jumps of the front of an interatomic crack represent a quasi-steady process because, even at the rate of missile impact, the interatomic bonds break at roughly the rate of only one per 100 thermal vibrations of an atom. Consequently, on the atomic scale, the crack jump probability must be the same as the crack jump frequency. So, following Bažant and Pang (2007) and Le et al. (this issue, Part I), we begin by analyzing the fatigue fracture of a nanoscale element.

As shown in Fig. 1(a), we consider the structure to be subjected to a cyclic load, which can be characterized by two quantities: the stress amplitude $\Delta\sigma = \sigma_{max} - \sigma_{min}$ and the stress ratio $R = \sigma_{min}/\sigma_{max}$. The corresponding stress history for a nanoscale element is hard to determine, especially for the first few cycles during which the residual stress field builds up rapidly. However, when focused on the high cycle fatigue, the first few cycles are not of particular interest. After a few cycles, the stress profile for the nanoscale element stabilizes (Fig. 1(b)). The stress amplitude on the nanoscale $\Delta\tau = \tau_{max} - \tau_{min}$ and the nanoscale stress ratio $R_\tau = \tau_{min}/\tau_{max}$ can thus be related to the stress amplitude $\Delta\sigma$ and the stress

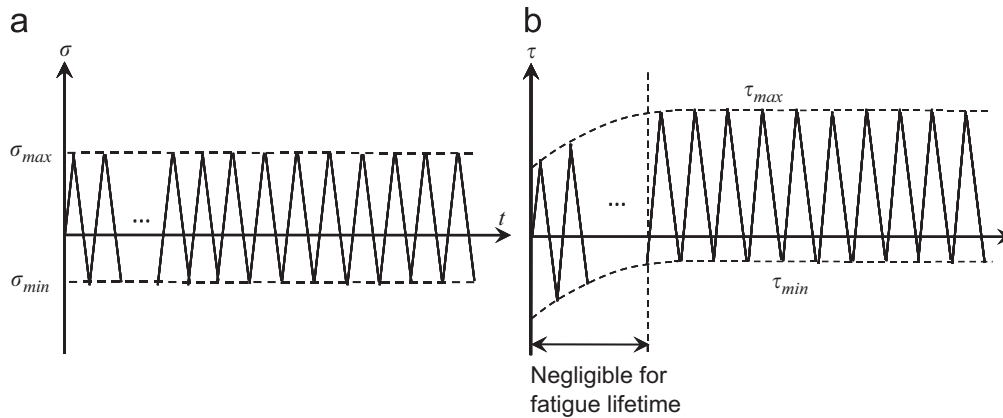


Fig. 1. (a and b) Stress-history at macro and nano-scales.

ratio R on the macroscale: $\Delta\tau = c_1\Delta\sigma$ and $R_\tau = c_2R$. Parameters c_1 and c_2 are empirical but could conceivably be determined through a detailed micro-mechanical analysis of the build-up of residual stresses.

Consider the fracture of a nano-element, either an atomic lattice block or a disordered nano-structure (Fig. 1 in Le et al., this issue, Part I). From the transition rate theory (Eqs. (4)–(6) of Part I), the frequency of failure of a nano-element under constant stress τ can be written as

$$f_a = v_T e^{-Q_0/kT} \left[\int_{\alpha_0}^{\alpha_c} V_a(\alpha) d\alpha \right] \frac{\tau^2}{E_1 kT} \quad (1)$$

where Q_0 is the dominant activation energy barrier on the free energy potential surface, k the Boltzmann constant, T the absolute temperature, and $v_T = kT/h$, $h = 6.626 \times 10^{-34}$ Js = Planck constant = (energy of a photon)/(frequency of its electromagnetic wave), where $V_a(\alpha)$ is the activation volume, α the relative crack length = a/l_a , a the effective crack length based on the equivalent linear elastic fracture mechanics, l_a the characteristic dimension of the nano-element, and E_1 the Young's elastic modulus of the nano-element.

For the cyclic stress at the nanoscale, $\tau = \tau(t)$, it may be assumed that the energy bias between two subsequent equilibrium states depends only on the current stress, but not on the stress history. Therefore, for a given number of cycles N_0 , the frequency of occurrence of failure events is

$$f_a = \frac{v_T e^{-Q_0/kT}}{N_0 t_c} \left[\int_{\alpha_0}^{\alpha_c} V_a(\alpha) d\alpha \right] \int_0^{N_0 t_c} \frac{\tau^2(t)}{E_1 kT} dt \quad (2)$$

where t_c the duration of each cycle. At the atomic scale, there is no residual stress build-up at the crack tip, and an applied compressive stress cannot cause any breakage of atomic bonds or any rupture of nano-particle connections. Therefore, the compressive stress does not contribute to the failure of the nano-element. For the stress history depicted in Fig. 1(b), Eq. (2) becomes

$$f_a = \frac{e^{-Q_0/kT}}{3E_1 h} \left[\int_{\alpha_0}^{\alpha_c} V_a(\alpha) d\alpha \right] (\tau_{max}^2 + \tau_{max} \langle \tau_{min} \rangle + \langle \tau_{min} \rangle^2) \quad (3)$$

where $\langle x \rangle = \max(x, 0)$. Since it is realistic to assume a quasi-steady process (Le et al., this issue), the failure probability P_f of the nano-element is proportional to the frequency of failure events. Therefore,

$$P_f \propto C_T f(R_\tau) \Delta\tau^2 = C_T f(R_\tau) (c_1 \Delta\sigma)^2 \quad (4)$$

where $f(R_\tau) = (1 + \langle R_\tau \rangle + \langle R_\tau \rangle^2) / (1 - R_\tau)^2$, $C_T = H_T \left[\int_{\alpha_0}^{\alpha_c} V_a(\alpha) d\alpha \right]$, and $H_T = e^{-Q_0/kT} / 3E_1 h$. Eq. (4) shows that the distribution of fatigue strength of a nano-element follows a power law with zero threshold.

3. Fatigue growth rate of subcritical crack at different scales

In the previous studies (Bažant et al., 2009; Le et al., 2009; Bažant and Le, 2009; Le et al., this issue), it was shown that the growth rate of subcritical crack provides a link between the cdf of monotonic strength and the cdf of creep lifetime. The cyclic crack growth law can provide the same, and it has also been used as the damage accumulation law (Christensen, 2008) to account for the cyclic loading history with varying loading amplitude.

In fatigue analysis, a realistic damage accumulation law is needed for all material scales involved in the multi-scale transition of the fatigue strength statistics (see the next section). Similar to the previous studies of lifetime (Bažant et al., 2009; Le et al., 2009), the crack growth rate law at RVE scale is again used to relate the probability distribution of fatigue strength and the probability distribution of fatigue lifetime. Based on the frequency of crack jumps in the nano-element,

the velocity of nano-crack growth under constant stress τ is (Eq. (27) of Le et al., this issue, Part I):

$$\dot{a} = \delta_a f_1 = v_1 e^{-Q_0/kT} K_a^2 \quad (5)$$

where $\dot{a} = da/dt$, K_a is the stress intensity factor of nano-element, $v_1 = \delta_a^2(\gamma_1 \alpha l_a)/E_1 h$, γ_1 the geometry constant such that $\gamma_1 a$ be the perimeter of the radially growing crack front, and δ_a the spacing of atoms or nano-particles. Consider now the case of cyclic stress. For each load cycle, the distance of nano-crack advance is given by $\delta a_{nano} = \int_0^{t_c} \dot{a}(t) dt$. So, the nano-crack growth rate per cycle can be written as

$$\frac{da}{dN} = v e^{-Q_0/kT} \Delta K_a^2 \quad (6)$$

where $v = v_1 t_c f(R_\tau)/3$. Therefore, the fatigue crack growth rate at nanoscale follows a power-law function of the stress amplitude with the exponent equal to 2. Furthermore, Eq. (6) also implies that the fatigue crack growth rate depends on the stress ratio for $R_\tau \geq 0$. For $R_\tau < 0$, the fatigue crack growth rate is independent of the stress ratio because the compressive stress does not contribute to the crack growth at the nanoscale. On the macroscale, extensive experimental observations document that the fatigue crack growth of quasibrittle materials follows the Paris law (e.g., Paris and Erdogan, 1963; Bažant and Planas, 1998; Bažant and Xu, 1991):

$$\frac{da}{dN} = A e^{-Q_0/kT} \Delta K^n \quad (7)$$

where A and n are the empirical parameters, and ΔK is the amplitude of the macroscale stress intensity factor.

Eq. (6) has the same form as the Paris law except for two features: (1) Parameter A of the Paris law is a function of the stress ratio only, but the parameter v in the equation for the fatigue crack growth rate at nanoscale is a function of both the stress ratio and the crack length. (2) The exponent of the power law for fatigue crack growth at nanoscale is 2, although experiments show that, for brittle as well as quasibrittle materials such as concrete and ceramics, the exponent is typically much higher, i.e., $n=10$ for concrete (Bažant and Xu, 1991), and $n=30$ for alumina ceramics (Ogawa, 1995) or zirconia dental ceramics (Studarta et al., 2007a) (while for metals typically $n=2$ to 4). As the macro-crack propagates under the fatigue loads, a fracture process zone (FPZ) forms at the crack tip (Fig. 2(a)). In that FPZ, the cyclic load produces microcracks. Compared to the FPZ under monotonic loading, the cyclic FPZ is expected to be narrower but longer. Since the size of cyclic FPZ does not change significantly as the fatigue crack propagates, the constant A must characterize the average of the growth rate of all the nanocracks with different lengths inside the cyclic FPZ. Hence, the constant A should not depend on the size of the macrocrack.

The difference between the exponents of the power-law for crack growth rates at the macro- and nano-scales is also found in the case of creep crack growth. In the recent studies (Bažant et al., 2009; Le et al., this issue, Part I), the power-law form of creep crack growth rate law with its high exponent value has been explained by considering the equality of nano and macro energy dissipation rates in the macro-FPZ. So, a similar approach will be used here. During each load cycle, the energy $\Delta \Pi^*$ dissipated in one load cycle by the macrocrack must be equal to the sum of the energies dissipated in that cycle by all the active nanocracks a_i ($i = 1, 2, \dots, N_a$) in the cyclic FPZ. This requires that

$$\Delta \Pi^* = \sum_{i=1}^{N_a} \Delta \Pi_i^* \quad (8)$$

Here the energy dissipation $\Delta \Pi_i^*$ for a nanocrack a_i during one load cycle can be expressed as

$$\Delta \Pi_i^* = \int_0^{t_c} \left(\frac{d\Pi_i^*}{dt} \right) dt = \int_0^{t_c} G \dot{a}_i dt = B_i(R_{\tau i}) e^{-Q_0/kT} \Delta K_{a_i}^4 \quad (9)$$

and

$$B_i(R_\tau) = \frac{v_i t_c (1 + \sum_{i=1}^4 \langle R_{\tau i} \rangle^i)}{5 E_i (1 - R_{\tau i})^4} \quad (10)$$

where K_{a_i} is the stress intensity factor of nanocrack a_i , E_i the elastic modulus of the nano-element containing the nanocrack a_i , and $v_i = \delta_a^2(\gamma_1 a_i)/E_i h$.

It is reasonable to expect that the amplitudes of the nanoscale stress intensity factors are roughly proportional to the amplitude of the macroscale stress intensity factor, i.e., $\Delta K_{a_i} = \omega_i \Delta K$ where ω_i are some constants. At the same time, the nanoscale stress ratios can be considered to be proportional to the macroscale stress ratio, i.e., $R_{\tau i} = c_i R$. Within the first few cycles, the residual stress field builds up and the stress on the cyclic FPZ gets stabilized. Thereafter, c_i will not vary significantly with the number of cycles. So, Eq. (8) may be re-written as

$$\Delta \Pi^* = e^{-Q_0/kT} \left[\sum_{i=1}^{N_a} \frac{v_i t_c (1 + \sum_{i=1}^4 \langle c_i R \rangle^i) \omega_i}{5 E_i (1 - c_i R)^4} \right] \Delta K^4 \quad (11)$$

The stress history of the cyclic FPZ is illustrated by the stress history of the nano-structure sketched in Fig. 1(b).

During each load cycle, the varying stress causes the macro-crack to propagate with a varying velocity. Since only structures that fail after very many load cycles are considered here, the variation of macro-crack velocity within one load

cycle is not of particular interest. What matters is the overall crack advance during one cycle. Hence, it is useful to consider the same crack under a constant load σ_e that would have the same rate of energy dissipation as the crack during one load cycle:

$$\Delta\Pi^* = \int_0^{t_c} \mathcal{G}\dot{a} dt = \mathcal{G}(\sigma_e)\Delta a \tag{12}$$

Here the stress intensity factor corresponding to σ_e can always be written as $K(\sigma_e) = \mu(R)\Delta K$. With Eq. (11), one thus obtains the rate of crack propagation per load cycle as

$$\frac{da}{dN} = e^{-Q_0/kT} \left[\sum_{i=1}^{N_a} \frac{B_i E}{\mu^2(R)} \right] \Delta K^2 \tag{13}$$

The number of active nanocracks N_a in the cyclic FPZ can be expressed in a multiscale framework. In the cyclic FPZ at the tip of the macro-crack, there are q_1 mesocracks, which have their own cyclic meso-FPZs. In each of these meso-FPZs, there are q_2 microcracks which contain their own cyclic micro-FPZs. In each of these micro-FPZs, there are q_3 sub-microcracks, etc., all the way down to the nanoscale. If there are s scales between the macro- and nano-scales, then the number of nanocracks in the macro-FPZ is

$$N_a = q_1 q_2 \dots q_s \tag{14}$$

Consider the cyclic FPZ at the i th material scale. During one load cycle, the load-deformation curve of the FPZ can be represented by Fig. 2(b). The energy dissipation during one load cycle is W_i , as shown by the area enclosed by the hysteresis loop in Fig. 2(b). It has been argued that the load-deformation hysteresis loop in the cyclic FPZ could be described by a constitutive law that does not depend on the maximum or the minimum loads (Fig. 2(c)) (Rice, 1967). Therefore, the energy dissipation per cycle, which governs the number of active sub-scale cracks in the cyclic FPZ, is a function of loading amplitude ΔP_i at i th material scale.

Since $\Delta P_i \propto \Delta K_i$, the number of active sub-scale cracks in the FPZ at i th material scale must be a function of ΔK_i , i.e., $q_i = \phi(\Delta K_i)$. It may be expected that there is no characteristic value of ΔK_i at which the function ϕ changes its behavior. Therefore, the function ϕ should be self-similar, i.e., a power law (Barenblatt, 2003), which gives $q_i \propto \Delta K_i^r$. Noting that the amplitude of the stress intensity factor for the FPZ at all the scales is approximately proportional to the macro-scale stress intensity factor ΔK , one obtains the number of active nanocracks inside the macroscale cyclic FPZ as

$$N_a = \kappa \Delta K^{rs} \tag{15}$$

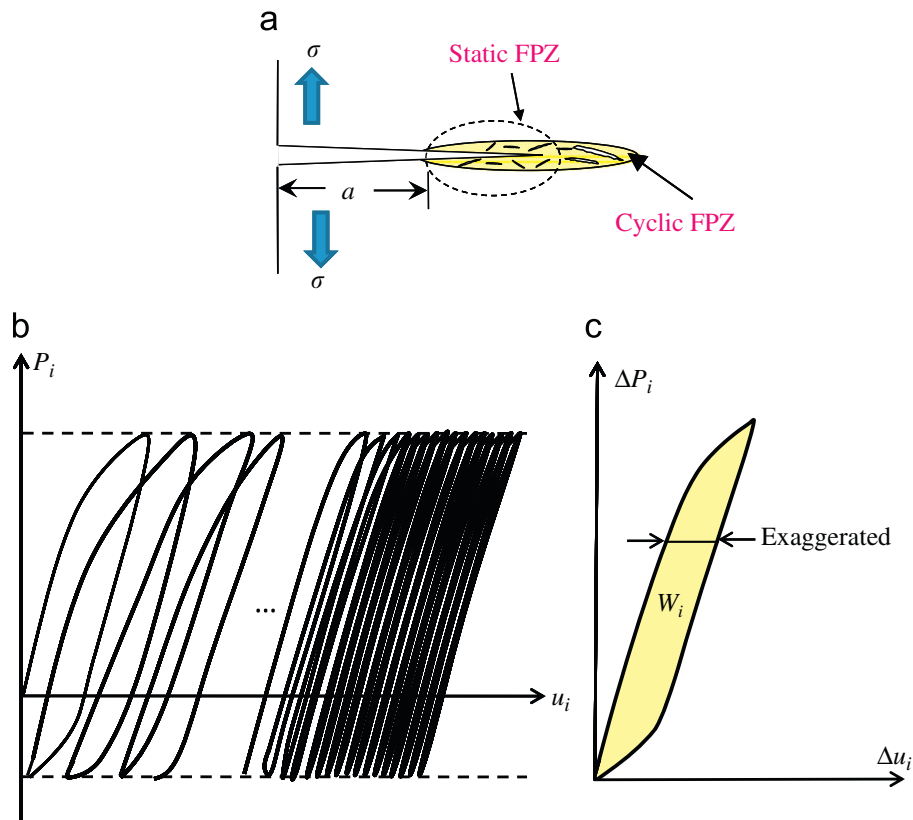


Fig. 2. (a) Cyclic fracture process zone, (b) and (c) Load-displacement curve of meso-scale cyclic FPZ.

It is obvious that N_a increases very rapidly as ΔK increases, whereas the ratio in the function B_i depends only weakly on ΔK . Therefore, one may replace v_i , c_i , E_i and ω_i by some effective mean values v_a , c_a , E_a and ω_a . By this replacement and with Eq. (15), one could re-write Eq. (13) as

$$\frac{da}{dN} = e^{-Q_0/kT} F(R) \Delta K^{rs+2} \tag{16}$$

where

$$F(R) = \frac{v_a t_c E \omega_a (1 + \sum_{i=1}^4 \langle c_a R \rangle^i)}{5 E_a (1 - c_a R)^4 \mu^2(R)} \tag{17}$$

Setting $rs + 2 = n$, one obtains the Paris law for fatigue crack growth rate, Eq. (16). The present analysis shows that the exponent of Paris law at nanoscale is 2, and the exponent increases to $n \approx 10\text{--}30$ at macroscale. The reason is that the number of active nanocracks in the macro-cyclic FPZ rapidly increases with the applied stress amplitude.

It has been documented that the growth rate of fatigue cracks mildly depends on the stress ratio (Bažant and Planas, 1998; Andersons et al., 2004). The present analysis implies such dependence, though not in a precise explicit manner.

It must be emphasized that the present analysis is based on certain hypotheses about the self-similarity of the function ϕ . Plausible though they seem to be, they do not lead to a rigorous mathematical proof. Experimental verification, based on other predictions of the theory, especially the size effect, is essential.

The characteristics of self-similarity are expected to hold for a wide range of medium stress amplitudes but not for very small or very large amplitudes. In fact, the growth rate of fatigue cracks is known to deviate from the power-law form for very small or very large stress amplitude, as confirmed by many experiments (Bažant and Planas, 1998; Andersons et al., 2004; Ogawa, 1995; Studarta et al., 2007a). For small stress amplitudes, the reason may be that the distinction between the static and cyclic FPZs gets blurred. For very large amplitudes, the reason may be that the maximum stress intensity factor during the load cycle is approaching the fracture toughness (Suresh, 1998), at which the crack propagates dynamically. However, the practical interest usually falls into the medium amplitude range.

Bažant and Xu (1991) observed the crack growth in a series of geometrically similar notched concrete beams under fatigue loading. The subsequent effective crack lengths were determined from the measured stiffness values. A marked size effect on the Paris law was observed (Fig 3(a)). The following size-dependent Paris law has been proposed (Bažant and Xu, 1991):

$$\frac{da}{dN} = A' \left(1 + \frac{D_0}{D}\right)^{n/2} \Delta K^n \tag{18}$$

where D_0 is a constant characterizing both the material property and specimen geometry, D the size (or characteristic dimension) of the structure, and A' an empirical constant. As for exponent n , Fig. 3a suggests that it decreases slightly with the structure size D and may be approximately considered as constant ($n=10.6$). This seems to be a general feature of quasibrittle materials, whereas the tests on metals show n to increase with D (Barenblatt and Botvina, 1981; Ritchie, 2005). But since Eq. 18 is here used only at the RVE level, the size dependence of n is not of concern here. Optimum fitting of experimental data (Fig. 3(a)) with Bažant's size effect law with parameters determined from LFM functions (Bažant and Planas, 1998; Bažant, 2005) indicated that the FPZ at load cycling with the amplitude of 80% of the maximum monotonic load is about 10 times longer than it is for monotonic loading. Such a big difference in the FPZ size needs to be further verified by numerical simulations with, e.g., the lattice-particle model.

Similar to the size effect on the Paris law, it has been experimentally observed that the threshold of stress intensity factor amplitude, at which the crack growth rate becomes too slow to discern, is also subjected to a size effect (Kitagawa and Takahashi, 1976; Tanaka et al., 1981). If we assume that there is a threshold value of the fatigue growth rate v_{th} which cannot be experimentally detected (Suresh, 1998), then Eq. (18) leads to

$$A' \left(1 + \frac{D_0}{D}\right)^{n/2} \Delta K_{th}^n = v_{th} \tag{19}$$

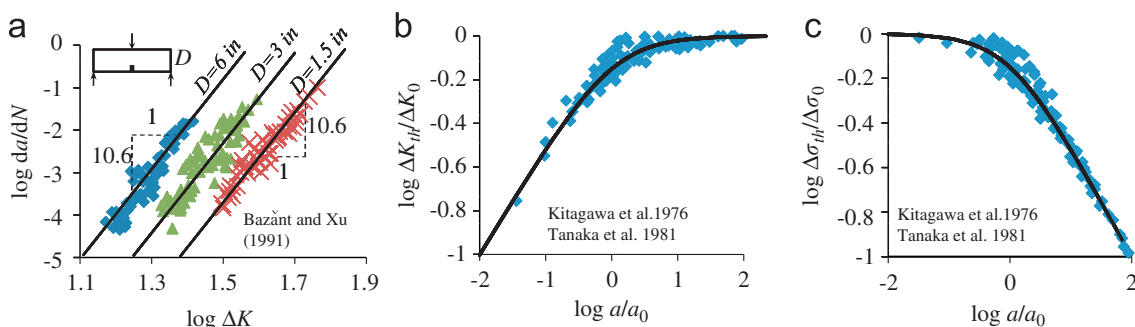


Fig. 3. (a) Size effect on the fatigue crack growth rate, (b) and (c) Size effect on the threshold of stress intensity factor amplitude.

$$\text{or : } \frac{\Delta K_{th}}{\Delta K_0} = \frac{1}{\sqrt{1+D_0/D}} \tag{20}$$

$$\text{or : } \frac{\Delta \sigma_{th}}{\Delta \sigma_0} = \frac{1}{\sqrt{1+D_0/D}} \tag{21}$$

where $\Delta K_0 = (v_{th}/A)^{1/n}$, $\Delta \sigma_0 = \Delta K_0 D_0^{-1/2} k(\alpha)^{-1}$, $k(\alpha)$ is the dimensionless stress intensity factor. Figs. 3(b) and (c) show that Eqs. (19) and (20) agree well with the measured size effect on the threshold of stress intensity factor amplitude for various engineering alloys (Kitagawa and Takahashi, 1976; Tanaka et al., 1981). The original data were referred to the initial crack length a_0 , which can be considered as the characteristic dimension, D , of the structure (a_0 was much smaller than the specimen size).

4. Multi-scale transition of statistics of fatigue strength

To relate the probability distributions of fatigue strength at nano- and macro-scales, a certain approximate statistical multiscale transition framework is required. The capability of numerical simulations of the multi-scale transition of statistics is limited, for two reasons: (1) the uncertainties in the physical laws across various scales are difficult to quantify (Graham-Brady et al., 2006; Williams and Baxer, 2006), and (2) our interest in the far-out tail probability ($P_f < 10^{-6}$) would require at least 10^8 simulations, which is currently beyond conventional computational means (methods such as the importance sampling would not help because they depend on a prior hypothesis about the tail; Bažant et al., 2007).

In the previous studies (Bažant and Pang, 2006, 2007; Le et al., this issue), the multiscale transition of strength distribution is represented by a hierarchical model (Fig. 3c in the preceding paper Le et al., this issue), which consists of series couplings (the chain model) and parallel couplings (the fiber bundle model). Physically, the parallel coupling represents the load re-distribution mechanisms at different scales as well as the condition of compatibility between one scale and its sub-scale. The series model represents (in the sense of the weakest-link model) the localization of damage at each scale.

4.1. Chain model

Consider a chain of elements (or links) subjected to cyclic loading with a prescribed number of cycles and stress ratio. The fatigue strength $\Delta \sigma_c$ of the chain, i.e., the critical stress amplitude that leads to failure, is determined by the smallest fatigue strength of all the elements. Since the chain survives if and only if all its elements survive, one can calculate the survival probability of the chain, $1 - P_f$, from the joint probability theorem. Assuming that the random fatigue strengths of the elements are statistically independent, one concludes that the failure probability of the chain with n_c elements is

$$P_{f,chain}(\Delta \sigma_c) = 1 - \prod_{i=1}^{n_c} [1 - P_i(\Delta \sigma_c)] \tag{22}$$

Using this equation and the same method as used in Bažant and Pang (2007) for static loads, one can easily prove for cyclic loading two essential asymptotic properties of the chain model: (1) If the cdf's of fatigue strengths of all the elements have a power-law tail of exponent p , then the cdf of fatigue strength of the whole chain has also a power-law tail and its exponent is also p ; and (2) when n_c is large enough, the cdf of fatigue strength of the chain approaches the Weibull distribution $P_f = 1 - e^{-n_c(\Delta \sigma_c/s_0)^p}$, where s_0 is a scaling constant.

4.2. Bundle model

Part I of this paper Le et al. (this issue) investigates the strength distribution of a bundle model with softening elements (Fig. 3(b) in Le et al., this issue). In Part II, we are interested in the cdf of the fatigue strength $\Delta \sigma_b$ of the bundle for a prescribed stress ratio R and a given number of cycles N_0 . We will analyze some asymptotic properties of this cdf by considering a bundle with two elements having random strength and the same cross section, although a generalization to any number of elements in the bundle would be straightforward.

Consider a bundle under cyclic loading with a prescribed stress ratio R . For a given stress ratio R and for N_0 loading cycles, the fatigue strength $\Delta \sigma_i$ ($i=1, 2$) of the elements is assumed to be known. The elements are numbered so that $\Delta \sigma_1 < \Delta \sigma_2$. Fig. 4(a-c) shows the loading histories of both the bundle and its two elements. The bundle reaches its strength limit and fails at the N_0 th cycle. After the first N_1 cycles, the first element fails and the second element carries the entire load for the remaining $N_0 - N_1$ cycles.

The first element is subjected to a cyclic load with stress amplitude $\Delta \sigma_b$ and stress ratio R . Under cyclic load, some subcritical crack inside the element grows from its original length a_0 to a critical length a_c at which the first element fails. The growth rate of the subcritical crack can be described by the Paris law (Eqs. (7) or (16)). By separating the variables and integrating the Paris law from the original crack length to the length a_c , one obtains

$$\Delta \sigma_b^{n_e} N_1 = e^{Q_0/kT} I_1 \tag{23}$$

where n_e is the exponent of the Paris law for one element, $I_1 = A^{-1} l_{e1}^{1-n_e/2} \int_{\alpha_0}^{\alpha_c} k_{e1}^{-n_e}(\alpha) d\alpha$, l_{e1} the characteristic size of the first element, $\alpha = a/l_e =$ relative crack length and k_{e1} the dimensionless stress intensity factor of the first element. It is clear that, for a particular element, I_1 must be a constant for different cyclic loads as long as the stress ratio is kept constant.

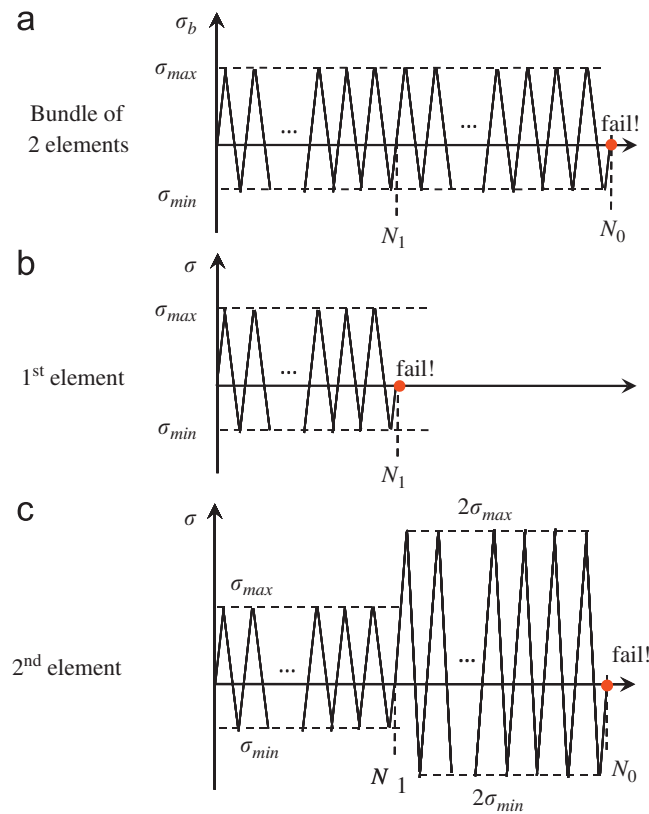


Fig. 4. (a–c) Loading history of bundle and its fibers.

Therefore, one can easily obtain the critical number of cycles N_1 of the first element in terms of its fatigue strength:

$$N_1 = N_0 \Delta\sigma_1^{n_e} / \Delta\sigma_b^{n_e} \quad (24)$$

The second element experiences, for the first N_1 cycles, the same load history as the first element does. After the first element fails, the stress in the second element doubles, i.e., the stress amplitude becomes $2\Delta\sigma_b$, because both elements have the same elastic stiffness and the same deformation. However, the stress ratio in the second element still remains to be R . The second element eventually fails at N_0 th cycle (Fig. 4(c)). Therefore, one can integrate the Paris law for the second element taking into account its increased stress amplitude:

$$\Delta\sigma_b^{n_e} N_1 + (2\Delta\sigma_b)^{n_e} (N_0 - N_1) = e^{Q_0/kT} I_2 \quad (25)$$

where $I_2 = A^{-1} l_{e2}^{1-n_e/2} \int_{a_0}^{a_c} k_{e2}^{-n_e}(\alpha) d\alpha$; l_{e2} is the characteristic size of the second element, and k_{e2} the dimensionless stress intensity factor of the second element. Similar to the analysis for the first element, one can replace $e^{Q_0/kT} I_2$ of the second element by $\Delta\sigma_2^{n_e} N_0$. Therefore,

$$\Delta\sigma_b^{n_e} N_1 + (2\Delta\sigma_b)^{n_e} (N_0 - N_1) = \Delta\sigma_2^{n_e} N_0 \quad (26)$$

Substituting Eq. (24) into Eq. (26), one can express the fatigue strength of the bundle as a function of the fatigue strengths of each element:

$$\Delta\sigma_b = [\Delta\sigma_1^{n_e} (1 - 1/2^{n_e}) + \Delta\sigma_2^{n_e} / 2^{n_e}]^{1/n_e} \quad (27)$$

If the fatigue strength of the bundle does not exceed a certain value S , then the fatigue strengths of elements are bounded by the region $\Omega_2(S)$ shown as Fig. 5. Assuming that the fatigue strengths of two elements are independent random variables, then the cdf of fatigue strength of the bundle is given by

$$G_2(S) = 2 \int_{\Omega_2(S)} f_1(\Delta\sigma_1) f_2(\Delta\sigma_2) d\Delta\sigma_1 d\Delta\sigma_2 \quad (28)$$

where f_i is the probability density function (pdf) of the fatigue strength of the i th element ($i=1,2$).

The foregoing analysis can be readily extended to a bundle with n_b elements. Eq. (27) can be generalized as

$$\Delta\sigma_b = \left\{ \sum_{i=1}^{n_b} [\beta_i(n_e) \Delta\sigma_i]^{n_e} \right\}^{1/n_e} \quad (29)$$

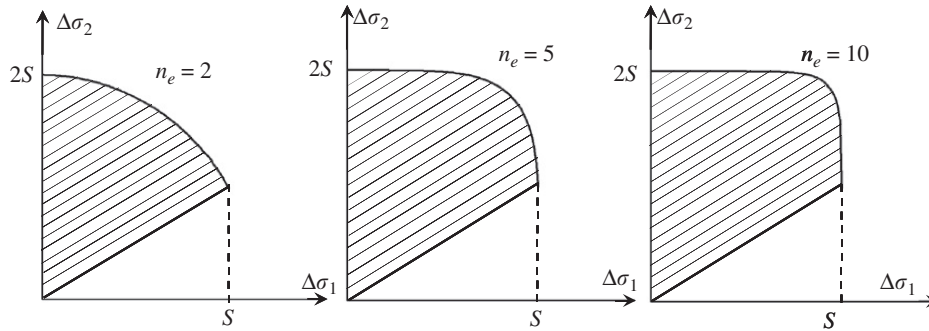


Fig. 5. Feasible region of fatigue strengths.

where $\beta_i(n_e) = [(n_b - i + 1)^{n_e} / n_b^{n_e} - (n_b - i)^{n_e} / n_b^{n_e}]^{1/n_e}$. One can easily show that $\beta_i = 1/n_b$ for $n_e = 1$, and $\beta_i = (n_b - i + 1)/n_b$ for $n_e \rightarrow \infty$. The cdf of fatigue strength of the bundle can then be written as

$$G_{n_b}(S) = n_b! \int_{\Omega_{n_b}(S)} \prod_{i=1}^{n_b} f_i(\Delta\sigma_i) d\Delta\sigma_1 d\Delta\sigma_2 \dots d\Delta\sigma_{n_b} \tag{30}$$

Here $\Omega_{n_b}(S)$ is the feasible region of fatigue strengths of in all the elements, which is defined by the following inequalities:

$$\left[\sum_{i=1}^{n_b} \beta_i(n_e) \Delta\sigma_i^{n_e} \right]^{1/n_e} \leq S \tag{31}$$

$$\Delta\sigma_1 \leq \Delta\sigma_2 \leq \dots \leq \Delta\sigma_{n_b-1} \leq \Delta\sigma_{n_b} \tag{32}$$

Two important asymptotic properties of the cdf of fatigue strength of the bundle are of particular interests. The first is the type of cdf of fatigue strength of large bundles. Consider the following two extreme values of n_e :

- 1) When $n_e = 1$, the fatigue strength of the bundle is simply the sum of the fatigue strengths of all the elements. This is the same as the mathematical representation of the cdf of strength of a plastic bundle, in which each element deforms at constant stress after its strength limit is reached. By virtue of the Central Limit Theorem, the cdf of fatigue strength must follow the Gaussian distribution except for its far left tail.
- 2) When $n_e \rightarrow \infty$, the fatigue strength of the bundle may be written as

$$\Delta\sigma_b = \max \left[\Delta\sigma_1, \frac{n_b-1}{n_b} \Delta\sigma_2, \dots, \frac{1}{n_b} \Delta\sigma_{n_b} \right] \tag{33}$$

where $\Delta\sigma_1, \Delta\sigma_2, \dots, \Delta\sigma_{n_b}$ are the fatigue strengths of the elements ordered according to the sequence of their breaks, i.e., according to increasing strength. This is the same as the mathematical formulation of the cdf of strength of a brittle bundle, in which the stress in each element drops to zero as soon as its strength limit is reached. The strength distribution of a brittle bundle can be described by the recursive equation of Daniels (1945), who further showed that the monotonic strength distribution of brittle bundles approaches the Gaussian distribution as the number of elements tends to infinity.

Therefore, one may expect that the cdf of fatigue strength of large bundles should approach the Gaussian distribution for any value of $n_e \geq 1$. Also, the rate of convergence to the Gaussian distribution should be bounded by the rates of convergence to the Gaussian distribution for the brittle and plastic bundles, which are $O(n_b^{-1/3} (\log n_b)^2)$ (Smith, 1982) and $O(n_b^{-1/2})$ (Bažant and Pang, 2007), respectively.

Another important property is the tail of the cdf of fatigue strength of the bundle. Let us assume that the fatigue strength of each element has a cdf with a power-law tail, i.e., $P_i(\Delta\sigma) = (\Delta\sigma/s_0)^{p_i}$. Considering the transformation $y_i = \Delta\sigma_i/s_0$, we can re-write Eq. (30) as

$$G_{n_b}(S) = n_b! S^{p_1 + p_2 + \dots + p_{n_b}} \int_{\Omega_{n_b}(1)} \left(\prod_{i=1}^{n_b} \frac{p_i y_i^{p_i-1}}{s_0^{p_i}} \right) dy_1 dy_2 \dots dy_{n_b} \tag{34}$$

where $\Omega_{n_b}(1)$ is the corresponding feasible region of the normalized fatigue strength. Thus it is proven that, if the fatigue strength of each element has a cdf with a power-law tail, then the cdf of fatigue strength of the bundle will also have a power-law tail, and the power-law exponent will be the sum of the exponents of the power-law tails of the cdf's of fatigue strength of all the elements in the bundle. As shown in Part I (Le et al., this issue), this tail property also holds true for the cdf of monotonic strength of bundles consisting of elements with arbitrary load-sharing rules.

The reach of the power-law tail is also an important property (Bažant and Pang, 2007). Based on the aforementioned two extreme cases ($n_e = 1$ and $n_e \rightarrow \infty$), the reach of the power-law tail of cdf of fatigue strength of the bundle can be

estimated. The mathematical representation of the cdf of fatigue strength of bundle is the same as the mathematical representation of the cdf of strength of a plastic bundle for $n_e=1$, or a brittle bundle for $n_e \rightarrow \infty$. As previously shown (Bažant and Pang, 2007), the reach of the power-law tail of the cdf of strength of a bundle rapidly decreases with an increasing number n_b of elements, and does so at the rate of $(P_{t1}/n_b)^{n_b}$ for a plastic bundle and at the rate of $(P_{t1}/n_b)^{n_b} - (P_{t1}/3n_b)^{n_b}$ for a brittle bundle, where P_{t1} is the reach of the power-law tail of the cdf of fatigue strength of one element. Therefore, one may expect that, for $n_e \geq 1$, the reach of the power-law tail will shrink with an increasing number of elements at the rate of $(P_{t1}/n_b)^{n_b} - (P_{t1}/3n_b)^{n_b}$.

4.3. Probability distribution of fatigue strength of one RVE

Recent studies (Bažant and Pang, 2006, 2007) showed that the representative volume element (RVE) can statistically be represented by a hierarchical model consisting of bundle of chains, each of which consists of sub-bundles of sub-chains, each of which consists of sub-sub-bundles of sub-sub-chains, etc., down to nano-scale elements (Fig. 3(c) in Le et al., this issue). No more than two chains can be coupled in parallel to prevent the reach of the power-law tail from being too short, and the chains must be long enough to extend the reach of the tail. The hierarchical model from Fig. 3(c) in Le et al. (this issue) may now be used to calculate the cdf of fatigue strength of one RVE.

The cdf of fatigue strength of each sub-chain can be calculated from the joint probability theorem (Eq. (22)). For the cdf of fatigue strength of sub-bundles, one must specify the exponent of the Paris law. Based on the aforementioned analysis of the multi-scale transition of fracture kinetics, the exponent of the Paris law must be equal to 2 at the nanoscale and then increase through the higher scales. Comparing the foregoing derivations of the cdf's of the fatigue and monotonic strengths of bundles, one would expect that the cdf of fatigue strength of a bundle at the nanoscale should be similar to the cdf of monotonic strength of a plastic bundle, while the cdf of fatigue strength of a bundle at an upper scale should be similar to the cdf of strength of a brittle bundle.

Fig. 6(a) and (b) display the calculated cdf of fatigue strength of one RVE on the Weibullian and Gaussian probability papers, respectively. On the Weibull scale (Fig. 6(a)), the lower portion of the calculated cdf of fatigue strength is seen to be a straight line, which represents the Weibull distribution (whose tail is a power-law). This result is consistent with the conclusion of the foregoing analysis: In the chain and bundle models, the power-law tail of cdf of fatigue strength is indestructible.

The upper part of the calculated cdf begins to diverge from the straight line at $P_f \approx 3 \times 10^{-4}$. Hence the cdf core does not follow the Weibull distribution. As shown in Fig. 6(b), the upper portions of the cdf's can be fitted quite closely by straight lines on the Gaussian probability paper. Therefore, the cdf of fatigue strength of one RVE can be approximately described by a Gaussian distribution with a Weibull tail grafted on the left at the probability of about $10^{-4} - 10^{-3}$, which can be mathematically described as follows:

$$P_1(\Delta\sigma_f) = 1 - e^{-(\Delta\sigma_f/s_0)^m} \quad (\Delta\sigma_f \leq \Delta\sigma_{gr}) \tag{35}$$

$$P_1(\Delta\sigma_f) = P_{gr} + \frac{r_f}{\delta_G \sqrt{2\pi}} \int_{\Delta\sigma_{gr}}^{\Delta\sigma_f} e^{-(\sigma' - \mu_c)^2 / 2\delta_c^2} d\sigma' \quad (\Delta\sigma_f > \Delta\sigma_{gr}) \tag{36}$$

Here $\Delta\sigma_f$ is the nominal fatigue strength, which is a critical load parameter of the dimension of stress; $\Delta\sigma_f = c_n \Delta P_m / bD$ or $c_n \Delta P_m / D^2$ for two- or three-dimensional scaling; ΔP_m is the maximum load amplitude under which the structure fails for a given number of cycles N_0 and a prescribed stress ratio R ; c_n the parameter chosen such that $c_n P / bD$ or $c_n P / D^2$ represent the maximum principal stress in the structure; b the structure thickness in the third dimension; D the characteristic

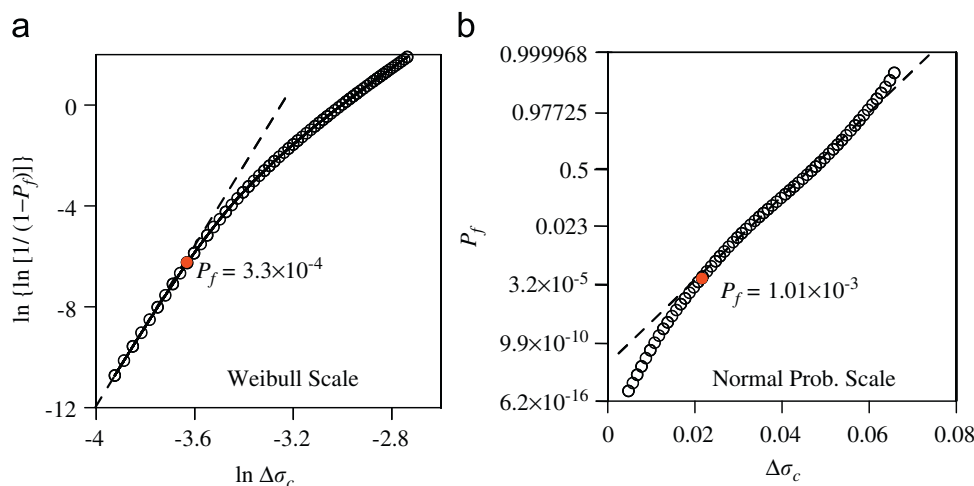


Fig. 6. (a and b) Calculated cdf of fatigue strength of one RVE.

structure dimension or size; m is the Weibull modulus (equal to the tail exponent); s_0 the scale parameter of the Weibull tail; μ_G and δ_G are the mean and standard deviations of the Gaussian core if $\Delta\sigma_f$ is considered extended to $-\infty$; r_f the scaling parameter required to normalize the grafted cdf such that $P_1(\infty)=1$; and P_{gr} the grafting probability $=1-\exp[-(\Delta\sigma_{gr}/s_0)^m]$. Finally, continuity of the probability density function at the grafting point requires that $(dP_1/d\Delta\sigma_f)|_{\Delta\sigma_{gr}^+} = (dP_1/d\Delta\sigma_f)|_{\Delta\sigma_{gr}^-}$.

Note that, for one RVE, the cdf of fatigue strength has a similar form as the cdf of monotonic strength as calculated in the preceding paper (Le et al., this issue). The locations of grafting points P_f of these two cdf's are similar, too. The reason is that the chain models for fatigue strength and monotonic strength share the same equation, and that the formulations of the bundle models for the fatigue strength and the monotonic strength are analogous.

5. Probabilistic distribution of fatigue lifetime

Now consider the tests of fatigue strength and fatigue lifetime made on the same RVE. In the fatigue strength test, the RVE is subjected to a cyclic load with a prescribed number of cycles N_0 and a given stress ratio R , and the critical load amplitude (i.e., the fatigue strength $\Delta\sigma_f$), at which the RVE fails, is recorded. In the fatigue lifetime test, the load amplitude ΔP_0 and the stress ratio R are prescribed, and recorded is the critical number of cycles N_f at which the RVE fails.

The cyclic failure of the RVE consists of two stages: (1) crack initiation and (2) crack propagation. In this study, we consider the growth of the dominant subcritical crack in the RVE. In the crack initiation stage, this dominant subcritical crack represents the distributed damage based on the equivalent linear elastic fracture mechanics. An RVE fails under cyclic load when the dominant subcritical crack grows from its original length a_0 to a critical length a_c .

The growth rate of this subcritical crack follows the Paris law (Eq. (7)). By separation of variables,

$$\Delta\sigma^n N = \int_{\alpha_0}^{\alpha_c} \frac{d\alpha}{Ak^n(\alpha)l_0^{n-1}} \tag{37}$$

where $\Delta\sigma = (P_{max}-P_{min})/bl_0$ is the nominal stress amplitude, $\alpha = a/l_0$ the dimensionless crack size, $k(\alpha)$ the dimensionless stress intensity factor of the RVE, and l_0 the RVE size. Applying Eq. (37) to the tests of both fatigue strength and fatigue lifetime, one can relate the fatigue strength for the given number of cycles to the fatigue lifetime N_f for the given load amplitude:

$$\Delta\sigma_f = \Delta\sigma_0(N_f/N_0)^{1/n} \tag{38}$$

Although the Paris law has been here physically justified as a mean behavior, it is now used for one RVE to link the randomness of fatigue strength and of fatigue lifetime. This is a simplification. Eq. (37) implies that the randomness of fatigue strength or fatigue lifetime is caused by the randomness of the dominant subcritical crack, whereas the dominance of cracks is determined by their geometry, size and local fracture energy. This is consistent with the conclusion drawn from the random particle model (Grassl and Bažant, 2009).

Note that the foregoing analysis is valid only for the case of constant loading amplitude. For variable amplitude fatigue, the crack growth rate is strongly influenced by the load history. For instance, single tensile overloads or high amplitude–low amplitude block loading sequences can retard the crack advance (Suresh, 1998). The present framework can possibly be extended to variable amplitude fatigue provided that the effects of stress ratio and load history on the crack growth rate are explicitly known. However, this is a more complicated subject, which is beyond the scope of this paper.

Substituting Eq. (38) into Eqs. (35) and (36), one obtains the probability distribution of fatigue lifetime of one RVE:

$$\text{for } N_f < N_{gr} : P_1(N_f) = 1 - \exp[-(N_f/s_N)^{\bar{m}}]; \tag{39}$$

$$\text{for } N_f \geq N_{gr} : P_1(N_f) = P_{gr} + \frac{r_f}{\delta_G \sqrt{2\pi}} \int_{\gamma N_{gr}^{1/n}}^{\gamma N_f^{1/n}} e^{-(N' - \mu_G)^2 / 2\delta_G^2} dN' \tag{40}$$

where $\gamma = \Delta\sigma_0 N_0^{-1/n}$, $N_{gr} = (\Delta\sigma_{gr}/\Delta\sigma_0)^n N_0$, $s_N = s_0^n N_0 \Delta\sigma_0^{-n}$, and $\bar{m} = m/n$. Similar to the cdf of fatigue strength, the tail probability distribution of fatigue lifetime follows the Weibull distribution, which has a power-law tail. The core of the cdf of fatigue lifetime, which is expressed by Eq. (40), does not follow the Gaussian distribution.

For structures that fail at the initiation of a macro-crack from one RVE, the RVE must be defined as the smallest material volume whose failure triggers the failure of the structure. Statistically, such structures can be modelled as a chain of RVEs. According to the joint probability theorem and the assumption that the fatigue lifetimes of the RVEs are independent random variables, the cdf of structure lifetime under a prescribed cyclic load can be written as

$$P_f(N_f, \Delta\sigma_0) = 1 - \prod_{i=1}^{n_s} [1 - P_1(N_f, \Delta\sigma_0 s(\mathbf{x}_i))] \tag{41}$$

$$\text{or } \ln(1 - P_f) = \sum_{i=1}^{n_s} \ln[1 - P_1(N_f, \Delta\sigma_0 s(\mathbf{x}_i))] \tag{42}$$

where n_s is the number of RVEs in the structure, $\Delta\sigma_0 s(\mathbf{x}_i)$ the amplitude of maximum principal stress at the center of the i th RVE, $\Delta\sigma_0$ the amplitude of maximum principal stress in the structure, and $s(\mathbf{x}_i)$ the dimensionless stress field (such that $\max s(\mathbf{x}_i) = 1$). Here we assume that the amplitudes of the minor and medium principal stresses are fully statistically correlated to the maximum one. If they were uncorrelated, each principal stress amplitude would require a separate element in the chain.

For sufficiently large structures, the tail part of the lifetime cdf of one RVE determines the failure of the entire structure. The approximation $\ln(1-x) = -x$ then furnishes the cdf of fatigue lifetime of large structures:

$$P_f(N_f) = 1 - \exp \left[- \left(\int_V s(\mathbf{x}_i)^{n_m} \frac{dV(\mathbf{x})}{V_0} \right) \left(\frac{N_f}{S_N} \right)^m \right] \quad (43)$$

where $V_0 = l_0^3$ is the RVE size. Eq. (43) indicates that the cdf of fatigue lifetime of large-size structures follows the Weibull distribution. This distribution corresponds to the perfectly brittle failure behavior, to which the extreme value statistics (or infinite weakest-link model) apply. Based on this distribution, one may conveniently define an equivalent number of RVEs as $N_{eq,N_f} = \int_V s(\mathbf{x}_i)^{n_m} dV(\mathbf{x})/V_0$, which represents the number of RVEs for which a chain of N_{eq,N_f} elements subjected to a uniform stress amplitude $\Delta\sigma_0$ gives the same lifetime cdf as Eq. (41) does.

For structures of intermediate and small sizes, the cdf of fatigue lifetime does not follow the Weibull distribution. Then the equivalent number of RVEs depends on the failure probability. Therefore, one must rely on the original equation of the weakest-link model (Eq. (41)). In the preceding paper (Le et al., this issue), a nonlocal boundary layer model is adopted to calculate the cdf's of strength and creep lifetime of structures with general geometry (Eq. (26) of the preceding paper (Le et al., this issue)). This method is now used for the probability distribution of fatigue lifetime. The logarithmic form of the finite chain model (Eq. (42)) can then be re-written as

$$\ln[1 - P_f(\Delta\sigma_0, N_f)] = \frac{l_0}{V_0} \int_{\Omega_M} \ln\{1 - P_1[s(\mathbf{x}_M)\Delta\sigma_0, N_f]\} d\Omega + \int_{V_l} \ln\{1 - P_1[\bar{s}(\mathbf{x})\Delta\sigma_0, N_f]\} \frac{dV(\mathbf{x})}{V_0} \quad (44)$$

where P_1 is the cdf of fatigue lifetime of one RVE for a given stress amplitude, and $\bar{s}(\mathbf{x})\Delta\sigma_0$ the amplitude of nonlocal stress for one RVE. For very large structures, the boundary layer becomes negligible compared to the structure size and the nonlocal stress in the interior becomes the local stress. Therefore, Eq. (44) eventually leads to Eq. (43).

6. Optimum fits of fatigue lifetime histograms

Experimental studies of statistics of fatigue lifetime have been pursued for decades. The two-parameter Weibull distribution has been widely used to fit the observed histograms (Studarta et al., 2007a,b; Hoshide, 1995; Bigleya et al., 2007), but significant deviations have consistently been found.

Fig. 7 presents the optimum fits of lifetime histograms of various quasibrittle structures, such as ceramics and cortical bones, by both the two-parameter Weibull distribution and the present theory. The experiments are summarized as follows: (a)–(e) Structural alumina ceramics (99% Al_2O_3): Round bar specimens were tested under fully reversed cyclic load produced by a rotating bending machine (Sakai and Fujitani, 1989; Sakai and Hoshide, 1995). Five stress levels were used and 20 specimens were tested for each stress level. (f) and (g) Dental ceramic composites: Glass infiltrated Al_2O_3 – ZrO_2 with feldspathic glass (Inc-VM7) (Fig. 7f) and yttria-stabilized ZrO_2 with feldspathic glass (TZP-CerS) (Fig. 7(g)). For each material, 30 specimens with size 4 mm \times 5 mm \times 50 mm were tested under fully reversed cyclic bending (Studarta et al., 2007a, 2007b). (h) and (i) Equine cortical bones: Specimens of different sizes, with dimensions 10.5 mm \times 10 mm \times 3 mm (Fig. 7(h)) and 21 mm \times 10 mm \times 3 mm (Fig. 7(i)), were extracted from 14 race horses with ages between 2 and 6 years. For each size, six specimens were subjected to direct tensile cyclic loads (Bigleya et al., 2007). Since these specimens came from different horses, the statistical parameters obtained from the histogram fitting represent average values for the tested group of horses.

As seen in Fig. 7, the lifetime histograms do not follow a straight line on the Weibull scale. Instead, they consist of two parts separated by a kink. The lower part of the histogram follows a straight line, whereas the upper part of the histogram diverges to the right from the straight line. Clearly, the two-parameter Weibull distribution cannot fit such histograms closely. On the other hand, the present theory gives an excellent fit for both parts of the histogram.

The Weibull modulus is determined by the slope of the lower part of the histogram, which can be much larger than the Weibull modulus obtained by using the Weibull distribution to fit the entire histogram. This makes a large difference for very low failure probability such as 10^{-6} . Furthermore, the present theory can match quite well the location of the kink, which characterizes the quasi-brittleness of structure.

To improve the fits, the three-parameter Weibull distribution, which has a finite threshold, has also been adopted for fatigue lifetime (Sakai and Hoshide, 1995). However, for monotonic strength, significant deviations to the right have been found in the high probability range provided that a sufficient number of specimens (at least 500) have been tested (e.g., Weibull, 1939).

Unfortunately, for the cdf of fatigue lifetime, the number of specimens for histogram testing has typically been small (about 30). In that case, the deficiency of the three-parameter Weibull distribution cannot be observed experimentally. Nevertheless, its use is unsound for other reasons. For example, it implies that a cyclic load below a certain threshold will never lead to failure. This contradicts the well-established transition rate theory with random walk

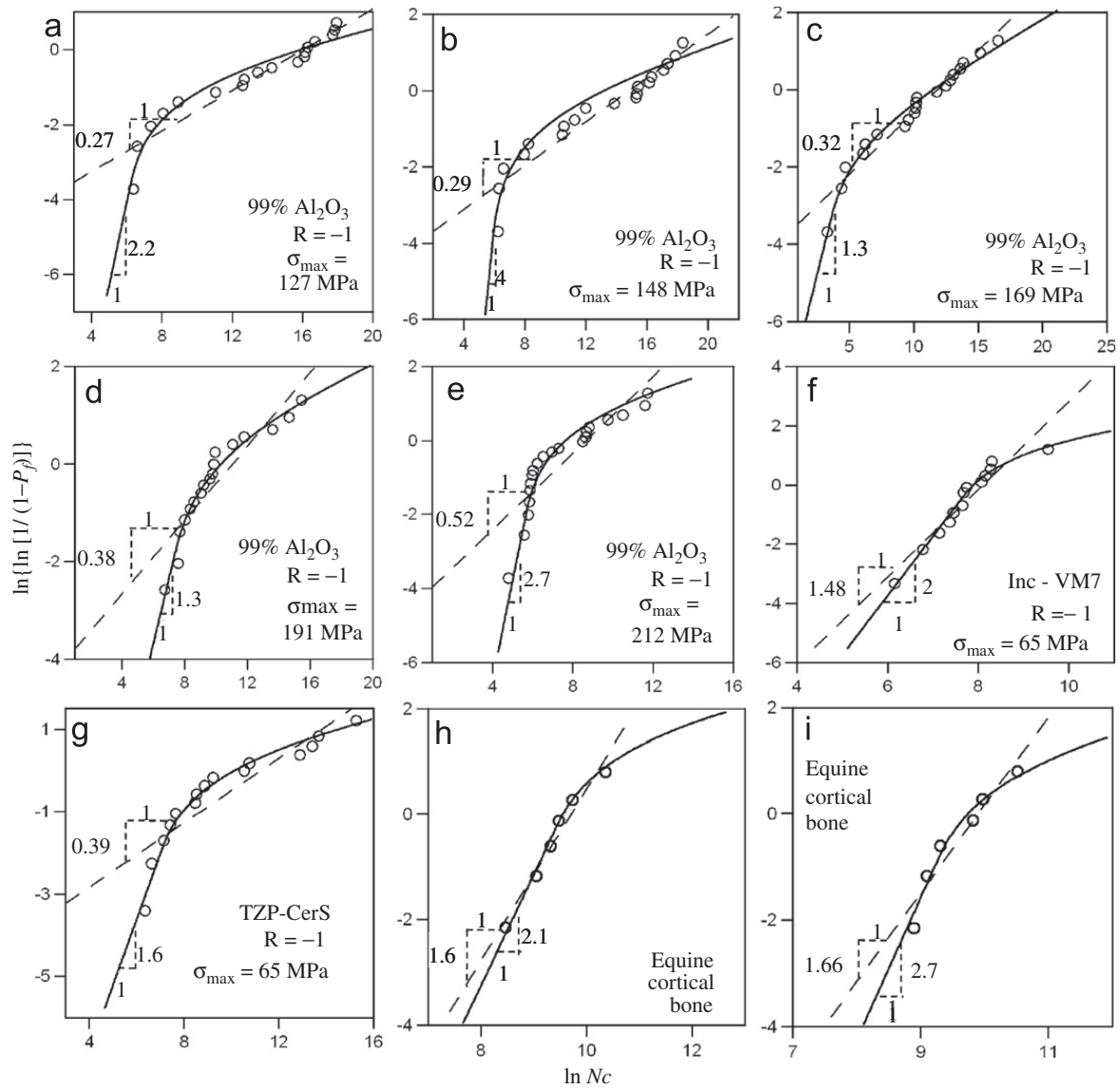


Fig. 7. (a–i) Optimum fits of histograms of fatigue lifetime.

analysis (Redner, 2001), which shows that the lifetime is finite under arbitrarily small loads (even a zero load) although it may be longer than the age of the universe.

7. Size effect on stress-life curve

The foregoing analysis (Eq. (41)) shows that the cdf of fatigue lifetime depends on the structure size as well as the geometry (which is introduced through the stress distribution). Naturally, the mean fatigue lifetime \bar{N}_f , too, must depend on the structure size and geometry. According to the weakest-link model,

$$\bar{N}_f = \int_0^\infty \prod_{i=1}^{n_s} [1 - P_1(\Delta\sigma_0 s(\mathbf{x}_i), N')] dN' \quad (45)$$

An analytical expression for \bar{N}_f seems impossible. However, similar to previous analysis of the size effect on the mean strength and creep lifetime (Bažant, 2004, 2005; Bažant and Novák, 2000; Le et al., this issue), one may use the approximation:

$$\bar{N}_f = \left[\frac{C_a}{D} + \left(\frac{C_b}{D} \right)^{\psi/\bar{m}} \right]^{1/\psi} \quad (46)$$

where \bar{m} is the Weibull modulus of fatigue lifetime. The values of C_a , C_b and ψ ensue by matching three asymptotic conditions: $[\bar{N}_f]_{D \rightarrow l_0}$, $[d\bar{N}_f/dD]_{D \rightarrow l_0}$, and $[\bar{N}_f D^{1/\bar{m}}]_{D \rightarrow \infty}$.

In the derivation of the cdf of fatigue strength of one RVE, the Paris law was integrated to obtain a simple equation that relates the fatigue lifetime and the applied stress amplitude (Eq. (37)). Consider now that two cyclic load histories with the same stress ratio but different stress amplitudes ($\Delta\sigma_{01}$ and $\Delta\sigma_{02}$) are applied to the same RVE. Based on Eq. (37), one finds that the fatigue lifetimes of RVE for these two load histories are related by

$$N_2 = \frac{\Delta\sigma_{01}^n}{\Delta\sigma_{02}^n} N_1 \tag{47}$$

Similarly, consider further that two cyclic load histories that give the same nominal stress ratio ($\sigma_{1,min}/\sigma_{1,max} = \sigma_{2,min}/\sigma_{2,max}$) but different nominal stress amplitudes ($\Delta\sigma_1$ and $\Delta\sigma_2$) are applied to the same structure. Since the stress in each RVE is proportional to the nominal stress, the ratio of stress amplitudes on each RVE for these two load cases is $\Delta\sigma_1/\Delta\sigma_2$.

For the first loading history, having nominal stress amplitude $\Delta\sigma_1$, the failure probability of the whole structure is $P_f = 1 - \prod_{i=1}^{n_s} [1 - P_1(N_f)]$. Based on Eq. (47), the failure probability of the structure under the second load history, having nominal stress amplitude $\Delta\sigma_2$, can be written as: $P_f = 1 - \prod_{i=1}^{n_s} \{1 - P_1[(\Delta\sigma_1^n/\Delta\sigma_2^n)N_f]\}$. Therefore, the mean fatigue lifetimes for these two load histories are related by $\Delta\sigma_1^n \bar{N}_{1c} = \Delta\sigma_2^n \bar{N}_{2c}$. This leads to a general relation between the mean fatigue lifetime and the nominal stress amplitude:

$$\bar{N}_f \Delta\sigma_0^n = C \tag{48}$$

where C is a constant. This is the well-known power law form for the stress-life (S-N) curve (or Basquin's law) for the fatigue loading, which is supported by numerous test data on quasibrittle materials such as ceramics (Kawakubo, 1995; Sakai and Hoshide, 1995; Lee et al., 1995) and cortical bones (Turner et al., 2001). It should nevertheless be emphasized that the S-N curve is here derived from the Paris law, which can be physically justified by assuming self-similarity of the function relating the number of microcracks to the applied stress amplitude. For very small or very large stress amplitudes, self-similarity may not be valid. Therefore, similar to the Paris law, one may expect the S-N curve to deviate from the power-law form for very low or very large stress amplitudes (Suresh, 1998). Note also that the slope of S-N curve is determined by the Paris law exponent n at the level of one RVE, and thus is not affected by size dependence of n .

Because of the size effect on the mean fatigue lifetime (Eq. (46)), constant C in Eq. (48) must depend on the structure size and geometry:

$$\bar{N}_f \Delta\sigma_0^n = C = \Delta\sigma_0^n \left[\frac{C_a}{D} + \left(\frac{C_b}{D} \right)^{\varphi/m} \right]^{1/\varphi} \tag{49}$$

Eq. (49) implies that, on a bilogarithmic plot, the S-N curve must shift horizontally to the left as the structure size increases. Fig. 8 shows the experimentally measured S-N curves of Sintered SiC under three-point bending and uniaxial tension fitted by Eq. (49) (Okabe and Hirata, 1995). Due to the difference in stress distribution, for the same specimen, the equivalent size of the specimen under three-point bending is much smaller than it is under uniaxial tension. As indicated as Fig. 8, there is a marked size effect on the S-N curve. For the same applied nominal stress amplitude, the lifetime of

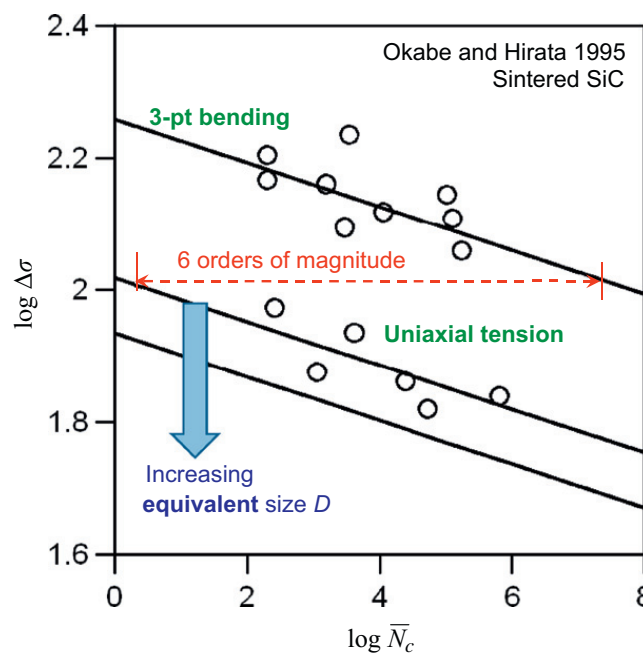


Fig. 8. Size effect on the S-N curve.

specimen under three point bending is about six orders of magnitude longer than the lifetime of specimen under uniaxial tension.

Eq. (49) is particularly important for the design process since it allows one to determine the mean lifetime of full-scale structures under relatively low stress amplitude from the laboratory tests on prototypes under relatively high stress amplitude.

8. Closing: three essential points

1. The only scale at which the probability distribution of failure properties can be clearly and easily determined is the nanoscale. The reason is that the breakage of interatomic bonds is a quasi-steady process, for which the probability is proportional to the frequency.
2. One property whose multiscale transition is known to be simple and easy is the activation energy control of rate processes. But it is not the only such property. Another is the tail of the probability distribution of strength. The finding that a power-law tail of cdf of fatigue strength is indestructible and that its exponent increases through multiscale transitions is an enabling feature of the present theory of fatigue as well as the preceding analogous theory of monotonic strength. The power-law tail of cdf with varying exponent across the scales is justified by the analysis of series and parallel couplings. Furthermore, the power-law for the mean rate of growth of a fatigue crack is physically explained by the equality of energy dissipation rates on the macro- and nano-scales.
3. The size effect is a salient feature of all quasibrittle failure. It affects not only the monotonic strength and static (or creep) lifetime, but also the fatigue strength and the type of its probability distribution. It leads to marked deviations from the Weibull distribution of lifetime, and its form deviates from the classical Weibull size effect. Considering brittle fracture as the large-size limit of quasibrittle fracture also enhances the understanding of brittle fracture itself.

Acknowledgments

The theoretical development was partially supported under Grant CMS-0556323 to Northwestern University (NU) from the U.S. National Science Foundation. The applications to concrete and to composites were partially supported by the U.S. Department of Transportation through the NU Infrastructure Technology Institute under Grant 27323, and also under Grant N007613 to NU from Boeing, Inc., respectively.

References

- Andersons, J., Hojo, M., Ochiai, S., 2004. Empirical model for stress ratio effect on fatigue delamination growth rate in composite laminates. *Int. J. Fatigue* 26, 597–604.
- Barenblatt, G.I., 2003. *Scaling*. Cambridge University Press.
- Barenblatt, R.I., Botvina, L.R., 1981. Incomplete self-similarity of fatigue in the linear range of crack growth. *Fatigue of Engrg. Mater. & Structures* 3, 193–212.
- Basquin, O.H., 1910. The exponential law of endurance tests. *Proc. A Mater. ASTEA* 10, 625–630.
- Bažant, Z.P., 2004. Scaling theory of quasibrittle structural failure. *Proc. Natl. Acad. Sci. USA* 101 (37), 13397–13399.
- Bažant, Z.P., 2005. *Scaling of Structural Strength*, second ed., Elsevier, London.
- Bažant, Z.P., Le, J.-L., 2009. Nano-mechanics based modeling of lifetime distribution of quasibrittle structures. *J. Eng. Failure Ana.* 16, 2521–2529.
- Bažant, Z.P., Le, J.-L., Bazant, M.Z., 2009. Scaling of strength and lifetime distributions of quasibrittle structures based on atomistic fracture mechanics. *Proc. Natl. Acad. Sci. USA*, pp. 11484–11489.
- Bažant, Z.P., Novák, D., 2000. Energetic-statistical size effect in quasibrittle failure at crack initiation. *ACI Mater. J.* 97 (3), 381–392.
- Bažant, Z.P., Pang, S.-D., 2006. Mechanics based statistics of failure risk of quasibrittle structures and size effect on safety factors. *Proc. Natl. Acad. Sci. USA* 103 (25), 9434–9439.
- Bažant, Z.P., Pang, S.-D., 2007. Activation energy based extreme value statistics and size effect in brittle and quasibrittle fracture. *J. Mech. Phys. Solids* 55, 91–134.
- Bažant, Z.P., Planas, J., 1998. *Fracture and Size Effect in Concrete and Other Quasibrittle Materials*. CRC Press.
- Bažant, Z.P., Vořechovský, M., Novák, D., 2007. Energetic-statistical size effect simulated by SFEM with stratified sampling and crack band model. *Int. J. Numer. Meth. Eng.* 71, 1297–1320.
- Bažant, Z.P., Xu, K., 1991. Size effect in fatigue fracture of concrete. *ACI Mater. J.* 88 (4), 390–399.
- Bigleya, R.F., Gibelingb, J.C., Stoverc, S.M., Hazelwooda, S.J., Fyhriea, D.P., Martin, R.B., 2007. Volume effects on fatigue life of equine cortical bone. *J. Biomech.* 40, 3548–3554.
- Christensen, R.M., 2008. A physically based cumulative damage formalism. *Int. J. Fatigue* 30, 595–602.
- Coffin, L.F., 1962. Low cycle fatigue—a review. *Appl. Mater. Res.* 1 (3).
- Daniels, H.E., 1945. The statistical theory of the strength of bundles and threads. *Proc. R. Soc. London A* 183, 405–435.
- Duckett, K., 2005. Risk analysis and the acceptable probability of failure. *The Struct. Eng.* 83 (15), 25–26.
- Goodman, J., 1899. *Mechanics Applied to Engineering*. Longmans Green, London.
- Gerber, H., 1874. Bestimmung der zulässigen Spannungen in Eisen-konstruktionen. *Zeitschrift des Bayerischen Architekten und Ingenieur-Vereins* 6, 101–110.
- Graham-Brady, L.L., Arwade, S.R., Corr, D.J., Gutiérrez, M.A., Breyse, D., Grigoriu, M., Zabarab, N., 2006. Probability and materials: from nano- to macro-scale: a summary. *Prob. Eng. Mech.* 21 (3), 193–199.
- Grassl, P., Bažant, Z.P., 2009. Random lattice-particle simulation of statistical size effect in quasi-brittle structures failing at crack initiation. *J. Eng. Mech. ASCE* 135 (2), 85–92.
- Hoshida, T., 1995. Proof testing and subsequent fatigue characteristics in ceramics. In: Kishimoto, H., Hoshida, T., Okabe, N. (Eds.), *Cyclic Fatigue in Ceramics*. Elsevier Science B. V. and The Society of Materials Science, Japan, pp. 207–232.

- Kawakubo, T., 1995. Fatigue crack growth mechanics in ceramics. In: Kishimoto, H., Hoshide, T., Okabe, N. (Eds.), *Cyclic Fatigue in Ceramics*. Elsevier Science B. V. and The Society of Materials Science, Japan, pp. 123–137.
- Kitagawa, H., Takahashi, S., 1976. Applicability of fracture mechanics to very small cracks or the cracks in the early stage. In: *Proceedings of the Second International Conference on Mechanical Behavior of Materials*, Metals Park, American Society for Metals, pp. 627–631.
- Le, J.-L., Bažant, Z.P., 2009. Finite weakest link model with zero threshold for strength distribution of dental restorative ceramics. *Dent. Mater.* 25 (5), 641–648.
- Le, J.-L., Bažant, Z.P., Bazant, M.Z., 2009. Crack growth law and its consequences on lifetime distributions of quasibrittle structures. *J. Phys. D Appl. Phys.* 42, 214008.
- Le, J.-L., Bažant, Z.P., Bazant, M.Z. Unified nano-mechanics based probabilistic theory of quasibrittle and brittle structures: I. Strength, static crack growth, lifetime and scaling. *J. Mech. and Phys. Solids*, this issue, doi:10.1016/j.jmps.2011.03.002.
- Lee, H.L., Park, S.E., Hahn, B.S., 1995. Modeling of cyclic fatigue stress for life prediction of structural ceramics. *J. Mater. Sci.* 30, 2521–2525.
- Mihashi, H., 1983. A stochastic theory for fracture of concrete. In: Witterman, F.H. (Ed.), *Fracture Mechanics of Concrete*. Elsevier Science Publishers B.V., Amsterdam, The Netherlands, pp. 301–339.
- Melchers, R.E., 1987. *Structural Reliability, Analysis & Prediction*. Wiley, New York.
- Morrow, J.D., 1968. *Fatigue Design Handbook—Advances in Engineering*, vols. 4, Sec. 3.2, Society of Automotive Engineers, Warrendale, P.A., pp. 21–29.
- NKB, 1978. (Nordic Committee for Building Structures). Recommendation for loading and safety regulations for structural design. NKB Report, No. 36.
- Ogawa, T., 1995. Fatigue crack growth of monolithic and composite ceramics. In: Kishimoto, H., Hoshide, T., Okabe, N. (Eds.), *Cyclic Fatigue in Ceramics*. Elsevier Science B. V. and The Society of Materials Science, Japan, pp. 167–188.
- Okabe, N., Hirata, H., 1995. High temperature fatigue properties for some types of SiC and Si₃N₄ and the unified strength estimation method. In: Kishimoto, H., Hoshide, T., Okabe, N. (Eds.), *Cyclic Fatigue in Ceramics*. Elsevier Science B. V. and The Society of Materials Science, Japan, pp. 245–276.
- Pang, S.-D., Bažant, Z.P., Le, J.-L., 2008. Statistics of Strength of ceramics: finite weakest link model and necessity of zero threshold. *Int. J. Frac. (Special Issue on Physical Aspects of Scaling)* 154, 131–145.
- Paris, P.C., Erdogan, F., 1963. A critical analysis of crack propagation law. *J. Basic Eng.* 85, 528–534.
- Phoenix, S.L., 1978a. The asymptotic time to failure of a mechanical system of parallel members. *SIAM J. Appl. Math.* 34 (2), 227–246.
- Phoenix, S.L., 1978b. Stochastic strength and fatigue of fiber bundles. *Int. J. Frac.* 14 (3), 327–344.
- Redner, S., 2001. *A Guide to First-Passage Processes*. Cambridge University Press.
- Rice, J.R., 1967. Mechanics of crack tip deformation and extension by fatigue. in: *Fatigue Crack Propagation*, Special Technical Publication 415, American Society for Testing and Materials, Philadelphia, pp. 247–309.
- Ritchie, R.O., 2005. Incomplete self-similarity and fatigue-crack growth. *Int. J. Frac.* 132, 197–203.
- Sakai, T., Fujitani, K., 1989. A statistical aspect on fatigue behavior of alumina ceramics in rotating bending. *Eng. Frac. Mech.* 32 (4), 653–664.
- Sakai, T., Hoshide, T., 1995. Statistical aspect on fatigue fracture of structural ceramics under cyclic loads. In: Kishimoto, H., Hoshide, T., Okabe, N. (Eds.), *Cyclic Fatigue in Ceramics*. Elsevier Science B. V. and The Society of Materials Science, Japan, pp. 189–206.
- Smith, R.L., 1982. The asymptotic distribution of the strength of a series-parallel system with equal load sharing. *Ann. Probab.* 10 (1), 137–171.
- Sobczyk, K., Spencer Jr., B.F., 1992. *Random Fatigue: From Data to Theory*. Academic Press, San Diego, CA.
- Soderberg, C.R., 1939. Factor of safety and working stress. *Trans. Am. Soc. Mech. Eng.* 52, 12–28.
- Sturdanta, A.R., Filser, F., Kochera, P., Gauckler, L.J., 2007a. Fatigue of zirconia under cyclic loading in water and its implications for the design of dental bridges. *Dent. Mater.* 23, 106–114.
- Sturdanta, A.R., Filser, F., Kochera, P., Lüthy, H., Gauckler, L.J., 2007b. Cyclic fatigue in water of veneer framework composites for all-ceramic dental bridges. *Dent. Mater.* 23, 177–185.
- Suresh, S., 1998. *Fatigue of Materials*. Cambridge University, Cambridge.
- Tanaka, K., Nakai, Y., Yamashita, M., 1981. Fatigue growth threshold of small cracks. *Int. J. Frac.* 17, 519–533.
- Tierney, L.-J., 1983. Asymptotic bounds on the time to fatigue failure of bundles of fibers under local load sharing. *Adv. Appl. Prob.* 14 (1), 95–121.
- Turner, C.H., Wang, T., Burr, D.B., 2001. Shear strength and fatigue properties of human cortical bone determined from pure shear tests. *Calcif. Tissue Int.* 69, 373–378.
- Weibull, W., 1939. The phenomenon of rupture in solids. *Proc. R. Swed. Inst. Eng. Res. Stockholm* 153, 1–55.
- Weertman, J., 1966. Rate of growth of fatigue cracks calculated from the theory of infinitesimal dislocation distributed on a crack plane. *Int. J. Frac.* 2, 460–467.
- Williams, T., Baxer, S.C., 2006. A framework for stochastic mechanics. *Prob. Eng. Mech.* 21 (3), 247–255.
- A. Wöhler, 1860. Versuche über die Festigkeit der Eisenbahnwagenachsen. *Zeitschrift für Bauwesen*. 10; English summary (1867). *Engineering* 4, 160–161.
- Yang, J.N., Salivar, G.C., Annis, C.G., 1983. Statistical modeling of fatigue-crack growth in a Nickel-based superalloy. *Eng. Frac. Mech.* 18 (2), 257–270.
- Yang, J.N., Donath, R.C., 1983. Statistical crack propagation in fastener holes under spectrum loading. *J. Aircraft* 20 (12), 1028–1032.
- Yang, J.N., Manning, S.D., 1991. A simple second order approximation for stochastic crack growth analysis. *Eng. Frac. Mech.* 53 (5), 677–686.